National Library
of Canada

Bibliothèque nationale
du Canada

Canadian Theses Service

Service des thèses canadiennes

Ottawa, Canada
K1A 0N4

NOTICE

The quality of this microform is heavily dependent upon the quality of the original thesis submitted for microfilming. Every effort has been made to ensure the highest quality of reproduction possible.

If pages are missing, contact the university which granted the degree.

Some pages may have indistinct print especially if the original pages were typed with a poor typewriter ribbon or if the university sent us an inferior photocopy.

Previously copyrighted materials (journal articles, published tests, etc.) are not filmed.

Reproduction in full or in part of this microform is governed by the Canadian Copyright Act, R.S.C. 1970, c. C-30.

AVIS

La qualité de cette microforme dépend grandement de la qualité de la thèse soumise au microfilmage. Nous avons tout fait pour assurer une qualité supérieure de reproduction.

S'il manque des pages, veuillez communiquer avec l'université qui a conféré le grade.

La qualité d'impression de certaines pages peut laisser à désirer, surtout si les pages originales ont été dactylographiées à l'aide d'un ruban usé ou si l'université nous a fait parvenir une photocopie de qualité inférieure.

Les documents qui font déjà l'objet d'un droit d'auteur (articles de revue, tests publiés, etc.) ne sont pas microfilmés.

La reproduction, même partielle, de cette microforme est soumise à la Loi canadienne sur le droit d'auteur, SRC 1970, c. C-30.

NL-339 (r. 88/04)

Canada

THE UNIVERSITY OF ALBERTA

Delayed Hydride Cracking of Zr-2.5%Nb

by

(C) Richard Robert Smith

A THESIS

SUBMITTED TO THE FACULTY OF GRADUATE STUDIES AND RESEARCH
IN PARTIAL FULFILMENT OF THE REQUIREMENTS FOR THE DEGREE
OF DOCTOR OF PHILOSOPY
IN
METALLURGICAL ENGINEERING

DEPARTMENT OF MINING, METALLURGICAL AND PETROLEUM
ENGINEERING

EDMONTON, ALBERTA
Fall 1987

Permission has been granted to the National Library of Canada to microfilm this thesis and to lend or sell copies of the film.

The author (copyright owner) has reserved other publication rights, and neither the thesis nor extensive extracts from it may be printed or otherwise reproduced without his/her written permission.

L'autorisation a été accordée à la Bibliothèque nationale du Canada de microfilmer cette thèse et de prêter ou de vendre des exemplaires du film.

L'auteur (titulaire du droit d'auteur) se réserve les autres droits de publication; ni la thèse ni de longs extraits de celle-ci ne doivent être imprimés ou autrement reproduits sans son autorisation écrite.

ISBN 0-315-41023-X

THE UNIVERSITY OF ALBERTA

RELEASE FORM

NAME OF AUTHOR Richard Robert Smith

TITLE OF THESIS Delayed Hydride Cracking of Zr-2.5%Nb

DEGREE FOR WHICH THESIS WAS PRESENTED DOCTOR OF PHILOSOPY

YEAR THIS DEGREE GRANTED Fall 1987

Permission is hereby granted to THE UNIVERSITY OF ALBERTA LIBRARY to reproduce single copies of this thesis and to lend or sell such copies for private, scholarly or scientific research purposes only.

The author reserves other publication rights, and neither the thesis nor extensive extracts from it may be printed or otherwise reproduced without the author's written permission.

(SIGNED) R R Smith

PERMANENT ADDRESS:

8608 - 157 Street
Edmonton, Alberta
T5R 2A5

DATED Sept 21 1987

THE UNIVERSITY OF ALBERTA

FACULTY OF GRADUATE STUDIES AND RESEARCH

The undersigned certify that they have read, and recommend to the Faculty of Graduate Studies and Research, for acceptance, a thesis entitled Delayed Hydride Cracking of Zr-2.5%Nb submitted by Richard Robert Smith in partial fulfilment of the requirements for the degree of Doctor of Philosopy in Metallurgical Engineering.

Reg Eadie

Michael L. Wayman

Supervisors

Samuel A. Bradford

B.M. Patchett

C.E. Coleman

External Examiner

Date Sept. 8, 1987

Abstract

The effects of load and temperature on the delayed hydride cracking of Zr-2.5%Nb have been investigated by use of tapered double-cantilever beam specimens. These samples were manufactured from Candu pressure tube material that was subsequently hydrided to the range of 92-298 ppm hydrogen. The progress of the hydride fracture was monitored by recording the acoustic emissions that were generated by the cracking samples. This was followed by fractographic and metallographic studies of the specimens.

The steady state cracking rate has been found to depend on prior conditions of both temperature and load. Generally faster cracking rates resulted when the load was increased to the test load, or when the sample was cooled to the test temperature.

In terms of temperature, hydride cracking in samples containing at least 92 ppm hydrogen was found to be bounded below by cracking rates too low to be considered significant, and bounded above by a crack arrest temperature, Tcat, which occurred in the range of 320°C. Above this temperature the loaded samples went into a state of cracking remission. A long incubation period was then required to re-establish cracking.

Many features appeared on the fracture surfaces that could not be attributed to the progression of a purely brittle fracture. Comparison of the acoustic emission history with fractographic features of tests samples showed that the two were only related in a general way. This, and other observations, indicated that fracture processes other than the fracture of hydrides occur but do not produce significant acoustic emissions in the frequency range monitored.

Metallographic studies showed that the delayed hydride fracture produced multiple branching cracks that were often discontinuous in the plane of observation.

The delayed hydride fracture process is thought to consist of the propagation of two crack fronts: a brittle crack front, and a ductile crack front. A new qualitative five stage model has been developed for delayed hydride cracking which includes these two modes of fracture.

Acknowledgements

I wish to thank my supervisors Dr. R.L. Eadie and Dr. M.L. Wayman, both of whom were essential to the completion of this project.

My thanks also to those who went beyond the call of duty to lend their moral and physical support for this project. With a special thanks to John Czuroski for his photographic help, to Tom Forman for his electronic expertise, to Jacques Gibeau for his computer-graphics knowledge, and to Karan Smith for her artistic ability shown in the sketches.

This work was partially funded by a Natural Sciences and Engineering Research Council of Canada Scholarship, and partially by the Department of Mining, Metallurgical and Petroleum Engineering, University of Alberta.

Table of Contents

Chapter Page

1. Introduction 1

2. Literature Survey 5

  2.1 Introduction 5

  2.2 Hydrogen Motion in Zirconium and its Alloys 6

  2.3 Hydrides and Other Precipitates 8

  2.4 Terminal Solid Solubility 14

  2.5 The Zirconium-Niobium System 17

  2.6 Properties of Zirconium Hydrides 18

  2.7 Concept of Hydride Cracking 19

  2.8 Models of Crack Propagation 21

  2.9 Cracking Stages 24

  2.10 Hydride Cracking Variables 26

    2.10.1 Test Temperature 26

    2.10.2 Hydrogen 27

    2.10.3 Thermal Cycles 27

    2.10.4 Grain Structure 28

  2.11 Fractography 29

  2.12 Morphology of Hydrides Associated with Fracture 30

  2.13 Monitoring Hydride Cracking 31

  2.14 Research Topic Selection 32

3. Experimental 34

  3.1 Introduction 34

  3.2 Test Samples 34

  3.3 Loading Arrangement 35

  3.4 Acoustic Emission Monitoring 40

3.5 Temperature Control and Recording 40

3.6 Microscopic and Fractographic Techniques 41

4. Results and Discussion 42

4.1 Acoustic emission monitoring 42

4.1.1 Introduction 42

4.1.2 Acoustic Emission Monitoring 44

4.1.3 Effect of Load and Temperature on Steady State Cracking 47

4.2 Waxing and Waning Temperature Changes 61

4.2.1 Waxing temperature 62

4.2.1.1 Post Slow Cracking Mode 62

4.2.1.2 After Temperature Fall 66

4.2.1.3 Post Fast Cracking Mode 67

4.2.2 Temperature Fall 68

4.2.2.1 Post Fast Cracking Mode 68

4.2.2.2 After Waxing Temperature 72

4.2.2.3 Post Slow Cracking Mode 73

4.2.3 Overall Effects of Waning and Waxing Temperature 74

4.3 The Effect of Load on Hydride Cracking 75

4.3.1 Load vs. Stress Intensity 75

4.3.2 Effect of a Waxing Load 75

4.3.3 Effect of a Waning Load 76

4.3.4 Effect of Prior Load on Acoustic Emissions 77

4.3.5 Tables Showing the Effect of Loading 77

4.3.6 Comparison of Load and Temperature Effects 80

4.3.7 Effect of Load Changes on Cracking Modes 82

4.4 Fractography 85

4.4.1 Optical Surface Features 85

4.4.2 Surface Features in the Scanning Electron Microscope 90

4.4.3 Acoustic Emission and Fractography 92

4.5 Metallography 97

4.5.1 As-Received Tubing 97

4.5.2 Hydride Orientation 101

4.5.3 Grain Structure and Hydrides 104

4.5.4 Microhardness 105

4.6 Artifacts in the Metallographic Preparation of Fractures 106

4.6.1 Fracture Path 108

4.6.2 Load and Crack Displacement 122

4.6.3 Fracture Appearance in the Radial-Tangential Plane 126

4.7 The Modelling of Delayed Hydride Fracture 132

4.7.1 Introduction 132

4.7.2 Components of Hydride Cracking 133

4.7.2.1 Hydrides 133

4.7.2.2 Hydrogen 135

4.7.2.3 Crack Morphology 136

4.7.2.4 Acoustic Emission 137

4.7.2.5 Temperature 138

4.7.2.6 Load 139

4.7.3 Limitations of the Current Hydride Cracking Model 140

4.7.4 The Proposed Delayed Hydride Cracking Model 143

4.7.5 Discussion of the Five Stage Model 147

4.7.5.1 Load 147
4.7.5.2 Striations 152
4.7.5.3 Temperature 154
4.7.5.4 Hydride Cracking Arrest 156
4.7.5.5 Literature Support for the Cracking Model 160
5. Conclusions 162
6. Further Study 166
7. Bibliography 169

List of Tables

Table Page

4.1 Conditions of Hydride Cracking Termination 49

4.2 Effect of Load Change at 119°C 78

4.3 Effect of Load Change at 140°C 79

4.4 Effect of Load Change at 200°C 79

4.5 Counts versus Fracture Surface Area on Sample 1804-2 94

4.6 Counts versus Fracture Surface Area on Sample 148-1 95

List of Figures

Figure Page

2.1 Phase Relations in the Zr-H System. 9

2.2 Terminal solid solubility curves for unalloyed zirconium. 14

2.3 A section of the Zr-Nb phase diagram. 17

2.4 Crack velocity versus stress intensity factors (Dutton,77a, Puls,82). 23

3.1 A constant K specimen. 35

3.2 The load suspension system and some of the acoustic emission monitoring apparatus. 36

3.3 The mechanical loading system. 37

3.4 The constant K sample in the pin and clevis coupling. 38

4.1 A noise calibration run. 45

4.2 Acoustic emissions during hydride cracking of sample 1804-1, 92 ppm hydrogen. 48

4.3 Crack tip hydrides in sample 1804-1, 10x. 50

4.4 A typical time-temperature profile. 53

4.5 Acoustic emission rate vs. temperature, slow cracking mode, sample 148-1, 298 ppm hydrogen. 55

4.6 Acoustic emission rate vs. temperature, slow cracking mode, sample 1804-2, 92 ppm hydrogen. 56

4.7 Acoustic emission rate vs. temperature, fast cracking mode, sample 1804-2, 92 ppm hydrogen. 58

4.8 Acoustic emission rate vs. temperature, fast cracking mode, sample 148-1, 298 ppm hydrogen. 59

4.9 Rising temperature plateaus. 62

4.10 Acoustic emission rate vs. periods of waxing temperature, slow cracking mode, sample 148-1. 64

Figure Page

4.11 Acoustic emission rate vs. periods of waxing temperature, slow cracking mode, sample 1804-2. 65

4.12 Temperature rise and fall. 66

4.13 A waxing temperature in the fast cracking mode. 67

4.14 A waning temperature in the fast cracking mode. 68

4.15 Acoustic emission rate vs. periods of waning temperature, fast cracking mode, sample 148-1. 70

4.16 Acoustic emission rate vs. periods of waning temperature, fast cracking mode, sample 1804-2. 71

4.17 A waning temperature after a temperature rise. 72

4.18 A waning temperature in the slow cracking mode. 73

4.19 The temperature profile and acoustic emissions generated during part of a load variation experiment. 84

4.20 The fracture path in the region of a saw cut, sample 148-1, 6x. 86

4.21 The fracture surface of sample 1804-2, 92 ppm hydrogen, 6x. 87

4.22 The fracture surface of sample 148-1, 298 ppm hydrogen, 6x. 88

4.23 Striations (oriented vertically), sample 1804-2, 40x. 90

4.24 Striations (oriented horizontally), 500x. 91

4.25 A striation line (shown with arrows), 1900x. 91

4.26 A temperature profile and acoustic emissions. 93

4.27 The orientation of three planes in the pressure tube. 97

Figure Page

4.28 The radial-longitudinal plane of a Zr-2.5%Nb tube, etched, 1400x. 98

4.29 The longitudinal-tangential plane, etched, 1400x. 99

4.30 The radial-tangential plane, etched, 1400x. 100

4.31 The hydride orientation in the radial-longitudinal plane, unetched, 110x. 101

4.32 The hydride orientation in the longitudinal-tangential plane, unetched, 110x. 102

4.33 Hydrides in the radial-tangential direction, unetched, 110x. 103

4.34 Hydrides at a crack tip before etching (left), and after etching (right), 1400x. 104

4.35 Hardness indents of 15 grams on the Zr-2.5%Nb matrix containing a hydride, 1400x. 106

4.36 The root of the hydride crack polished to show hydrides (above) and polished flat (below), 2000x. 109

4.37 The intergranular and transgranular components of the fracture path, 1400x. 110

4.38 The interface of zone 1 and zone 2, 2000x. 111

4.39 The powdery cracking of zone three, 1400x. 112

4.40 The final fracture separation with some of the zone three material, 650x. 113

4.41 The effect of heavy polishing scratches on the stage three material, 1400x. 114

4.42 A hardness indent of 15 grams on the stage three material, 600x. 115

4.43 An etched section of zone three, 1400x. 116

Figure Page

4.44 The oxide phase adjacent to the fracture surface of a tube sample as shown by a 45 degree taper section of sample 148-1, 1400x. 117

4.45 The oxide phase adjacent to the outside surface of a tube sample as shown by a 45 degree taper section of sample 148-1, 1400x. 118

4.46 Material found in a hydride crack (above) and material found in a crack-like defect created in the same sample (below), 1120x. 119

4.47 Hydrides associated with a drilled hole and plug in a hydrided zirconium sample, 320x. 120

4.48 An electron micrograph of a stressed hydride crack (the longitudinal direction of the crack extends from the lower left corner at ≃45°), 300x. 123

4.49 The hydride crack under load, 56x. 124

4.50 A prepared hydride crack without load (left) and with load (right). The upper crack of Figure 4.49 is shown above while the longer, lower crack is shown below, 800x. 125

4.51 The appearance of two regions of the hydride fracture viewed in the radial-tangential plane near the mouth of the crack, 112x. 127

4.52 A region of the hydride fracture at 240x (above) and 1400x (below) near the root of the crack in the radial-tangential plane, sample 1804-3. 128

4.53 Cracking parallel to the applied stress viewed in the radial-tangential plane near the crack tip, 1400x. 129

4.54 Transverse cracking ahead of the major crack in the radial-tangential plane, 225x. 130

4.55 The root of the fracture in the radial-tangential plane, 230x. 131

Figure Page

4.56 A schematic representation of the five stages of hydride cracking (not to scale). 144

1. Introduction

Each of us at some time or another has derived a form of satisfaction from breaking things. A small boy experiences great delight in breaking an iced puddle with a stick while a professor happily demonstrates the brittle fracture of a liquid nitrogen-cooled tygon tube with a hammer. The results of these tests are not frivolous, but provide a subliminal type of logic on which many of our living skills are based.

On a slightly more sophisticated level destructive tests are employed as a basis for engineering design. In this respect a test that determines the point of failure has an infinitely greater value than one that demonstrates a set of conditions under which failure does not occur. The merit of destructive tests evolves from the epitome of good engineering design, which is structural integrity at the lowest possible cost. This economic constraint often necessitates that the design be as close as possible to the point of failure and still allow, under the conditions in which the component was intended to operate, fulfillment of the service life. In order to have value it is obvious that destructive tests must somehow reflect the intended service conditions.

During the course of history it has become apparent that the evaluation of a metal component can not be fully achieved simply by loading to failure. In the first half of the 19th century two French engineers worked on the failure of stage coach axles, and recommended that a limit of 70,000 km be placed on the life of such axles. They had effectively, perhaps even before the word "fatigue" was coined for metals, found a solution for metal fatigue. Today, still following their advice, some metal components are replaced after a specified service life. The millions of fatigue tests conducted since this recommendation have increased our understanding of the phenomenon enabling a more accurate prediction as to when the failure of a component will take place.

Metals have shown other disconcerting methods of failing far below their ultimate strengths. One of the most recently discovered can be described as a delayed hydrogen fracture. Failure via this process requires a quantity of hydrogen in the metal matrix along with appropriate conditions of time, temperature, and stress. The concept of delay infers that time for the diffusion of hydrogen is necessary in the fracture process.

Over the course of time a distinction has been made between metals that display a stable hydride during cracking conditions and those that do not. This distinction manifests itself in the theoretical modeling of the fracture mechanism rather than the name given to the process. Thus for materials such as zirconium and vanadium, that form stable hydrides, the failure may be termed "delayed hydrogen cracking" or "hydride cracking."

To most people the topic of hydride cracking has a somniferous quality. In reality it should be exciting. Nuclear reactors have made extensive use of zirconium components because of their neutron transparency. The hydride cracking of zirconium alloys had been demonstrated in the early 1960's, but it wasn't until service failures in the reactors began to occur in the early 1970's that the topic came into vogue. Extensive work has been done on this topic since the first failure, and methods have been found to mitigate some of the problems with regard to the cracking of the pressure tubes in the Candu reactors, but our working knowledge of the phenomenon is far from complete.

The purpose of this study was to examine the effects of two variables, stress and temperature, on the hydride cracking of the commercial alloy, Zr-2.5%Nb. The use of acoustic emission to detect cracking allowed emphasis to be placed on the dynamic nature of the two variables. In order to ensure that any significant data resulting from this study would also have a practical significance, the test specimens were manufactured from Candu pressure tube material.

We cannot eliminate hydride cracking any more than we can eliminate metal fatigue, but by knowing the conditions under which it occurs and how the process or processes operate, we can design around the problem. Timely solutions such as reducing the amount of hydrogen in the material and lowering the residual stresses in working components have already provided some means of avoiding failures. The task is now to achieve a greater understanding of the phenomenon to allow designs of greater economy that utilize these materials and still maintain a respectable safety factor.

2. Literature Survey

2.1 Introduction

The time dependent stepwise cracking of a metal due to the effect of hydrogen had been conceptualized by the early 1950's (Petch,52). Work on the effect of hydrogen on the short term ductility of zirconium was also reported about this same time by the United States Atomic Energy Commission (Coleman,79).

By 1960 the delayed failure of metals containing hydrogen had been documented in steel and titanium, and a low strain rate hydrogen embrittlement had been observed in vanadium and niobium (Troiano,60). The susceptibility of zirconium and zirconium alloys to delayed failure hydrogen embrittlement was reported a few years later (Weinstein,64, Östberg,64), but it was not until the first service failures caused by delayed hydride cracking of the Candu reactor in the early 1970's (Perryman,78) that a concentrated research effort began on the subject.

Most studies of delayed hydride cracking have dealt with either pure zirconium or the common commercial grade alloys: Zircaloy 2 and 4 (essentially Zr-1.5%Sn) (Coleman,79), and Zr-2.5%Nb. Work has also been done on the cracking of the Excel alloy (Zr-3.5%Sn-0.8%Nb-0.8%Mo) (Cheadle,79) and precipitation studies have been carried out on the alloys Scank 1 (Zr-1%Nb), and Scank 4 (Zr-0.5%Nb-0.5%Cr) (Vitikainen,78).

These studies have revealed that three factors are necessary in order for delayed hydride cracking to take place: a suitable tensile stress within the zirconium metal, the transport of sufficient hydrogen in the metal to allow the hydride phase to form in the stressed region, and time for the crack to initiate and grow. The understanding of these factors is obfuscated by the effects of numerous metallurgical variables.

It is the intent of this literature survey to touch on the metallurgical variables mentioned above with a bias towards the Candu pressure tube material manufactured from Zr-2.5%Nb. This will be followed by a review of the present understanding of the delayed cracking phenomena. The way will thus be paved for considering the experimental program that was carried out. However, it must be noted that the explanations and interpretations of experimental results which are reported in this section are not necessarily the opinion of the writer. Furthermore some of the conclusions resulting from studies reported in the literature are in direct conflict with the findings of this study.

2.2 Hydrogen Motion in Zirconium and its Alloys

The transport of hydrogen in the zirconium matrix is one of the fundamental necessities of hydride cracking. Yet because of the difficulty in making measurements and the complexity of the system, relatively little is quantitatively known of this phenomenon. Measurements of bulk diffusion rate have been made by numerous workers (Sawatzky,81, Mazzolai,76, Kearns,72) expecially at temperatures above 200°C. Although this parameter would be expected to have an effect on cracking rate, it does not completely describe the hydrogen transport at the micro-level at which cracking takes place.

As an example, the diffusion of hydrogen has been studied in a two phase α-β zirconium system in which the diffusion rate of the hydrogen in the β phase was known to be higher than the diffusion rate in the α phase. This study compared the diffusion rates of samples that contained a continuous network of β filaments to samples in which the β phase was partially or completely decomposed. The diffusion coefficient for hydrogen was found to be the same in both cases (Sawatzky,81). A similar comparison was made to determine the effect of the β microstructure on cracking rate. The cracking velocities of the two sample groups were found to be different and the implication was made that this variation in cracking rate resulted from the change in the diffusivity of hydrogen due to the decomposition of the β phase (Simpson,84).

In the zirconium alloys hydrogen can move in several modes: interstitially in the matrix, along grain boundaries, through precipitates and secondary phases, and along dislocations. The system may be further complicated because of the movement of dislocations during the cracking process. For example, Bastien and Azou have suggested that moving dislocations might transport significant quantities of hydrogen in metals (Johnson,76).

Pressouyre gives a detailed description of hydrogen transport in a material during embrittling conditions which employs the concept of hydrogen traps. Two types of hydrogen traps are considered, reversible and irreversible. The reversible traps actively exchange hydrogen, while the irreversible traps act only as hydrogen sinks (Pressouyre,80). Thus if a dislocation sweeping through the material is carrying an atmosphere of hydrogen with it, the dislocation will lose hydrogen if the traps are empty and will not lose hydrogen if the traps are full. The hydrogen trapping ability of various traps, such as precipitates or other phases, could lower the effective hydrogen concentrations in the zirconium alloy. This could be similar to the effect of thoria particles in reducing the hydrogen embrittlement of Ni (Thompson,72).

2.3 Hydrides and Other Precipitates

Hydrogen is present as an impurity in refined zirconium metal typically at levels of ≃15 ppm (Ells,78). Over a period of time in a superheated water or steam atmosphere the zirconium will pick up hydrogen from the corrosion reaction (Weinstein,64). It is then possible for the hydrogen to migrate in the alloy due to the effects of a temperature gradient (Wilkins,69) or a stress gradient (Völkl,72). Figure 2.1 shows the phases present in the Zr-H system as proposed by Beck (1962) which is similar to that given by Mueller (1968). At high temperatures large amounts of hydrogen dissolve in zirconium as a solid solution. Upon cooling hydrogen comes out of solution in the form of hydrides, and a phase transformation takes place in the zirconium metal.

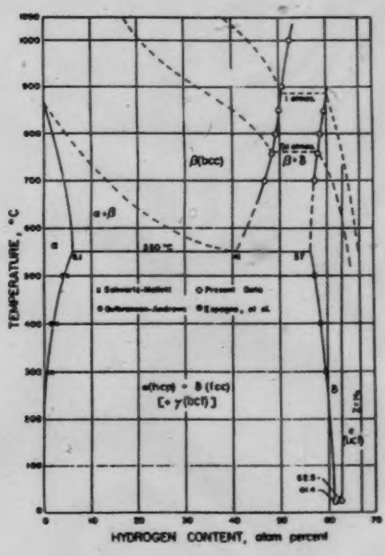

Figure 2.1 Phase Relations in the Zr-H System.

There are three possible hydrides in pure zirconium: the face centred tetragonal γ phase (ZrH), the face centred cubic δ phase (ZrH_x, where x lies in the range of 1.5 to 1.66) and the face centred tetragonal ε phase (ZrH_2) (Ells,68, Libowitz,62, Northwood,78a, Weatherly,81). The δ and the ε phases are considered to be stable while the γ phase is generally considered to be metastable. The occurrence of the γ phase has been described schematically on the zirconium-hydrogen phase diagram by a solvus line running below, but roughly parallel, to the equilibrium solvus line of the α phase (Nath,75). This concept of a metastable γ phase is not universally held. Barraclough and Beevers (1974) reported that at 300°C the γ hydride was stable rather than the δ hydride phase.

The crystal structure, distribution and morphology of the hydrides are dependent upon the cooling rate from the solid solution temperature (Bradbrook,72). Carpenter (1973) found γ hydride needles in rapidly cooled alloys. Decreasing the cooling rate leads to more δ hydrides and fewer γ hydrides (Bradbrook,72, Northwood,78a). In furnace cooled Zr-2.5.%Nb samples both the δ hydrides and γ hydrides were observed (Northwood,78a) whereas in pure zirconium only δ hydrides were observed after furnace cooling (Nath,75).

Work on zirconium and Zircaloy 2 has shown that hydrides appeared both intragranularly and at the grain boundaries, after high rates of cooling (Bradbrook,72). In these studies the grain boundary hydrides appeared as small needle-shaped precipitates or large irregular hydrides while the intragranular precipitates were uniformly distributed and needle-shaped. At very slow rates of cooling, large precipitates of δ hydride were found mainly at the grain boundaries (Bradbrook,72).

Other metallurgical and test variables have been investigated to determine their effects on the nature of the precipitating hydr~~ide~~ phase. Cann et al. (1984) have investigated four of these variables: grain size, solution heat treating temperature, specimen purity, and hydrogenation technique. Only specimen purity, specifically the oxygen content, was found to influence the hydride formation. Below oxygen levels of 200 ppm, the γ phase predominated; above 1000 ppm, the δ phase predominated.

Since the precipitation and growth of hydrides is thought to play an indispensible role in hydride cracking (Coleman,85), it is important to consider some of the characteristics of this precipitation process. The formation of a δ hydride in the zirconium matrix involves a 17% volume expansion (Carpenter,73) and a shear transformation (Carpenter,78). It is also thought that the formation of a single hydride plate will have an autocatalytic effect, promoting the formation of additional hydrides (Bradbrook,72).

Zirconium hydrides can occur in a wide range of morphologies. Both needle-shaped and large irregular hydrides have been documented by Bradbrook et al. (1972), and "clumping" of hydrides has been reported in fine grained specimens (Coleman,66). However for the case of Zr-2.5%Nb pressure tube the hydrides appear in a form that is usually described as platelets (Ells,80), or perhaps more picturesquely as a cornflake structure (Perovic,84).

Hydrides will not only precipitate out at grain boundaries, as previously mentioned, but also on dislocation lines, along the boundaries of previously existing hydrides (Arunachalam,67), and between the retained β phase and the α matrix (Perovic,84). This is especially significant to the Zr-2.5%Nb alloy since components of this material, such as pressure tubes, have α/β microstructures. Studies on α-β zirconium alloys (Perovic,83) indicate that stacks of δ hydrides form in the circumferential or radial direction of the Zr-2.5%Nb pressure tubes and have the relationship with the α matrix:

$$(111)_{\delta}\text{nearly}\,||\,(0001)_{\alpha};\ [1\bar{1}0]_{\delta}\text{nearly}\,||\,[11\bar{2}0]_{\alpha}$$

When a zirconium alloy is cooled under load, hydride plates tend to form with normals parallel to the tensile stress direction (Ells,68). This preferred orientation is increasingly marked if the material displays a strong crystallographic texture, with the basal plane normal parallel to the direction of stress. In the pressure tubes of the Candu there are some basal plane normals in the circumferential direction, and thus the Zr-2.5%Nb tubes could be susceptible to stress orientation of hydride into the radial-longitudinal planes (Ells,78). In cracking tests it was reported (Coleman,79) that cracks grew in the axial-radial plane (i.e. the radial-longitudinal plane) in all specimens. The analysis of the 1974 Pickering failure showed that radially precipitated hydrides existed in the cracked region, whereas the orientation of zirconium hydrides in the as-fabricated tubes is circumferential (Perryman,78).

It is well documented that the hydrides can reorient under an applied stress (Ells,68). Northwood and Gilbert (1978) found that hydrides which reoriented under the tensile stress were δ hydrides. However electron microscope studies of hydrides growing at the crack tip have shown that it is the γ hydrides that form and not the δ hydrides (Cann,80). Cann and Sexton also noted that in pure zirconium the hydrides formed at the crack tip whereas in the Zr-2.5%Nb the hydrides formed at, and also ahead of, the crack tip. After fracture the hydrides did not redissolve immediately. This is contrary to the behavior of vanadium in which the hydrides have been shown to dissolve immediately after the passage of the hydride crack (Takano,74).

Other precipitates also form in zirconium alloys. Vitikainen and Nenonen (1978) found four types of precipitates in Zircaloy 2. Two of these were hydrides, the γ hydride and a hydride most likely formed during electropolishing of the TEM specimens. In the Zr-1%Nb alloy two precipitates were found: the β_{Nb} phase and γ hydride needles. The needles showed poor coherency in the thickness direction. Often the hydride appeared to have nucleated on other precipitates in the material.

2.4 Terminal Solid Solubility

The temperature at which hydrides begin to form on cooling, or the temperature at which the last hydrides dissolve on heating is defined as the terminal solid solubility temperature, TSS. A plot of the TSS lines for zirconium under different conditions is shown in Figure 2.2 (Puls,81).

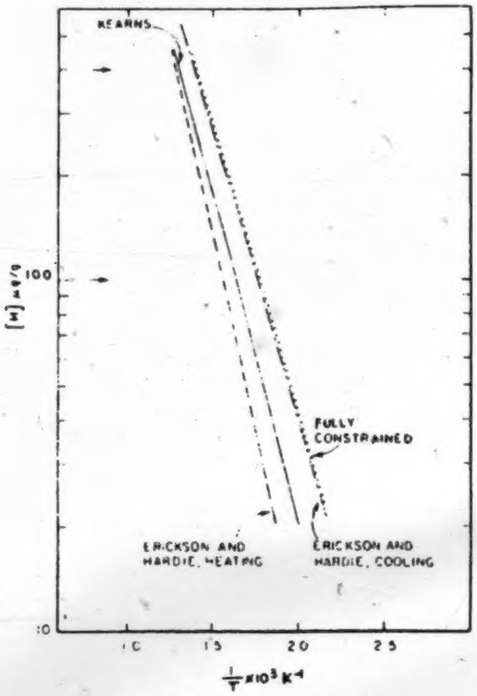

Figure 2.2 Terminal solid solubility curves for unalloyed zirconium.

A hysteresis is observed between the TSS lines measured on heating and on cooling. The extent of this hysteresis depends on the temperature, the holding time and the number of cooling cycles through which the system has been taken (Puls,81). The explanation of this phenomenon revolves around the fact that the hydrides forming from the matrix are less dense and occupy a greater volume than the metallic zirconium. Thus there is a strain energy associated with the precipitates. As the precipitate grows, the strain energy is partially relieved by plastic deformation of the matrix. On reheating the misfit strain cannot be fully recovered (Puls,81).

Applied stress affects the terminal solid solubility both in terms of the hydride formation and the hydrogen in solid solution. A tensile stress will increase the solubility of hydrogen. However since a volume expansion of the hydrides takes place during their formation, a tensile stress also increases the tendency to form hydrides which in turn tends to decrease the TSS (Puls,82). This may be the reason that little, if any, change in TSS with applied stress has been observed experimentally (Coleman,78).

If a thermal gradient is imposed on a zirconium rod containing hydrogen, the hydrogen will diffuse to the cool end and form a region of solid hydride (Wilkins,69). The hydrogen in solution at the high temperature end of the rod will be below the TSS line. Tests (Marshall,65) and simulations (Waisman,77) in titanium have also shown that hydrogen will redistribute towards the cold end of a specimen.

Dilatometric studies on alloys of zirconium with Nb,Ti,Hf,Y,In,Pb,Sb, and O have shown that above the β eutectoid temperature α stabilizing elements increase the TSS while β stabilizing elements decrease the TSS as compared to unalloyed zirconium. Below this eutectoid temperature (560°C) alloying elements have no significant effect on TSS (Erickson,64). However in the case where the β phase is present at room temperature, as in Zr-2.5%Nb alloy (Perovic,83) alloying elements may affect the TSS below the eutectoid temperature.

Variations in grain size are reported to have no effect on TSS and the effects of residual cold work are minor (Kearns,67).

A memory effect is also observed. When thermal cycling across the TSS takes place the hydrides will tend to dissolve and reform at the same locations. The Zr-2.5%Nb shows this memory effect, but only when the hydrogen concentration is below 46 ppm (Northwood,78a). In low hydrogen material the majority of the hydride in the as received condition is likely to be γ hydride, and after dissolution and quenching the γ hydride is again formed. On the other hand at higher hydrogen contents the original hydride is mainly the δ hydride. After resolution and reprecipitation the γ hydride forms but does not appear to precipitate at the original δ hydride sites (Northwood,78a)

In comparative tests Coleman and Ambler state that no difference in the TSS temperature was found between protium and protium-deuterium mixtures (Coleman,83). However, inspection of their data indicates that it may be possible to draw two separate TSS lines that cross-over at 230°C.

2.5 The Zirconium-Niobium System

The Zr-H system is complicated by the additions of Nb which acts as a β stabilizer. Figure 2.3 shows a section of the Zr-Nb phase diagram (Rogers,55).

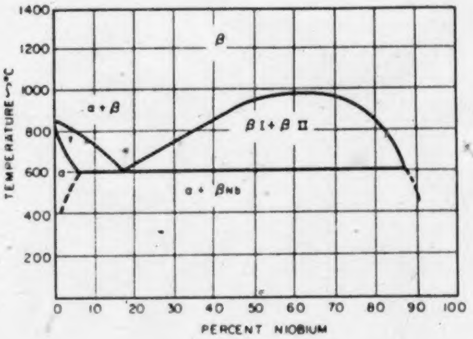

Figure 2.3 A section of the Zr-Nb phase diagram.

Extruded alloy components such as the Zr-2.5%Nb pressure tubes have an elongated grain structure and the microstructure contains approximately 10% of the retained β_{Zr} (≃20% Nb) (Perovic,83). The retained β_{Zr} phase is metastable below 610°C and decomposition reactions occur which result in the formation first of the ω phase and finally the β_{Nb} phase (≃85% Nb) (Hehemann,72).

It has been shown that hydrogen has a much higher rate of diffusion in the β phase then in the α phase, but no difference in diffusion rates has been detected between annealed and as-extruded Zr-2.5% Nb (Sawatzky,81).

The decomposition of the β phase has a profound effect on the precipitation of hydrogen. This has been shown by the observation of interphase hydride precipitation in samples where the β phase has not yet started to decompose. On decomposition of the retained β phase (to β_r and ω), hydride precipitation occurs as arrays of hydride plates in β between the ω phase particles (Perovic,84).

2.6 Properties of Zirconium Hydrides

The determination of many of the mechanical properties of zirconium hydride has proven to be very difficult. The major problems are the inherent brittleness of the hydride and the difficulty in obtaining relatively large crack-free test specimens (Mueller,68). However studies on the δ phase zirconium hydride have shown the fracture toughness to be ≃1 MPa$\sqrt{m}$ at 20°C perhaps rising to ≃3 MPa$\sqrt{m}$ at 300°C (Simpson,79a). These values are characteristic of a very brittle material. In comparison Zr-2.5%Nb samples oriented to show minimum toughness values display a fracture toughness of ≃40 MPa$\sqrt{m}$ at room temperature rising to values greater than 100 MPa$\sqrt{m}$ at 300°C (Coleman,85).

The Young's modulus of the δ zirconium hydride is $\approx 2/3$ of that of zirconium metal, but its thermal conductivity and expansion coefficient are higher. The thermal expansion coefficient of the hydride is ≈ 1.36 to 2.25 times that of the zirconium metal while the thermal conductivity is about 1.45 times that of the metal (Coleman,84a).

2.7 Concept of Hydride Cracking

If a notch is created in a sample normal to an applied tensile stress, the effective tensile stress at the notch tip is higher than at other regions in the sample. This effect of multiplying the applied stress in local regions of a material because of sample geometry is termed stress concentration. If the effects of load and stress concentration take a ductile material above its yield stress, a region of plastic deformation or a plastic zone will result at the tip of the notch, causing it to be blunted. A less ductile material undergoing the same load and notch configuration may respond by the formation of a running crack extending from the tip of the notch. The tendency to form a crack is a result of both the applied load and the geometry of the notched sample. A parameter, known as the stress intensity factor, K, depends on these two factors and is used to describe the magnitude of the stress state around the crack tip. Stress intensity usually has the units of $MPa\sqrt{m}$ and for the conditions of a tensile stress the notation K_I is used. Given the situation of a sharp crack of length a, in a large sample undergoing increasing load normal to the crack plane, the stress intensity factor, K_I, will increase until the crack begins to propagate. The critical stress intensity factor at which unstable crack propagation begins is called K_{IC}, and is a measure of the fracture toughness of the material. In the case of a sample undergoing hydride cracking the critical stress intensity is denoted as K_{IH}. The fact that K_{IH} is not equal to K_{IC} implies that hydride cracking represents a more involved process than just the instantaneous stretching of metal bonds at the tip of the notch.

A sample of zirconium metal that contains both hydrides and a stressed notch or crack has the prerequisites for hydride cracking. Hydrogen will dissolve from the hydrides in the matrix and migrate up the stress gradient to the vicinity of the notch tip where it again precipitates in the form of a hydride. Thus hydrides must be present both in the zirconium matrix and at the crack tip (Coleman,85). The re-precipitated hydrides continue to grow reducing the fracture toughness of the crack tip region to the point that the crack begins to move. It propagates rapidly through the hydrided region and arrests in the ductile matrix. The process is then repeated resulting in stepwise crack growth through the material (Puls,82).

2.8 Models of Crack Propagation

A generalized model for hydrogen embrittlement has been proposed by Westlake (1969) and several mathematical models appear in the literature specifically for the hydride cracking of zirconium (Cheadle,79, Dutton,78, Simpson,79b, Puls,82). The simplest of the crack velocity models is given by Cheadle and Coleman (1979):

$$V_c \propto D\ C\ \Delta\sigma_h$$

where:

V_c is crack velocity

D is diffusivity

C is terminal solid solubility

$\Delta\sigma_h$ is the stress gradient

In an attempt to compensate for other parameters affecting the diffusivity of hydrogen, this concept has been expanded (Puls,82, Dutton,77a) to a quantitative mathematical model where the cracking velocity, V_c, is equal to:

$$\frac{2\pi\Omega_{hyd}D_H C_H^S}{\Omega_{Zr}\Phi(\ell,L)\chi\tau} \exp\left[\bar{w}_t^{inc}/\chi RT\right]\left\{\exp\left[\bar{w}_t^{a}(L)/\chi RT\right]-\exp\left[w^{-a}_{t}(\ell)/\chi RT\right]\right\}$$

where:

Ω_{hyd} = the atomic volume of the hydride

x = the composition of the hydride phase, ZrH_x

D_H = the diffusion coefficient of hydrogen in α-Zr

C_H^S = the TSS at zero stress

Ω_{Zr} = the atomic volume of zirconium

$\Phi(L,\ell)$ = ln (L,ℓ)

L = the distance between the dissolving hydrides and the crack tip

ℓ = the distance between the precipitating hydride and the crack tip

τ = the thickness of the hydride

$\bar{w}_t^{inc}$ = total molal strain energy of matrix (Zr) and inclusion (hydride), which varies depending on whether the system is heated or cooled to test temperature

$\bar{w}_t^{a}$ = is the hydride molal interaction energy with an applied stress field

R and T are assumed to be the universal gas constant and the absolute temperature.

This model is based on the premise that the cracking rate is dependent on the diffusion of hydrogen to the precipitating hydride at the crack tip. It is assumed that the hydrides, some distance, L, away from the crack tip, dissolve and this atomic hydrogen diffuses to a distance, ℓ, from the crack tip where it precipitates. The major driving force for this diffusion is considered to arise from the stress gradient at the crack tip.

The predictions of the theoretical model have been compared to experimental data, assuming values for such constants as: L, ℓ, τ, χ, Ω_{hyd}, $\bar{w}_t^{inc}$, etc. Figure 2.4 shows how the predictions of the theoretical model compare with experimental data when the dependence of cracking velocity on stress intensity factors at different temperature is considered.

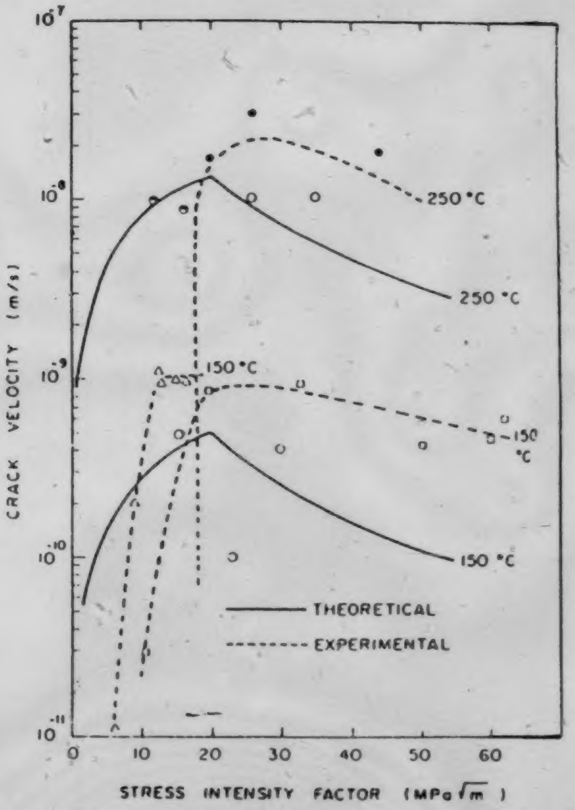

Figure 2.4 Crack velocity versus stress intensity factors (Dutton,77a, Puls,82).

In order to achieve the theoretical relationship in Figure 2.4, 2ℓ and τ were equated to the radius of the plastic zone and the crack-opening displacement, respectively. The radius of the plastic zone is given by: $K_I^2 / 6\pi\sigma_Y^2$, where σ_Y is the yield stress. Similarly one half of the crack opening displacement is given by $K_I^2 / \sigma_Y E$, where E is the Young's modulus (Dutton,77a).

2.9 Cracking Stages

The delayed hydride cracking process in Zr-2.5%Nb can be broken down into two or three divisions: an incubation time before cracking begins (Coleman,79), followed by one or two stages of crack propagation.

During the incubation period the hydrogen must first collect at the stress concentration, then a hydride must nucleate and grow until it reaches a critical size before it cracks (Coleman,79). It will be seen that the hydride precipitation and growth processes that take place according to this definition of incubation time also take place during crack propagation.

Stage I cracking is thought to occur at low stress intensities. In this configuration the plate-like hydride is assumed to be larger than the plastic zone. The tip of the hydride would then be exposed to the elastic field ahead of the crack tip. Since the driving force for diffusional growth of the hydride is the local hydrostatic stress at the hydride tip, the crack velocity during this stage of cracking would be dependent on K_I, the stress intensity factor (Dutton,77b).

During the stage II cracking, which occurs at higher stress intensities, the plastic zone is larger. The crack tip hydride is therefore assumed to grow within the plastic zone ahead of the crack. Thus the driving force for diffusion is relatively insensitive to K_I since increases in K_I will only serve to increase the plastic zone size rather than increase the tensile stress on the growing hydride. A negative dependence of K_I on cracking velocity is predicted based on the assumption that "the stress at $r=\ell$ remains fixed at $M\sigma y$, thus making the driving force for diffusion relatively insensitive to K_I, whereas the balance between the stress sensitivity of ℓ and ℓ' yields the overall negative K_I dependence of v" (Dutton,77a) ($M\sigma y$ = some value above the yield stress, v = crack velocity, ℓ' = effective crack tip radius, ℓ = distance between the precipitating hydride and the crack tip)

There is some experimental data indicating that stage II cracking commences only 1 or 2 $MPa\sqrt{m}$ above the stress intensity of the cracking threshold (K_{IH}). Between the cracking threshold and stage II cracking the crack velocity is very strongly dependent on K_I. Therefore Simpson and Puls (1979) suggest that stage I may not exist, leaving only the incubation time followed by one mode of cracking.

The stress intensity values given for the stages of cracking show considerable scatter. K_{IH}, the threshold stress intensity of hydride cracking given by Coleman and Ambler (1979), is apparently temperature dependent rising from ≃4.5 MPa$\sqrt{m}$ at 150°C to 10 MPa$\sqrt{m}$ at 260°C. Simpson and Puls (1979) give the K_I as ≃6 MPa$\sqrt{m}$ and the stage I to stage II transition as 7 to 8 MPa$\sqrt{m}$, with both values independent of temperature. It is also apparent that elimination of the stage I cracking would move the threshold value, K_{IH}, up or lower the onset of the stage II with respect to K_I.

2.10 Hydride Cracking Variables

The effects of stress intensity and the decomposition of the β phase on cracking behavior have been mentioned previously in sections 2.5 and 2.9. This section will describe the effects of other variables on hydride cracking.

2.10.1 Test Temperature

In cold worked Zr-2.5%Nb the delayed hydrogen crack growth rate increases with temperature when the specimens are cooled to the test temperature (Coleman,85). However the rate of delayed hydride cracking is not only affected by test temperature but it also depends on whether the test temperature was attained by heating from a lower temperature or cooling from a higher temperature. Ambler (1984) uses the parameter Tdat to characterize the effect of the direction of approach to temperature. Above the Tdat temperature, the cracking rate is reported to actually decrease if the test temperature is raised by heating from a lower temperature, while below Tdat the crack growth rates measured after heating to test temperature were similar to those measured after cooling to the same test temperature. Tdat has been found to depend on the rate of cooling and the amount of hydride precipitated during the cooling cycle prior to heating, but is typically ≈150°C (Ambler,84).

2.10.2 Hydrogen

Hydride precipitates are necessary for cracking to take place (Coleman,85). However once the TSS is exceeded the crack velocity and the time to failure are only slightly affected by the hydrogen content (Coleman,79). Studies using acoustic emission have also found the cracking rate to be insensitive to the amount of hydride present, in the range of 0.1 to about 3 weight percent hydride (Arora,81).

2.10.3 Thermal Cycles

When a specimen is cooled under load the hydrides can reorient so that the hydride plate is normal to the tensile stress (Cheadle,84). Work done on Zircaloy-2 has shown that as the number of temperature cycles is increased the number and size of reoriented hydrides also increases (Mishima,72). In Zr-2.5%Nb it has also been found that the degree of rearrangement of the hydride plates depends on: the stress, the temperature of stressing and the concentration of hydrogen in the material (Hardie,75). In the region near the crack tip it has been reported that a thermal cycle will also cause hydride reorientation (Simpson,77). It is suggested that reoriented hydrides as provided by thermal cycling may increase the cracking velocity and reduce the K_{IH}. However if all hydrides dissolve on heating, cracking may be postponed since the conditions for incubation may have to be reestablished (Coleman,79).

The cracking characteristics during a thermal cycle have also been studied. Results from these types of tests which involve crack growth during a thermal cycle in samples of Zr-2.5%Nb, have shown that most of the crack growth occurs during the cooling period, and that at high K_I values the crack velocity during cooling is dependent on the volume fraction of hydride precipitated during the cycle (Nuttall,77).

2.10.4 Grain Structure

In Zr-2.5%Nb tubing, cracks have been shown to grow faster in the axial direction than in the radial direction (Coleman,79). In the radial direction more grain boundaries per length of crack growth have to be crossed than is the case in the axial direction. The inference is thus made that the crossing of grain boundaries slows the cracking rate. This has been substantiated by time to failure tests in Zr-2.5%Nb where a material of smaller grain size took longer to fail than a material of larger grain size (Coleman,79).

2.11 Fractography

Most of the fractographic studies of hydride cracked Zr-2.5%Nb have taken place on regions of the surface corresponding to stage II crack propagation. Features known as striations have been observed running parallel to the thumbnail shaped crack front. Striations are described as a series of adjacent dimples, separated by thin ligaments (Simpson,77) and are reported to be bounded by distinct stretch zones separating the elongated fingers of brittle cleavage (Dutton,77b). The prominence of the striations varies from specimen to specimen (Simpson,80) and the conclusion has been reached by some workers that striations are a rather rare occurrence (Yuan,82). The spacing of striations is reported to be dependent on temperature, and is either essentially independent of K_I (Nuttall,79), or increases as K_I increases (Simpson,80). They are usually observed on fracture surfaces produced at test temperatures in the range of 150°C to 320°C (Nuttall,79). Increase in test temperature causes an increase in striation spacing which ranges from $\simeq$10 to 50 microns (Simpson,80). However the scatter is considerable, and a variation in the spacing size has been reported in the order of $\simeq$35 microns at 325°C (Nuttall,79).

The morphology of striations changes with stress and temperature. The size of the stretched regions within the striations increases with temperature and the size of the dimples within the striations increases with the stress intensity factor (Nuttall,79).

Striations are often grouped in growth bands which correspond to the number of thermal cycles (25°C-300°C) a cracking sample has undergone (Nuttall,77). Other subgroups may be differentiated, as the stretch marks of an individual striation are strongly dependent on K_I (Simpson,79b).

In terms of the fracture process it has been stated that each striation represents a period of crack arrest and is a manifestation of crack blunting (Dutton,77a). The striation spacing is reported to represent a critical length of hydride required to grow at the crack tip before rupture occurs (Nuttall,79). However crack initiation tests have shown that hydrides less than 20 microns in length do not crack (Coleman,77a) whereas striation spacings of less than 20 microns have been previously mentioned (Simpson,80).

2.12 Morphology of Hydrides Associated with Fracture

There appear to be various shapes, sizes and forms of hydrides associated with the hydride cracking process in Zr-2.5%Nb. Instead of attempting to differentiate these various morphologies with test conditions, it seems to be more productive to classify them according to laboratories in which the studies were carried out.

The AECL, Pinawa, Man. group depict the crack affiliated hydrides as being a series of clusters extending along the hydride crack. During isothermal testing at 325°C the striation spacing is reported to be ≈50 microns which corresponds to a cluster size of ≃60 microns (Dutton,77a). These clusters or clumps of hydrides become less distinct at higher values of K_I (Simpson,80).

The Metallurgical Sciences Laboratory at the University of Manitoba show regions of heavy hydriding along the crack front separated by regions where there is little or no hydride precipitation (Tangri,82). The reoriented hydride near the crack tip grows to a maximum size of about 270 microns in length, about 7 microns in width and about 2.5 microns in thickness (Yuan,82).

AECL Chalk River, Ontario show the hydride involved in the fracturing process to be somewhat carrot shaped, closely associated with the fracture (Coleman,77a,82). A variation on this is shown in the cracking of Zircaloy-2 in hydrogen gas (Coleman,84b). Here a large hydride (≃60 microns in thickness) at a crack tip is shown that appears to contain numerous small disjointed cracks.

2.13 Monitoring Hydride Cracking

An important feature of the hydride fracture is the occurrence of tunnelling. The thumbnail-shaped crack front clearly indicates that the maximum growth of the crack occurs in the midsection of the sample. This emphasizes the potential difficulties involved in obtaining crack velocity data from surface measurements (Simpson,77).

Initially the problems of surface observation were overcome to a certain extent by the use of heat tinting, that is, correlating the thermal history with the oxide bands visible on the fracture surface. By use of this technique an average crack velocity can be measured by calculating an area differentiated by the fracture surface oxide, and attributing the formation of this fracture area to a set of conditions that occurred over a specific time period (Simpson,77).

Other nondestructive tests are used to monitor hydride cracking. The increase in displacement (crack opening displacement), resistivity, and acoustic emission all indicate crack propagation (Coleman,77). The potential drop method (resistivity) utilizes the fact that as the crack grows the potential drop across the sample in the vicinity of the crack tip increases (Simpson,79b). The acoustic emission technique detects and counts the noise (acoustic emissions) within a certain frequency range that is emitted by the fracturing sample. In hydride cracking failure tests of zirconium alloys, all three parameters plotted against time have been shown to produce similar curves (Coleman,77).

2.14 Research Topic Selection

The range of unsolved problems suitable for research projects in the field of hydrogen delayed cracking is virtually unlimited. Even restricting the topic by selecting zirconium or one of its alloys as a host material still leaves a large number of variables that could have a significant effect on the hydride cracking mechanism. In order to standardize these metallurgical factors the Candu pressure tube material, Zr-2.5%Nb, was chosen for this research. This placed a stringent restriction on variables such as oxygen content, grain size, texture, and heat treatment while still retaining the possibility for the results to have a practical significance.

Acoustic emission was selected for monitoring the development of the hydride cracks in the pressure tube material. Justification for the use of this method arises from the numerous literature references (Ambler,77, Simpson,81, Tangri,77) that demonstrate its applicablity to the study of hydride cracking.

Having selected both a material and a method of investigation for this hydride cracking study it was necessary to consider the choice of test parameters. A comprehensive report on the delayed hydrogen cracking in Zr-2.5%Nb has been compiled by Coleman and Ambler (1979). In this report it was stated that, "Numerical evaluation of the temperature dependence of delayed hydrogen cracking is thus still unreliable." On this basis the experimental stages of this study began by monitoring the effects of test temperature on the acoustic emissions from samples of Zr-2.5%Nb undergoing hydride cracking at constant load. The scope of this study was later extended to include the effect of load changes on cracking behaviour.

3. Experimental

3.1 Introduction

The experimental procedure consisted of the production of a hydride crack and the monitoring of its progress under different test conditions. A Zr-2.5.%Nb alloy containing hydrogen was used as the host material for the hydride cracking while the variables in the testing conditions were limited to changes in load and temperature. The activity of the hydride crack was gauged by the sample's production of acoustic emissions. Visual characteristics of the hydride fracture were then determined by standard methods of microscopy and fractography.

3.2 Test Samples

Six test samples of Zr-2.5%Nb (by weight) containing either 92, 156, or 298 ppm of hydrogen were used in these experiments. They were prepared at CRNL, Chalk River, Ont. from flattened pressure tube material, 4 mm in thickness, into which hydrogen was charged prior to a 4 day anneal at 400°C. The hydrogen contents reported were calculated from the charging conditions; no subsequent hydrogen analyses were performed. These "constant K", or tapered double-cantilever beam specimens have profiles as shown in Figure 3.1. They had been machined to a shape (Mostovoy, 67) that provided a relatively linear correlation between the load and the compliance (1/slope of the load-deflection curve) over a given range of crack length. This allowed the crack to grow in the longitudinal direction (with respect to the original pressure tube) from a length of 5 to 15 mm at constant load without experiencing a significant change in K_I (Coleman,77b).

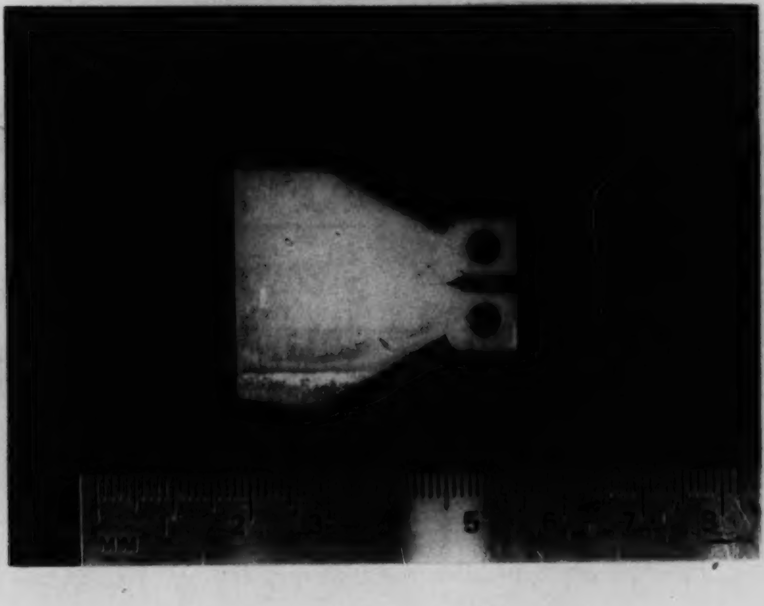

Figure 3.1 A constant K specimen.

3.3 Loading Arrangement

The load was applied to the samples by two forms of dead weight. In the initial stages of the experiments iron and lead weights were used. The weights were later superseded by a tank filled with water as shown in Figure 3.2. A sight glass was used to monitor the level of water in the tank. This level could be adjusted to provide a variation of load in the range of 29 to 182 kg.

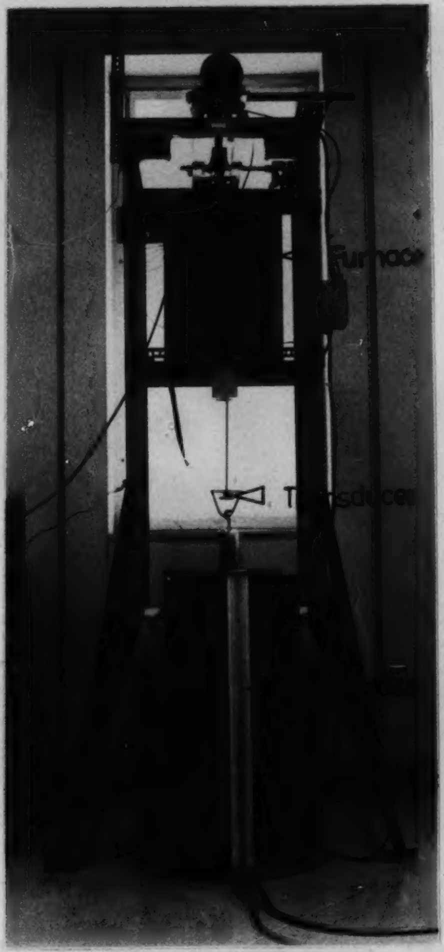

Figure 3.2 The load suspension system and some of the acoustic emission monitoring apparatus.

The suspension of the water tank began from a shaft supported by two pillow blocks as shown in Figure 3.3. The shaft was the center of motion for a drum and lever arm. Two parallel bands of steel formed the upper end of the load train that provided the mechanical link from the drum through the specimen to the weight (water tank). These bands were fastened to the drum in such a manner that a small rotation of the shaft caused the bands to wind on (or off) the drum, effecting a vertical displacement of the load train and weight.

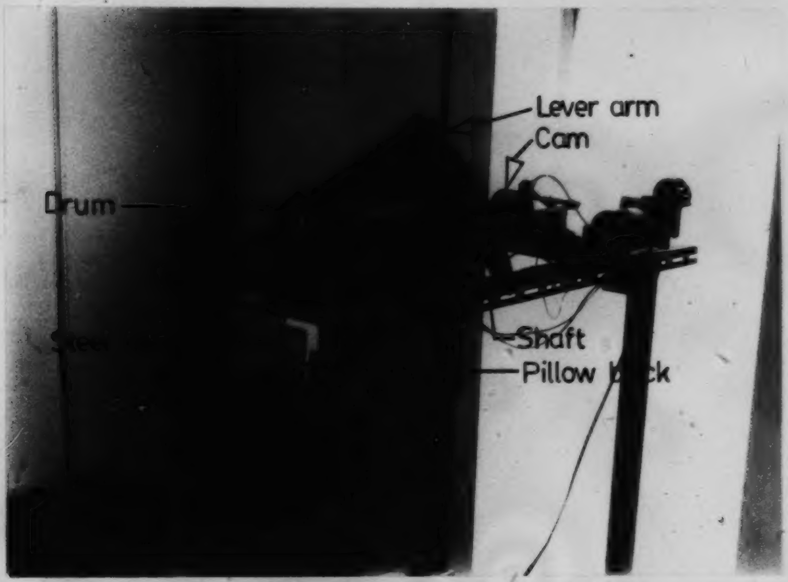

Figure 3.3 The mechanical loading system.

The rotational movement of the shaft was supplied by the action of a cam on the lever arm connected to the drum. The cam was turned by an electric motor that was controlled with a series of microswitches and a timer circuit in the furnace controller.

Ultimately in order to create a stress in the sample it had to be incorporated into the load train. For this purpose a fitting was used to connect the drum bands to a 4 mm steel rod. The sample was then connected to the lower end of this rod by a pin and clevis arrangement as shown in Figure 3.4. The rod length was selected in order to allow the sample to be positioned in the center of the furnace.

Figure 3.4 The constant K sample in the pin and clevis coupling.

Another rod ran from the lower sample clevis down to the transducer plate. A U-shaped rod welded onto this plate formed the final flexible link with the hook and bracket attached to the top of the water tank.

The loading of the sample was thus accomplished in two ways: first the motion of the cam and lever arm lifted the tank off the floor, and then the level of water could be varied while the tank was suspended above the floor. There were a number of advantages to this loading arrangement:

(1) The bands and drum at the top of the load train applied a purely vertical displacement to the load.

(2) The pin and clevis coupling eliminated the possibility of any large bending moment being applied to the sample.

(3) The hook and U-shaped rod allowed the tank to find its center of gravity when lifted without putting a bending moment on the rod.

(4) The tranducer was isolated from the furnace by the plate and a sufficient distance so that operation of the furnace would not significantly affect the operation of the transducer.

(5) The electric motor and timer permitted the loading of the sample to take place at any time, or alternately to have the loading coordinated with the furnace temperature programming.

(6) The dead weight gravity system of loading allowed a constant force to be applied to the sample accommodating any

minor changes in rod and sample length due to temperature and load changes.

(7) Changing the level of water in the tank allowed smooth adjustments in load to be applied to the sample.

3.4 Acoustic Emission Monitoring

Acoustic emissions were monitored with a Dunegan/Endevco acoustic emission apparatus, using a 0.1-0.3 MHz filter, a 40 dB preamplifier, and a model S9204 transducer. Total amplification was set at 87 dB. A two pen recorder was used to record temperature and acoustic emissions simultaneously on a single strip chart. Full scale on the recorder was set at 100,000 counts of acoustic emission; when full scale was reached an automatic reset to zero took place.

3.5 Temperature Control and Recording

The temperature of the sample was controlled by use of a Barber Coleman 570 furnace controller coupled with a vertical tube furnace. This system had the ability to consistently reproduce a multitude of temperature-time profiles. Two thermocouples were used to measure temperature. One was used with the controller to regulate the furnace temperature while the other was used in conjunction with the strip chart recorder and a digital panel meter to measure sample temperature.

3.6 Microscopic and Fractographic Techniques

Fracture surfaces were viewed with a low power binocular microscope and a scanning electron microscope.

The metallographic samples were prepared by either: grinding to a 600 grit finish, mechanical abrasion (as with a fine tooth file), or lapping with "Lapmaster 3400 compound" on a "Lapmaster 12" lapping machine. Following this, samples were prepared by hand using: 6,3,1, and 1/4 micron diamond paste. When required a mixture of 1.2 parts (by volume) hydrofluoric acid, 20 parts lactic acid, and 10 parts nitric acid was then used to etch the metallographic samples.

Examinations of metallographic samples were carried out using conventional optical microscopy, scanning electron microscopy, energy dispersive X-ray analysis, and microhardness techniques.

4. Results and Discussion

4.1 Acoustic emission monitoring

4.1.1 Introduction

The object of these experiments was to study the effect of temperature and stress on the hydride cracking of Zr-2.5%Nb. Much of this work involved monitoring of acoustic emission. The data from these experiments is contained on strip chart paper on which both the temperature profiles and corresponding acoustic activity are recorded as a function of time. In order to present some of this data in a manageable form, sections of the strip chart have been reproduced in photographs. When interpreting the photographs it is important to note that the temperature pen leads the acoustic emission pen by ≃2.5 of the small units on the strip chart paper or ≃30 minutes in time. Therefore in order to correlate the two events the temperature curve has to be displaced backward with respect to the chart direction, or forward with respect to time (i.e. to the left in the strip chart photographs). The acoustic emission line represents the cumulative, total counts of acoustic activity. Thus while the chart paper moves at a constant rate, the recorder pen is deflected across the paper, proportionately to the number of incoming acoustic counts, until full scale (100,000 counts) is reached. At this point the recorder pen resets to zero producing a nearly vertical line on the paper as the process continues. Thus the number of resets can be used in calculating the total acoustic counts and the spacing of the vertical lines gives an indication of count rate.

Since the connotation of a word often varies among individuals a few of the terms used throughout this section will now be defined.

"Dynamic" refers to a continual change, that is, not in a condition of steady state.

"Waxing and waning" refer to increasing and decreasing. For example, a temperature rise which starts at 30°C would be referred to as a waxing temperature of 30°C, while a temperature fall terminating at 30°C would be referred to as a waning temperature of 30°C.

"Steady state" means that the magnitude of the variables in the system do not change with time. An example of this would be a condition of constant stress intensity and temperature producing a crack propagating at constant velocity.

"Plateau" indicates a halt in progress. A temperature plateau corresponds to a period of time in which the temperature is constant.

"Temperature profile" is a number of programmed temperature changes occurring over a finite time.

"Test series" refers to a number of repetitions of the the same temperature profile.

Since the characteristics of a hydride crack propagating at a single test temperature (above ≈150°C) were quite different depending on whether this test temperature was approached from above or below, the concept of two modes of cracking has been introduced. The "fast cracking mode" refers to test conditions where the test temperature was approached from a temperature at least 30°C higher; conversely the "slow cracking mode" refers to test conditions where the test temperature was approached from a temperature at least 30°C lower.

4.1.2 Acoustic Emission Monitoring

In total over 15,500 hours of testing was carried out and recorded on strip chart paper. During the course of testing, especially after some change of design in the apparatus, a verification was made as to the source of the acoustic emissions. Figure 4.1 shows an early run where change of temperature was monitored with no load. This graph shows that over a period of 60 hours with ≈80 temperature changes approximately 5000 counts were picked up. This number of counts is insignificant when compared to the acoustic emission counts that were produced during hydride cracking.

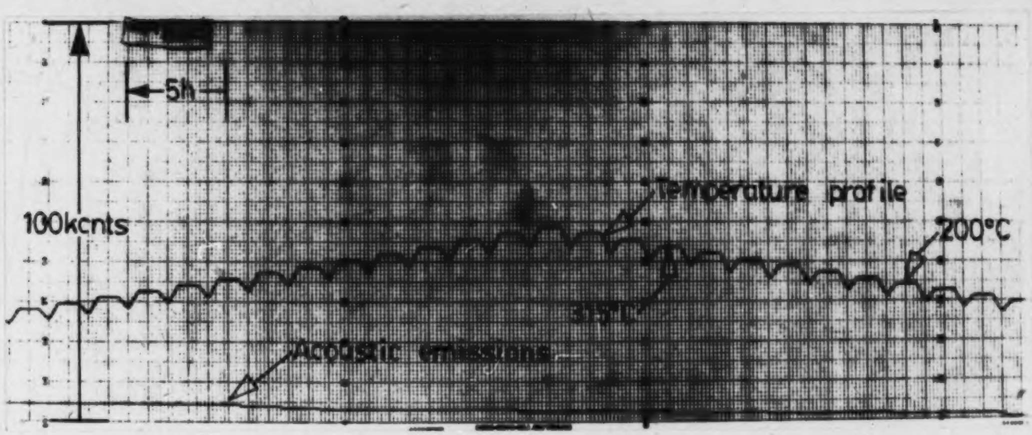

Figure 4.1 A noise calibration run.

In addition to these calibration runs a test was conducted using a fixed load of 130 kg on a steel sample instead of the normal Zr-2.5%Nb test sample. In the 55 hour duration with 28 temperature changes in the range of 90°C to 380°C about 3000 counts were measured. The counts measured in this case would represent the acoustic emission background of a loaded test sample.

After the water tank was installed to permit variable loads, emissions during test conditions were monitored during the filling and emptying of the tank. Initially it was found that some noise was generated if the water was quickly added or subtracted. To eliminate this noise, restrictive orifices were installed in the fill and return lines. These orifices allowed about 140 kg of water to be added to the dead weight in 18 minutes generating about 10,000 counts of acoustic emission. In view of the noise generated from the sample during cracking, this level of background during loading and unloading proved to be quite acceptable.

Overall the apparatus was acoustically quiet but sensitive to disturbances in the room caused by such factors as operation of a nearby impact tester, and the cleaning staff. In order to eliminate such disturbances they had to be identified. Since the chart recorder also acted as a clock, it proved to be a most valuable asset in this regard.

The transducer was coupled to the fracturing sample with approximately 550 mm of 4 mm steel rod. There was some concern that a significant proportion of the emissions generated by fracture were being absorbed in the steel rod. In order to assess this effect, a 0.5 mm pencil lead was broken on the rod at various points between the sample end and the transducer end of the rod. These tests showed that there was little, if any, attenuation along the length of the rod.

In terms of cracking area, "counts" can be conceptualized as a measuring stick with a variety of lengths, since a count is not a standardized unit of measure. However in this study the actual number of counts is not important in the interpretation of the results. It is also not mandatory that the constant of proportionality between the number of counts and cracking area remains independent of temperature and stress intensity, although such a relationship between number of counts and cracking area has been reported (Ambler,84). However there are two essential criteria that were fulfilled, and are important for this study. They are:

(1) A low ratio of background to acoustic emissions during cracking.

(2) A stipulation that changes in count rate resulting from variations in test conditions are detectable and reproducible in a qualitative sense.

4.1.3 Effect of Load and Temperature on Steady State Cracking

The boundary between dynamic and steady state cracking is somewhat arbitary as the acoustic emissions occur as a series of bursts. Even under conditions of constant load and temperature the acoustic emission rate continues to oscillate around an average value even after days of cracking. Thus the term steady state cracking rate refers to the most reasonable average value of counts per hour that occurred over a period of time.

In order to establish the ~~range of~~ temperature over which hydride cracking occurred the lower temperature boundary was investigated. However instead of reaching a boundary the cracking continued at an ever decreasing rate as the temperature was lowered, until the cracking rates became too low to be considered significant.

The upper temperature boundary was investigated by subjecting test samples to a temperature profile as shown in Figure 4.2.

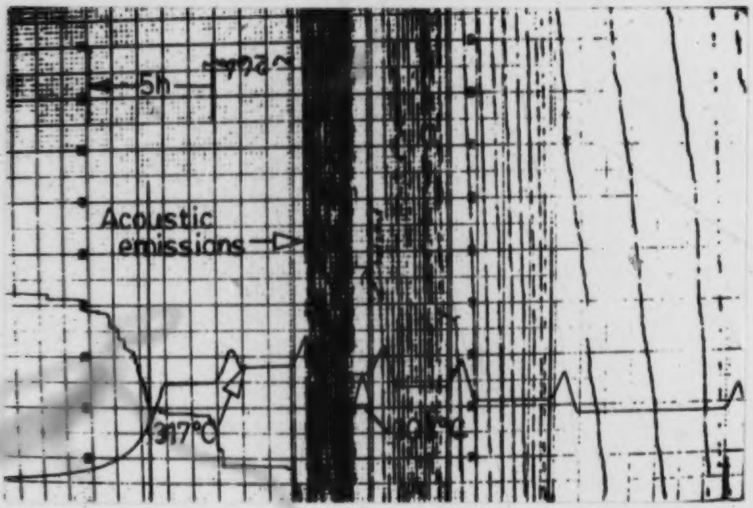

Figure 4.2 Acoustic emissions during hydride cracking of sample 1804-1, 92 ppm hydrogen.

This configuration allowed the highest rates of cracking to take place, that is, the fast cracking mode, since each progressive temperature plateau was approached from a temperature 60°C higher.

This series of tests showed an ever increasing acoustic emission rate with increases in test temperature until the emissions suddenly ceased during the 60°C rise on the first stage of the approach to the next higher temperature plateau. This caused a halt in crack growth that would return if the temperature was lowered, although a short initiation period was sometimes required. The temperature at which emissions ceased is termed the crack arrest temperature or Tcat. Approximate values of this temperature and the conditions under which it occurred are shown in Table 4.1.

Another effect which is perhaps best described as cracking remission was found to occur at temperatures above Tcat. This condition resulted at the end of each run as given in Table 4.1. Once cracking remission took place a long period of time was required at lower temperatures before cracking could be restarted. For example in order to restart the hydride cracking after run #4 (Table 4.1) was completed, a time period of 150 hours was required at 150 kg load while the test temperature was cycled between 157°C and 219°C.

TABLE 4.1 - CONDITIONS OF HYDRIDE CRACKING TERMINATION

Run	Test Sample	Hydrogen Content ppm	*TSS °C	Load kg	Tcat °C
1	1804-1	92	330	130	295 to 317
2	148-2	156	380	130	288 to 317
3	1804-4	92	330	130	328 to 358
4	1804-4	92	330	150	325 to 352
5	1804-4	92	330	100	280 to 315

* Approximate value from (Coleman, 78)

It was noted from the output of the strip chart paper that the process of cracking remission seemed to be a product of time and temperature. Therefore it is assumed that a specific time at a temperature at or above Tcat would be necessary in order for the cracking remission to occur.

A visual opening of the crack was also noted after cooling the sample under load when cracking remission had been achieved. This indicates extensive local plastic deformation which was not previously apparent in the sample. Microscopic examination showed a series of hydrides surrounding the crack tip as shown in Figure 4.3.

Figure 4.3 Crack tip hydrides in sample 1804-1, 10x.

The dark horizontal line at the center of the figure represents the hydrided crack. At the crack tip, reoriented hydrides are seen which would suggest a zone of plastic deformation ≈8 mm in height.

At first glance it may be inferred that cracking remission is simply the result of exceeding the TSS. From the standpoint of the bulk of the sample this idea would conflict with the terminal solid solubility data reported by Coleman (1978) and would also not agree with the apparent independence of cracking remission to the hydrogen content of the sample as shown in Table 4.1. However the question of whether or not TSS is exceeded at the crack tip could be debated at length, simply because the hydrogen concentration and the change of TSS with stress conditions are not known in this region.

The results of these first two series of tests have outlined the temperature borders of hydride cracking. At low temperatures hydride cracking proceeds at rates too low to be considered significant while at high temperatures hydride cracking is stopped by one or more of three effects:

(1) TSS is exceeded.

(2) Tcat is exceeded.

(3) A condition of crack remission occurs which involves: hydride reorientation, bulk plastic deformation of the sample, and a long incubation time before the hydride cracking restarts.

A certain amount of validation for the two limits of temperature for hydride cracking is provided in the literature. At low temperatures hydride cracking is shown to decrease with decreasing temperature (Ambler,84, Simpson,79b). At high temperatures, less than 325°C, Simpson and Nuttall (1977) report that it is more difficult to obtain slow crack growth. Room is also provided in the literature for Tcat and cracking remission by an absence of data on temperature vs. cracking rates at temperatures above 300°C, as for example in studies by Ambler (1984) and Simpson (1979b).

In another series of experiments incremental loads were applied between temperature change profiles, one of which is shown in Figure 4.4. These tests showed two distinct trends depending on whether the test temperature was approached from above or below. If the test temperature was approached from above the acoustic emission rates were generally higher and therefore the fracturing sample was said to be in the fast mode of cracking; conversely if the test temperature was approached from below the fracturing sample was said to be in the slow cracking mode.

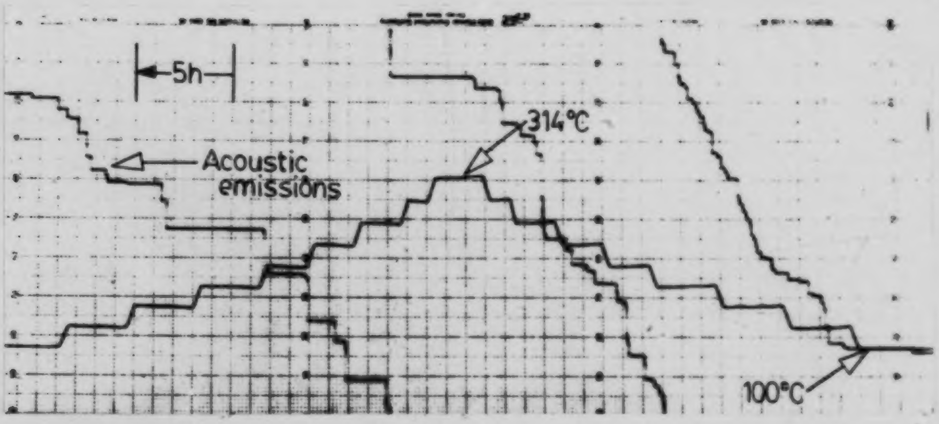

Figure 4.4 A typical time-temperature profile.

By observing the cracking rates that occurred on the temperature plateaus from each temperature profile, two sets of data were obtained. The plateaus that rise intermittently are representative of the slow cracking mode, conversely the plateaus cascading down are representive of the fast cracking mode. Load changes also took place after the completion of the temperature profile. Thus this series of tests showed the effect of load on cracking rates in both modes of cracking over a range of temperatures.

Graphs of the acoustic emission rate vs. temperature are given in Figure 4.5 and 4.6 for two samples in the slow cracking mode. Graphs that show two curves represent two sets of test data repeated under the same conditions. These figures do not show dramatic changes in the cracking rate vs. temperature relationship as load is added. The area under the count-temperature curve seems to increase with load to a maximum and then decline. There also appears to be a trend in the form of a shift in maximum count rate to higher temperatures as load is increased.

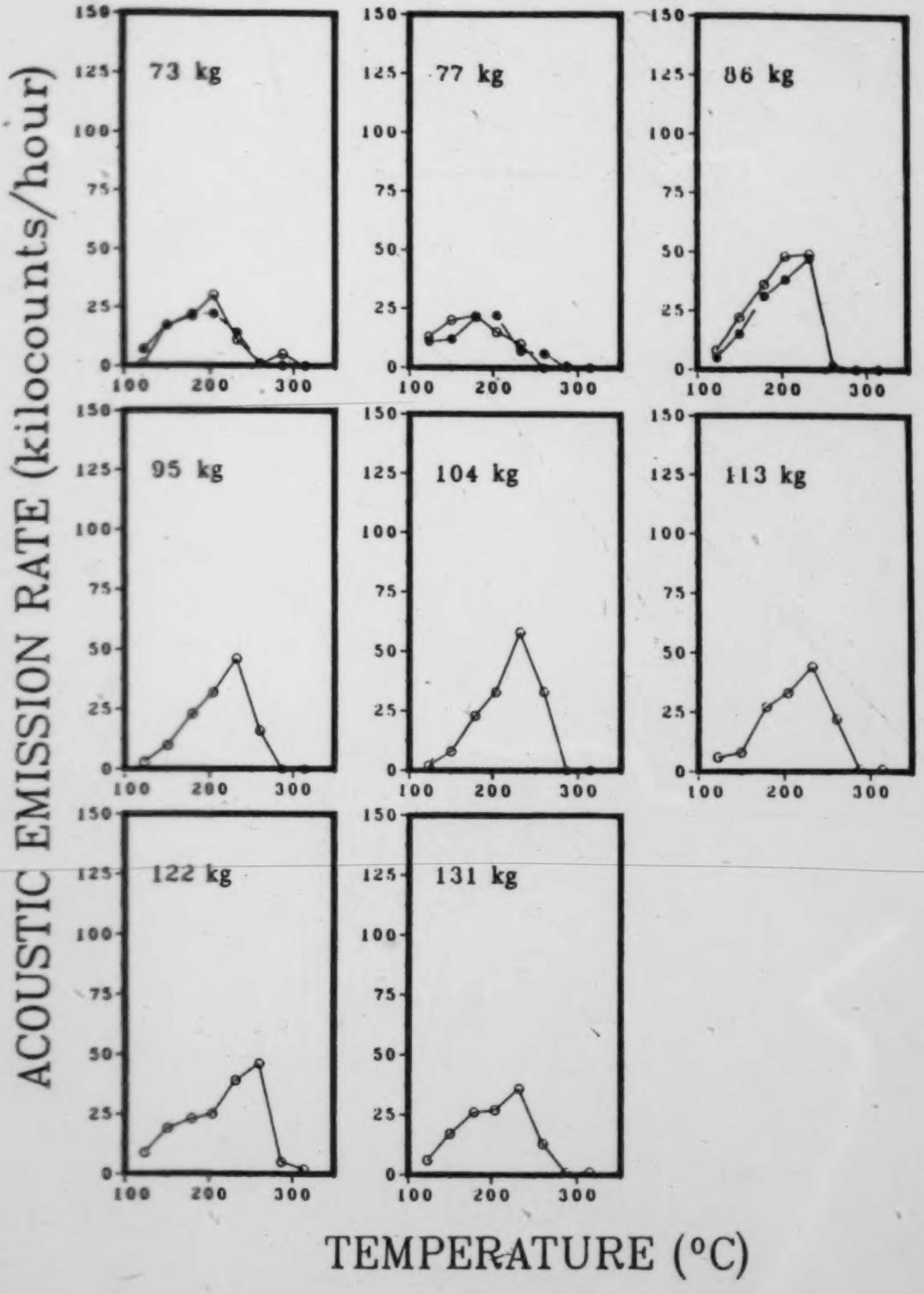

Figure 4.5 Acoustic emission rate vs. temperature, slow cracking mode, sample 148-1, 298 ppm hydrogen.

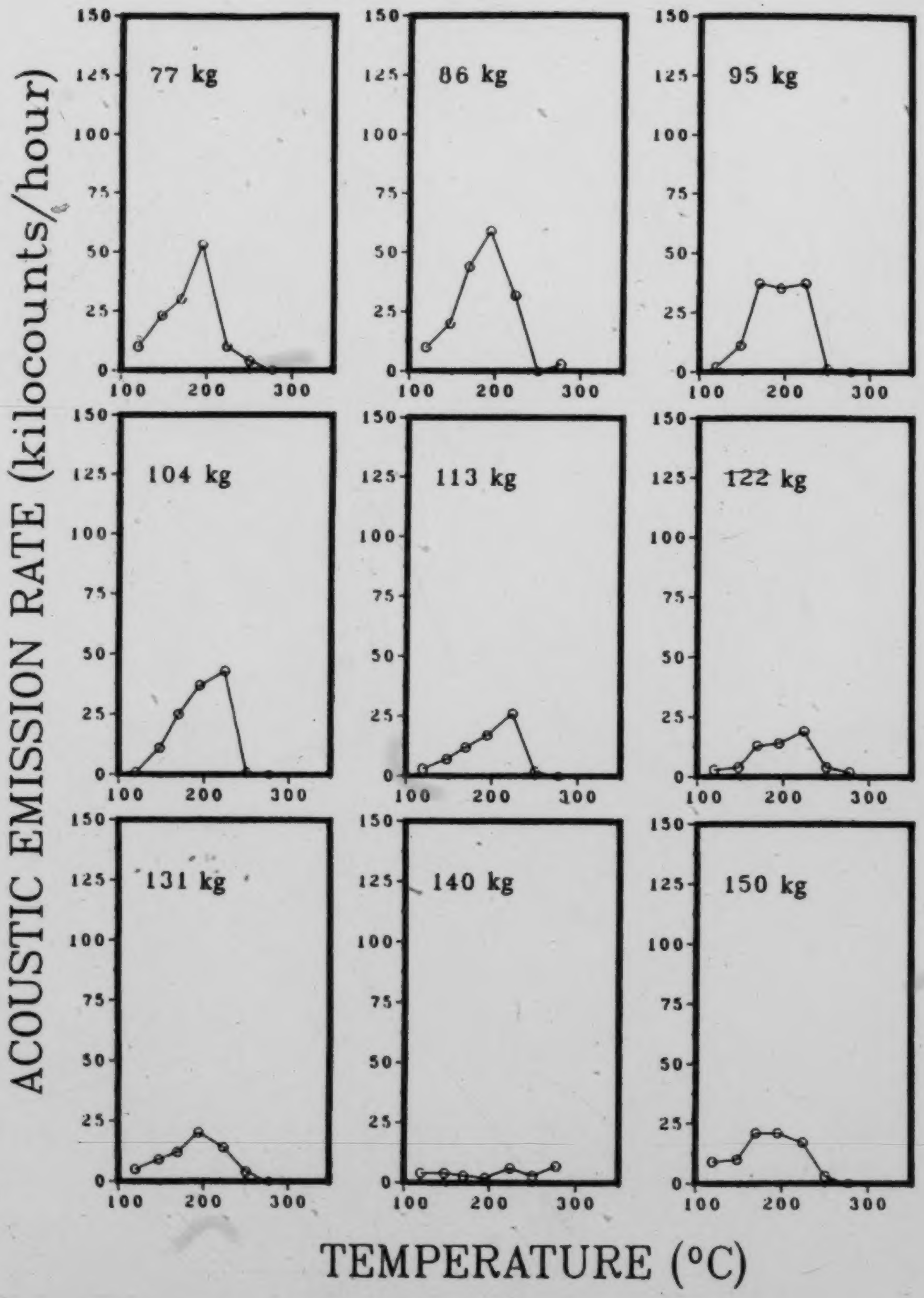

Figure 4.6 Acoustic emission rate vs. temperature, slow cracking mode, sample 1804-2, 92 ppm hydrogen.

The effect of load on acoustic emission was much more dramatic in the fast cracking mode, that is when the temperature was approached from above. Figure 4.7 and 4.8 show the effects of load during the fast cracking mode in the same layout as Figure 4.5 and 4.6 with the exception that the vertical axis extends to 800 kilocounts/hour instead of 150 kilocounts/hour.

The area under the acoustic emission rate vs. temperature curve is seen to increase with load to a maximum and then decline. The temperature that produces the highest acoustic emission rate increases with load to a maximum.

It is also apparent that more than just an increase in acoustic emission rates occurs when switching from the slow to the fast cracking mode. Comparison of Figures 4.4 through 4.8 shows that the temperature of maximum activity is higher in the fast cracking mode and also that Tcat occurs at a higher temperature. The shapes of the curves also appear to be somewhat different as the graphs of the slow cracking mode data appear more symmetrical than those of the fast cracking mode data.

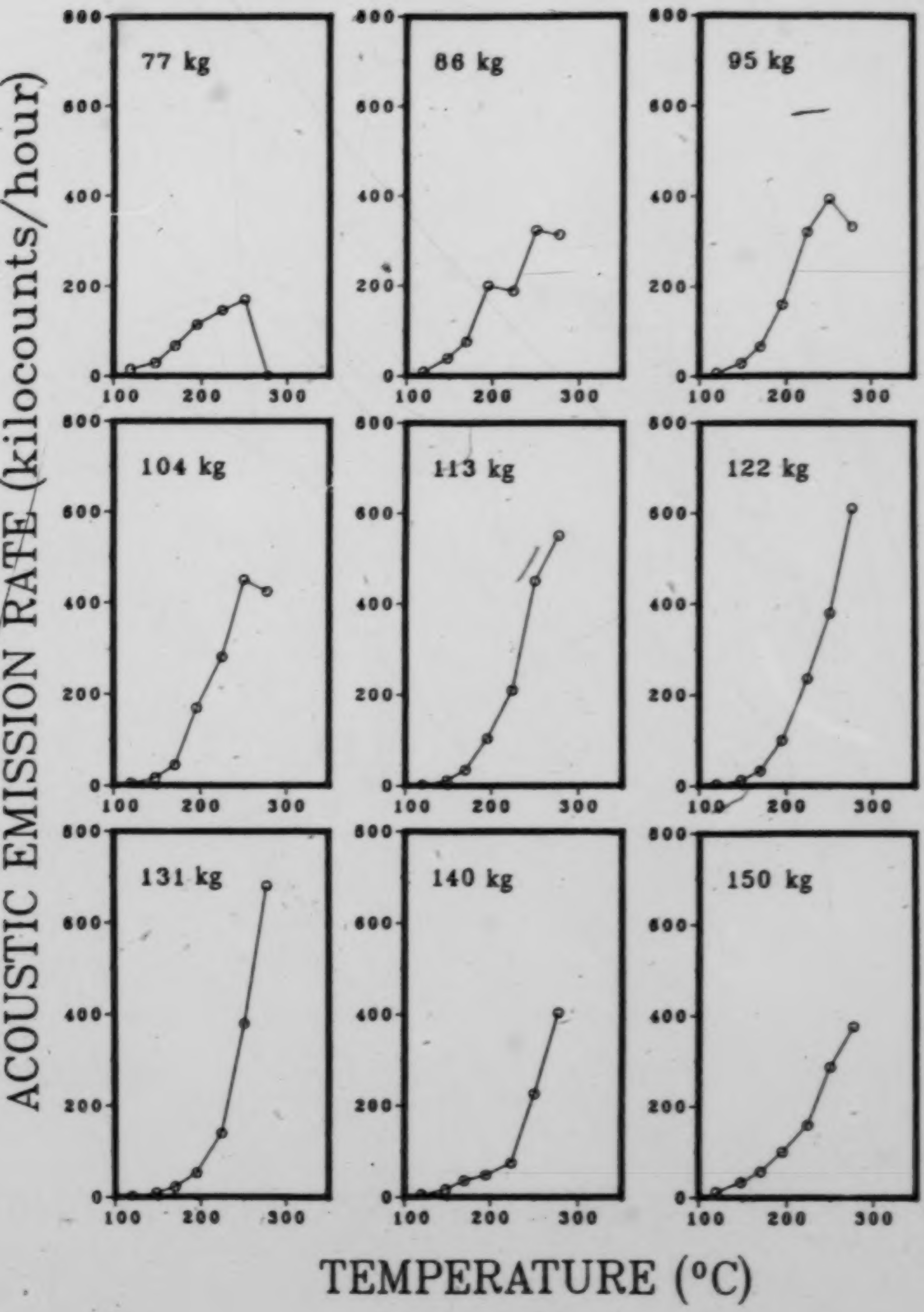

Figure 4.7 Acoustic emission rate vs. temperature, fast cracking mode, sample 1804-2, 92 ppm hydrogen.

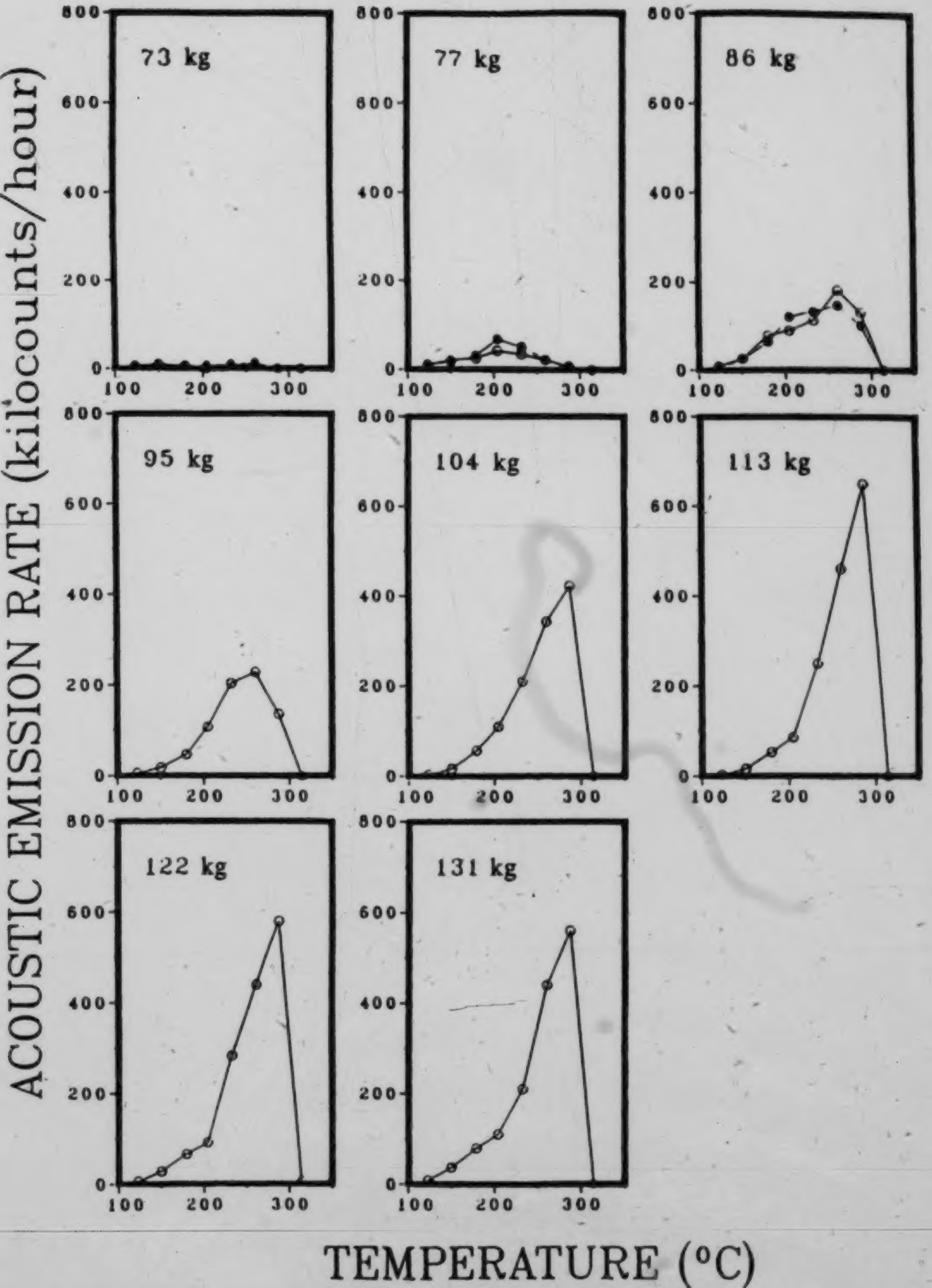

Figure 4.8 Acoustic emission rate vs. temperature, fast cracking mode, sample 148-1, 298 ppm hydrogen.

As the test temperature was lowered there was a point below which the two cracking modes seemed to produce acoustic emissions at similar rates. This temperature appeared to be load dependent, decreasing as the load increased. For sample 148-1 this temperature was: 180°C for 77 kg, 150°C for 95 kg, and 123°C for 131 kg. For sample 1804-2 the load dependence of this temperature was less marked, that is: 148°C for 77 kg, and 120°C for 140 kg.

This series of tests has demonstrated a substantial change in hydride cracking behavior in the different cracking modes. In the fast cracking mode it is apparent that at high loads the acoustic emissions drop off abruptly when the Tcat is approached. At lower loads and during conditions of the slow cracking mode, there is a more gradual decrease in acoustic activity as Tcat is approached. The limits of Tcat appear to be 260°C-300°C in the slow cracking mode and 290°C-314°C in the fast cracking mode.

4.2 Waxing and Waning Temperature Changes

In this section the effects of temperature changes will be considered from a dynamic point of view in terms of both immediate and long term effects. The immediate-effects represent changes in acoustic activity that transpired during a waxing or waning temperature. The long term effects represent changes in acoustic activity that take place after the temperature change. In this regard it was found that the effects of a waning or waxing temperature were dependent on:

(1) whether or not steady state conditions existed before the change.

(2) the range of temperature in which the testing was carried out.

(3) the cracking mode prior to the temperature change.

(4) the direction of the temperature progression.

To understand the effects of a changing temperature it is necessary to consider three cases of a waxing temperature and three cases of a waning temperature. To illustrate these six cases sections of the strip chart recorder paper have been reproduced in figures that contain the appropriate temperature sequences.

4.2.1 Waxing temperature

4.2.1.1 Post Slow Cracking Mode

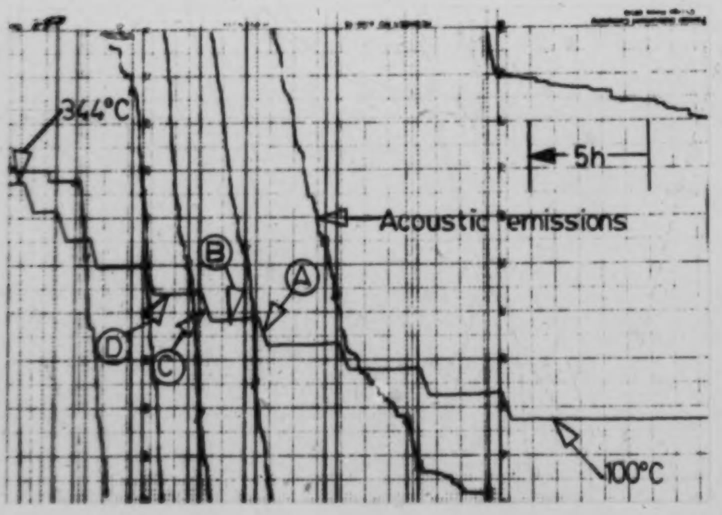

Figure 4.9 Rising temperature plateaus.

This case of waxing temperature refers to the situation after steady state conditions have prevailed in the slow cracking mode as shown in Figure 4.9. The temperature sequence represented in this case is: the rise in temperature (A) that establishes the slow cracking mode, the plateau (B) that ensures steady state conditions, the region (C) of waxing temperature, and the plateau (D) over which steady state is re-established.

In the lower range of temperature (below ≈150°C) the temperature rise (C) produces a burst of emissions in a cracking sample. As this sequence is transposed to higher temperatures, emissions during region (C) increase until a point is reached where further temperature increases cause a diminishing of emissions. This trend continues with increasing temperature until all emissions cease in the range of temperature around 300°C.

The effect of a waxing temperature on acoustic emissions has been plotted for different loads in Figure 4.10 and 4.11. The temperature on the horizontal scale refers to the starting temperature of the 30°C temperature rise. In cases where the test was repeated the appropriate graph contains two plots.

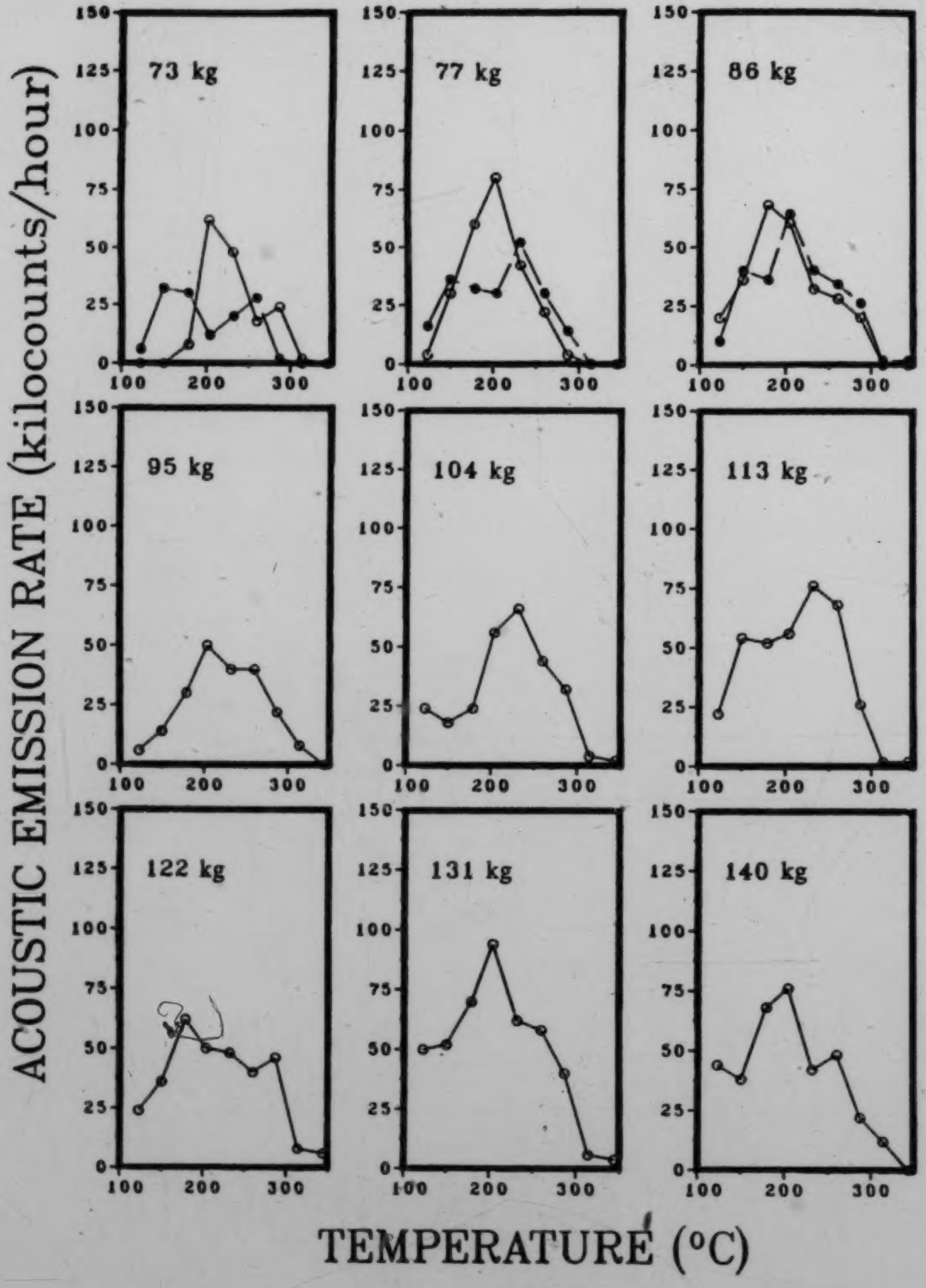

Figure 4.10 Acoustic emission rate vs. periods of waxing temperature, slow cracking mode, sample 148-1.

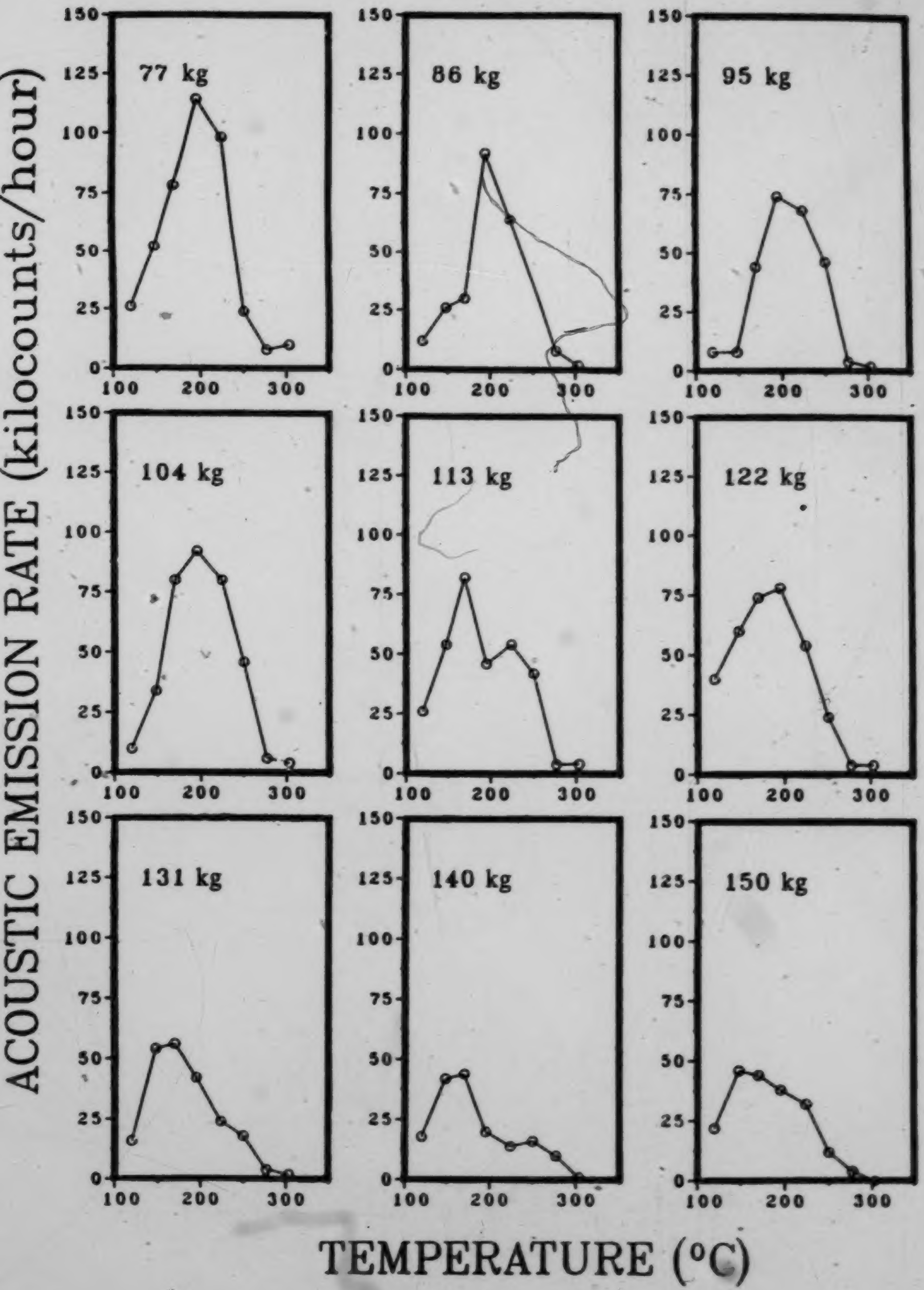

Figure 4.11 Acoustic emission rate vs. periods of waxing temperature, slow cracking mode, sample 1804-2.

4.2.1.2 After Temperature Fall

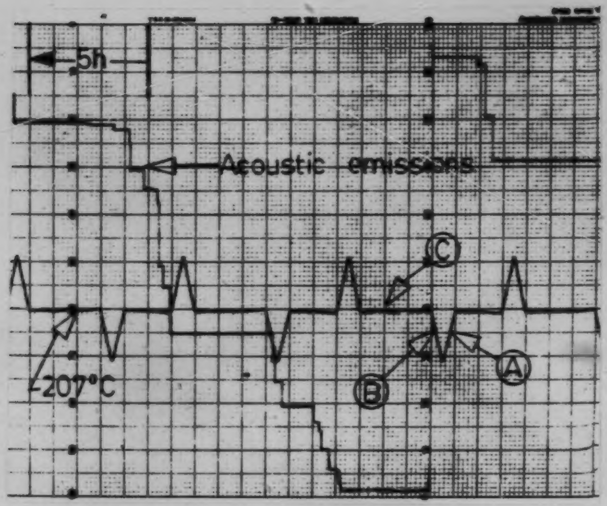

Figure 4.12 Temperature rise and fall.

This effect of a waxing temperature pertains to a case of dynamic conditions. The temperature sequence represented here is: a temperature fall (A), a waxing temperature (B), and a plateau (C) over which steady state is established.

At low temperatures (under ≈150°C) a waxing temperature (B) immediately after a fall (A) does not give a burst of emissions and has little effect on acoustic emission rate during the following plateau (C). If this sequence is transposed to higher temperatures, as shown in Figure 4.12, the waxing temperature will cause a reduction in acoustic emission rate if the fast cracking mode has been established immediately prior to the temperature fall.

4.2.1.3 Post Fast Cracking Mode

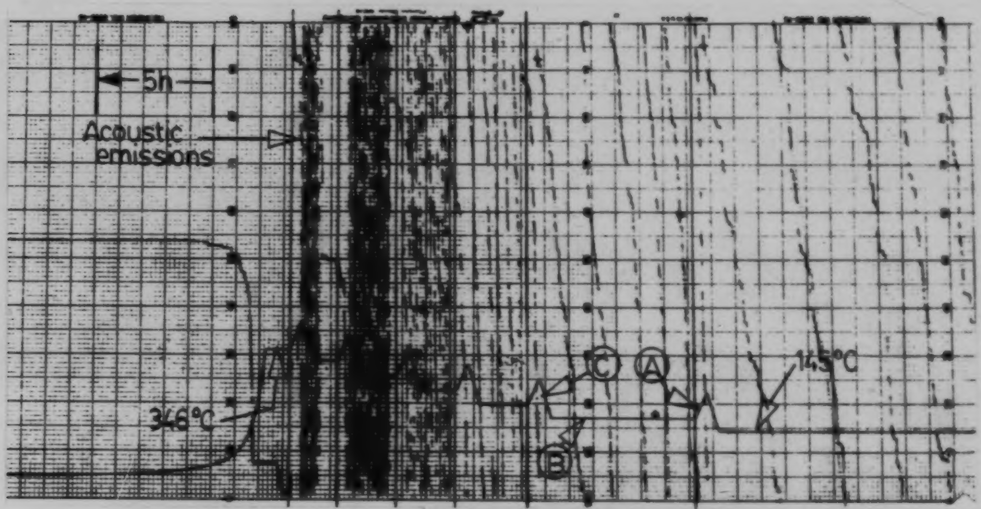

Figure 4.13 A waxing temperature in the fast cracking mode.

This case pertains to the situation where a temperature increase is imposed after steady state has been established in the fast cracking mode. The temperature sequence represented here is: a temperature fall (A) to establish the fast cracking mode, a temperature plateau (B) to establish steady state, and a waxing temperature (C).

In the lower temperature regions (below ≃150°C) a waxing temperature (C) as shown in Figure 4.13 produces a burst of emissions above the normal cracking rate. As this sequence is transposed to higher temperatures the difference between the acoustic emission rate during the waxing temperature (C) and the rate on the previous plateau (B) becomes less until no difference is noted. Finally transposing the sequence to still higher temperatures, a waxing temperature lowers the acoustic emission rate until all emissions stop at the crack arrest temperature, Tcat.

4.2.2 Temperature Fall

4.2.2.1 Post Fast Cracking Mode

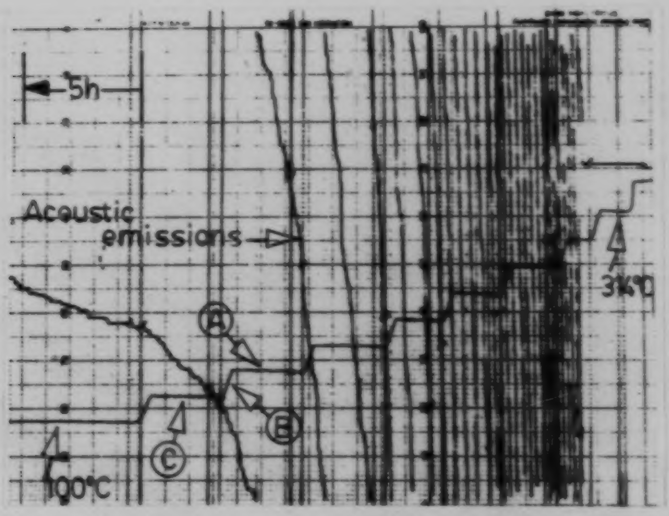

Figure 4.14 A waning temperature in the fast cracking mode.

This case of waning temperature pertains to the situation where steady state has been established in the fast cracking mode. The temperature sequence here is: a plateau (A) to establish the fast cracking mode, a waning temperature (B), and a plateau where steady state is again established.

At high temperatures there is a gradual decrease of emission on temperature fall as shown in Figure 4.14. However below ≃200°C, a decrease in temperature will cause a noticeable lull in emission rate. (i.e. the emission rate drops markedly for a time, then increases to a steady state value)

Figures 4.15 and 4.16 show the effect of load on the relationship between the acoustic emissions produced during a 30°C temperature wane and the temperature. The temperature scale at the bottom of the graphs refers to the final temperature of the change. For example, a temperature wane from 344°C to 314°C is represented by the point 314°C on the temperature scale. In cases where two plots are shown on the same graph the temperature profile was repeated twice at the same load.

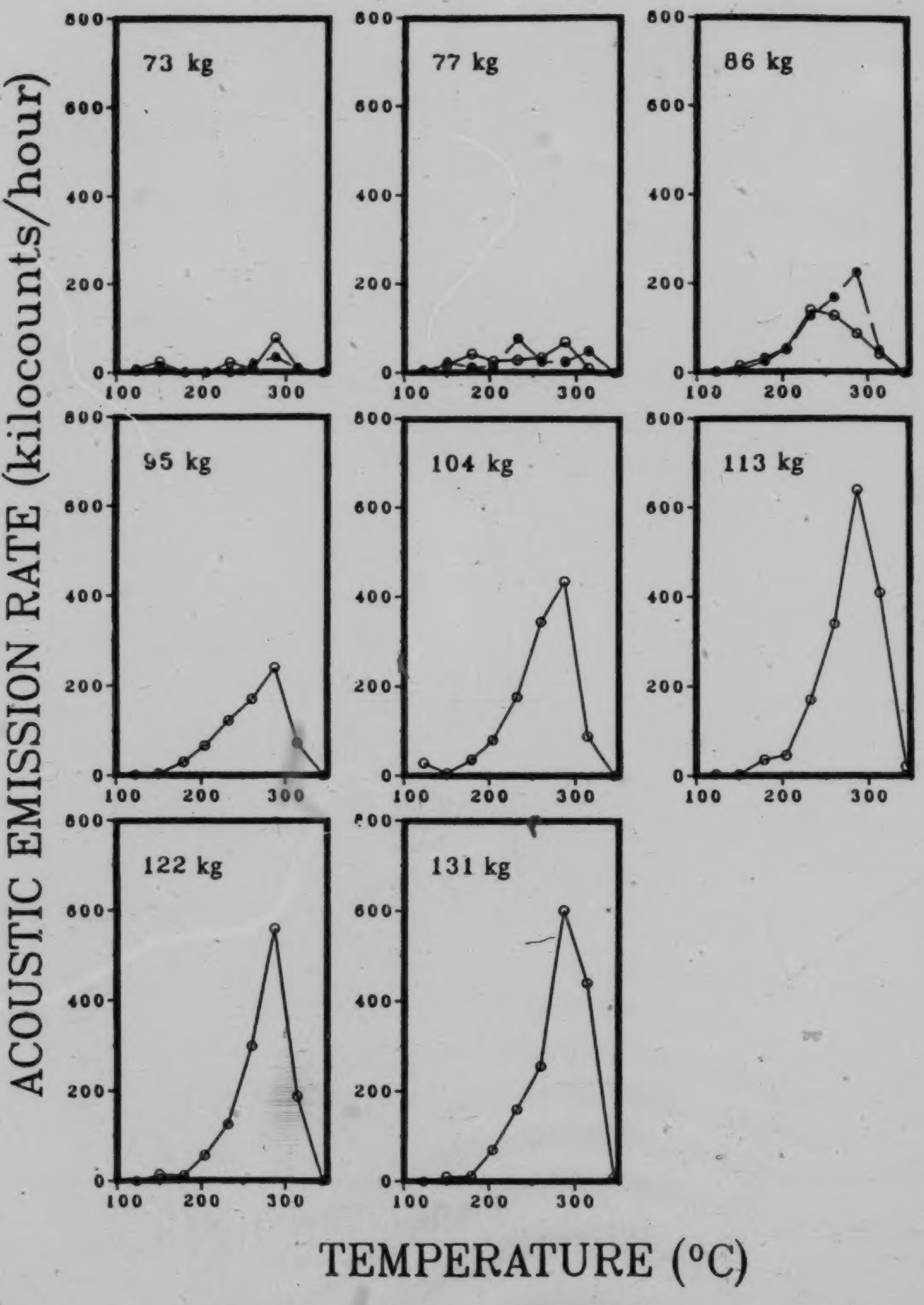

Figure 4.15 Acoustic emission rate vs. periods of waning temperature, fast cracking mode, sample 148-1.

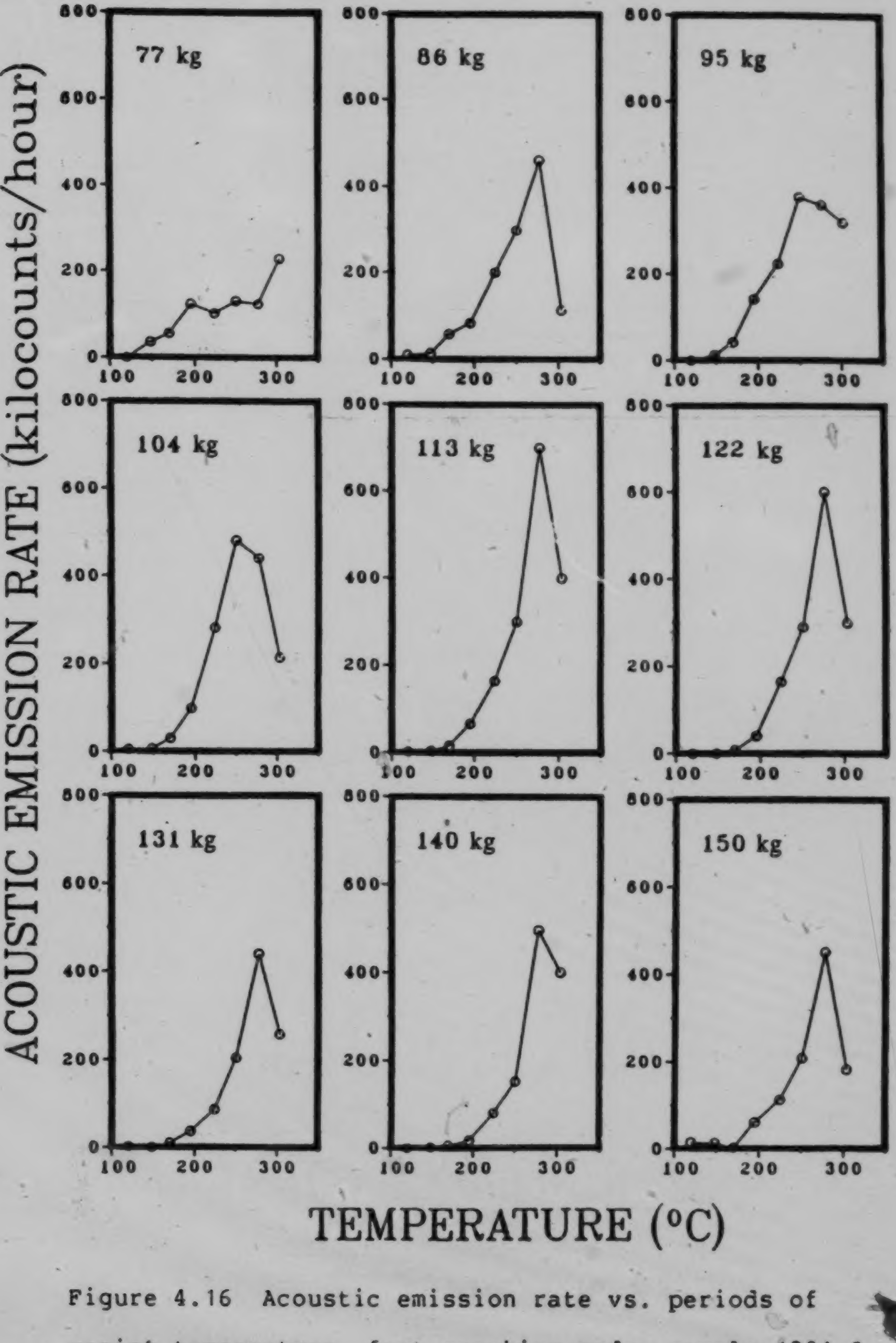

Figure 4.16 Acoustic emission rate vs. periods of waning temperature, fast cracking mode, sample 1804-2.

4.2.2.2 After Waxing Temperature

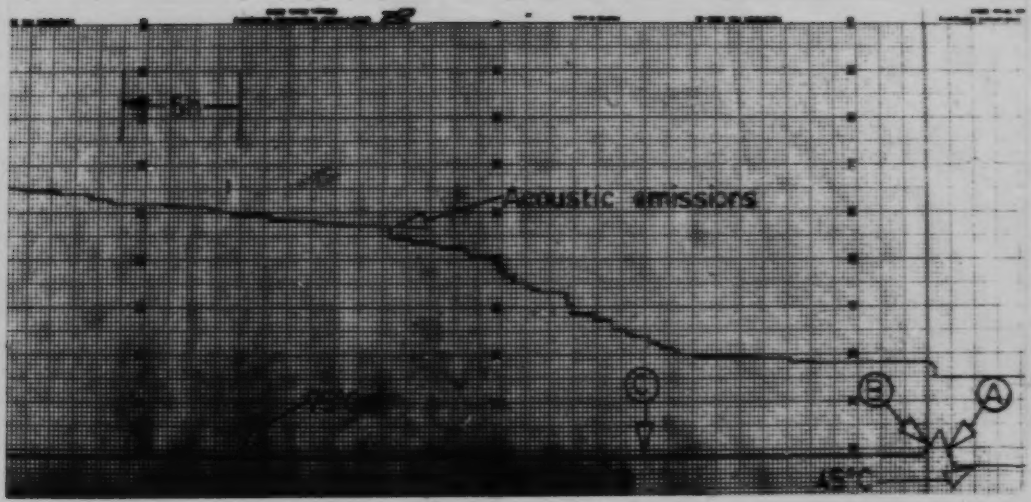

Figure 4.17 A waning temperature after a temperature rise.

This effect of waning temperature refers to a case of non-equilibrium conditions. The temperature sequence here is: a temperature rise (A), a waning temperature (B), and a plateau (C) over which steady state is established.

At high temperatures in the range of Tcat, a waning temperature as shown in Figure 4.17 will cause a lull or depression in acoustic emission rate. At midrange temperatures there appears to be little effect of a waning temperature. At lower temperatures as in the case of Figure 4.17, a cracking sample experiencing a waning temperature will again show a lull in the acoustic emission rate. Following this lull acoustic emissions occur at an accelerated rate before stabilization occurs. Above ≃150°C this temperature sequence causes a change in the cracking mode providing the slow cracking mode is in effect.

4.2.2.3 Post Slow Cracking Mode

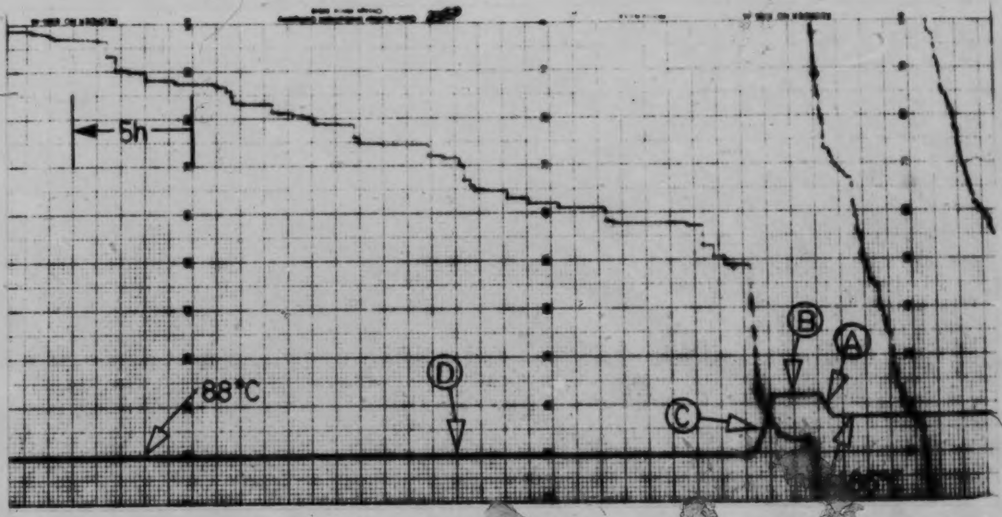

Figure 4.18 A waning temperatu[illegible]n the slow cracking mode.

This case of waning temperature refers to steady state conditions. The temperature sequence here is: a rise in temperature (A) to establish the slow cracking mode, the plateau (B) to establish steady state, a waning temperature (C), and the plateau (D) over which steady state is again established.

At lower temperatures, below ≈150°C, a waning temperature produces a lull in acoustic emissions. In the temperature range above ≈150°C a waning temperature as shown in Figure 4.18 causes increased cracking during the fall, as there is a tendency to change to the fast cracking mode. If the cracking has stopped as a result of exceeding the Tcat, a period of time is required on the fall before cracking begins. There may be an additional effect of waning temperature since Figure 4.18 gives a hint that an acceleration of emissions over the steady state conditions occurs during a waning temperature, and Figures 4.2 and 4.13 show that after cracking remission acoustic emissions will occur as the temperature falls.

4.2.3 Overall Effects of Waning and Waxing Temperature

In the sections above some of the long and short term effects on acoustic emission activity resulting from a waning and waxing temperature have been described. From the discussion on different modes of cracking in previous sections it is obvious that a thermal cycle of 30°C could have a long term effect on the rate of acoustic emissions. The dynamic temperature effects that could not have been predicted were the changes in acoustic emission rate which arose during a temperature change. The combination of these effects makes a determination of Tcat difficult. In addition it must be noted that a rising temperature can exhibit two opposing tendencies: the tendency for emissions to increase on the temperature rise, and the tendency for emissions to decrease as a result of a change in the cracking mode.

4.3 The Effect of Load on Hydride Cracking

4.3.1 Load vs. Stress Intensity

Care has been taken not to equate load with stress intensity. This is due to the fact that under constant load the stress state at the crack tip changes with time as a result of the migration of hydrogen and the formation of the hydrides. Therefore calculations of stress intensity which are based on the geometry of a simple fatigue cracked sample, as seen frequently in the literature, are incorrect when applied to hydride cracking. However in order to compare the dead weight load (kg) that was applied to constant K samples in this study, with the stress intensity factors given in other work, the relationship, $K_I = 0.132$ x load MPa$\sqrt{m}$, may be used (Coleman,77b).

4.3.2 Effect of a Waxing Load

A sample undergoing hydride cracking gives a burst of emissions during a load increase. In some cases load increases of 1 or 2 percent were sufficient to cause up to approximately 10,000 counts. Larger load increases were capable of increasing emissions up to at least 180,000 counts.

The acoustic emissions created by loading did not occur if the sample was unloaded and then immedately reloaded to the original value. However an extra burst of emissions occurred if this original load was exceeded or if the sample was left a period of time to crack at the lower load before reloading. In these circumstances, this accelerated emission rate continued for a time after the load was applied, but eventually the acoustic emission rate reached a steady state level. Some test results showing the effect of a waxing load are given in Tables 4.2 through 4.4 under the column "Immediate Effect".

4.3.3 Effect of a Waning Load

Reductions in load caused an immediate decrease in the rate of acoustic emissions. Emissions then continued at a low rate for a period of time before increasing to some stable value. Unloading sometimes caused cracking to stop completely, thus if cracking was to be monitored following a large decrease in load it was necessary to remove the load in stages. In some cases a cracking sample, subjected to a large unloading that caused crack stoppage for a period of time, had to be reloaded to a value higher than the value at which it had been originally cracking in order to restart the cracking. Some test results showing the effects of a waning load are given in Tables 4.2 through 4.4 in the column "Immediate Effect."

4.3.4 Effect of Prior Load on Acoustic Emissions

Monitoring the effect of load on the acoustic emission rate also revealed an effect of prior loading. Depending on the load history, different emission rates could be obtained at the same temperature and load. If a cracking sample experienced a load increase to reach a test load, the cracking rate would be higher than in the case in which the given test load was attained by reducing the load from a higher value. Some test results are presented in Tables 4.2 through 4.4 for both cracking modes.

4.3.5 Tables Showing the Effect of Loading

Tables 4.2 through 4.4 show the effect of loading on acoustic emission at three different temperatures. These tables show the results of a series of experiments involving smooth changes in load by use of the water tank as described in section 3.3.

The "Established Acoustic Emission Rate kcnt/h" indicates the rate of acoustic emissions given off by the sample before the load change. In places this column shows a "continue", indicating that the experiment was not finished and that additional load changes were carried out after various periods of time.

The "Load Change kg" specifies the sample load in kilograms before the load change and after the load change.

The "Immediate Effect" refers to the immediate change in acoustic activity, either in a burst of emissions or, alternatively, as a time required before some level of acoustic activity was achieved.

The "New Acoustic Emission Rate" refers to the newly established rate of acoustic emissions emitted by the cracking sample after the load change; "time held" refers to the time before the cracking sample went through another load change.

In the calculation of these tables at least 100,000 counts were allotted for the cracking rate to stabilize. If this criterion was not met the cracking rate is noted as an estimate only.

TABLE 4.2 - EFFECT OF LOAD CHANGE AT 119°C

Fast Cracking Mode　　Sample 1804-3

Established Acoustic Emission Rate	Load Change kg	Immediate Effect	New Acoustic Emission Rate
9.3 kcnts/h	170 to 136	Stop 14 h	7.6 kcnts/h
7.6 kcnts/h	136 to 104	Stop 13 h	5.3 kcnts/h
5.3 kcnts/h	104 to 73	Stop 52 h	1.1 kcnts/h
1.1 kcnts/h	73 to 104	105 kcnts	12.8 kcnts/h
12.8 kcnts/h	104 to 136	100 kcnts	18.9 kcnts/h

TABLE 4.3 - EFFECT OF LOAD CHANGE AT 140°C

Fast Cracking Mode   Sample 1804-3

Established Acoustic Emission Rate	Load Change kg	Immediate Effect	New Acoustic Emission Rate
14.0 kcnts/h	176 to 136	43.6 h to 100 kcnt	6.6 kcnts/h
6.6 kcnts/h	136 to 104	82.5 h to 100 kcnt	2.5 kcnts/h
2.5 kcnts/h	104 to 121	26 kcnts	6.8 kcnts/h
6.8 kcnts/h	121 to 136	62 kcnts	16.9 kcnts/h

TABLE 4.4 - EFFECT OF LOAD CHANGE AT 200°C

Fast Cracking Mode   Sample 1804-2

Established Acoustic Emission Rate	Load Change kg	Immediate Effect	Time Held or New Acoustic Emission Rate
7.1 (kcnts/h)	64 to 73	52 kcnts	< 0.1h
continue	73 to 64	Stop 2 h	10.1 (est.) kcnts/h
10.1 (est.) (kcnts/h)	64 to 73	42 kcnts	Hold 3.8 h
continue	73 to 64	Stop 15.5 h	9.5 kcnts/h
9.5 (kcnts/h)	64 to 91	103 kcnts	96.8 kcnts/h
96.8 (kcnts/h)	91 to 100	72 kcnts	0.1 h
continue	100 to 91	1.8 h to 100 kcnts	83.3 kcnts/h
83.3 (kcnts/h)	91 to 100	68 kcnts	0.2 h
continue	100 to 91	2.2 h to 100 kcnts	56.3 kcnts/h
56.3 (kcnts/h)	91 to 100	64 kcnts	75.0 kcnts/h
75.0 (kcnts/h)	100 to 91	5.2 h to 100 kcnts	52.6 kcnts/h
52.6 (kcnts/h)	91 to 64	110 h to 0.0 kcnts	0.0 kcnts/h
16.3 (kcnts/h)	64 to 91	180 kcnts	65.9 kcnts/h
65.9 (kcnts/h)	91 to 100	98 kcnts	< 0.1 h
continue	100 to 91	2.4 h to 100 kcnts	50.8 kcnts/h
50.8 (kcnts/h)	91 to 100	55 kcnts	0.4 h
continue	100 to 91	3.5 h to 100 kcnts	46.2 kcnts/h
46.2 (kcnts/h)	91 to 100	55 kcnts	57.1 kcnts/h
57.1 (kcnts/h)	100 to 91	4.7 h to 100 kcnts	29.6 kcnts/h
29.6 (kcnts/h)	91 to 82		< 0.1 h
continue	82 to 91		40.4 kcnts/h
40.4 (kcnts/h)	91 to 82	12.4 h to 100 kcnt	12.3 kcnts/h

4.3.6 Comparison of Load and Temperature Effects

It has been shown that a sample of Zr-2.5%Nb undergoing delayed hydride cracking is capable of producing acoustic emissions through a steady state process, and through a dynamic process. The steady state process would be one for which the amount of acoustic emissions is dependent only on time, and would be reached when all variables such as temperature, load, and cracking rate are constant. It is also possible by the manipulation of load or temperature to alter the acoustic emission rate of a cracking sample in a manner comparatively independent of time. This is referred to as a dynamic process.

In the case of hydride cracking there may be a whole range of cracking rates possible, that is, a variety of steady state conditions at the same load and temperature. It has been shown by approaching the test temperature from above (below) that a fast (slow) mode of cracking can result. In terms of the load parameter, if the test load is attained by loading from below, a faster rate of cracking occurs than if the test load is reached by unloading.

When obtaining two cracking rates by manipulation of load and temperature it is apparent that the two parameters have a different sense of direction. A test load achieved by a rising load produces fast cracking, and test temperatures achieved by rising temperature produce slow cracking. Alternatively, in terms of dynamic effects, increases in load or in temperature both produce an increase in acoustic emissions.

There were other differences between the load and temperature parameters in the way steady state conditions were approached. Changes in cracking mode appeared to stabilize quickly whereas changes in load drifted into steady state in a more asymptotic fashion.

The dynamic effects of load and temperature on hydride cracking have not been previously reported, whereas the present work has to a certain extent, validated the steady state effects reported in the literature. The two modes of cracking due to temperature are confirmed somewhat by Ambler (1984) in connection with his description of the Tdat temperature. In terms of the steady state changes due to load variations Coleman and Ambler (1979) reported that lowering the stress intensity results in delay times before hydrided cracking reappears. This has also been verified in the present work.

4.3.7 Effect of Load Changes on Cracking Modes

When the static and dynamic effects of load and temperature on acoustic emission were described above, it may have become obvious to the reader that the fast and slow cracking modes which result from different directions of approach to temperature could be simply explained in terms of load changes. In the literature section it was seen that hydride cracking deals with the fracture of hydrides and that the specific volume of the zirconium hydride is greater than that of the zirconium metal. In the last section it has been shown that a load increase to the test load will cause a faster rate of cracking than a load decrease to the test load, and that a Zr-2.5%Nb sample is very sensitive to load during steady state cracking, since small increases in load will produce a substantial amount of emissions. Further, it has been demonstrated that a waxing temperature will cause a burst of emissions. Thus, the logical hypothesis could be made that a rise in temperature causes a momentary local load surge, due to the expansion of the fractured hydride, which in turn causes a change from the fast cracking mode to the slow cracking mode.

A further investigation was made into this aspect of load variation. Figure 4.19 shows a photograph of the strip chart recorder paper used to monitor the temperature and acoustic emissions during part of this experiment. At a temperature of 207°C, sample #1804-3 (92 ppm hydrogen) was subjected to changes in cracking mode by ramping the temperature down to 157°C in a 30 minute time interval followed by a 30 minute ramp back to 207°C. After the cracking rate was established, the temperature was ramped to 257°C in 30 minutes. This was followed by a 30 minute fall to 207°C where steady state was again established. Prior to one of these downward spikes in temperature, the 178 kg weight was unloaded to 161 kg then reloaded to 178 kg after the spike. No difference in the steady state acoustic emission rate was detected by making the load change.

The test was repeated decreasing the level of water in the tank until a load of 91 kg was reached before reloading to 178 kg. This resulted again in no change in the slow cracking mode.

The test was repeated oppositely, that is, with an upward temperature spike just after a load drop to 161 kg. Following the temperature spike (test temperature again 207°C) the load was returned to 178 kg. The normal burst of emissions from the waxing temperature of the spike was not present, but there was no apparent change in the rate of the fast cracking mode after returning to the 178 kg load.

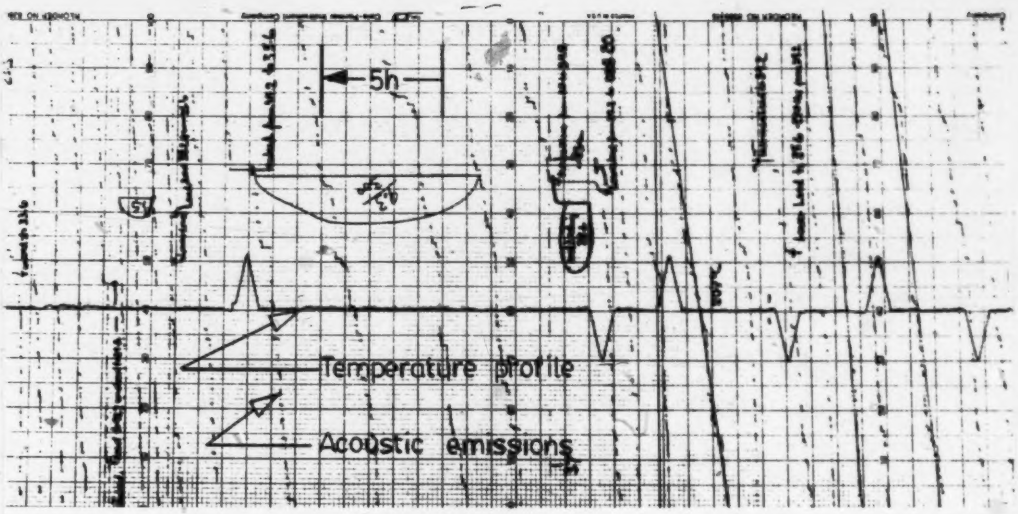

Figure 4.19 The temperature profile and acoustic emissions generated during part of a load variation experiment.

The results of this experiment indicate that the different cracking modes are not simply a result of prior load. It is also apparent that more information in terms of fractography and metallograpy would be helpful in combination with the acoustic emission data in attempting to explain the characteristics of hydride cracking.

4.4 Fractography

4.4.1 Optical Surface Features

In specimens 1804-2 and 148-1 hydride cracks were allowed to progress until the samples could no longer sustain the test load. The samples then deformed plastically until the weight came to rest on the floor. Since these were the sample specimens used to determine the acoustic emission rates vs. temperature at varying loads (section 4.1.3) their thermal, acoustic, and loading histories were known. The samples were each separated into halves to expose the surface features.

The final separation of the fracture surfaces was accomplished by making a shallow saw cut in the plane of fracture. This allowed the samples to be pulled apart by hand. The saw cut of sample 1804-2 is shown in Figure 4.21. However the saw cut was not visible in the fracture surface of sample 148-1, as shown in Figure 4.22. The fracture in sample 148-1 continued to propagate along its original plane rather than join the saw cut. The relationship between the facture surface and the saw cut of this sample is shown in Figure 4.20.

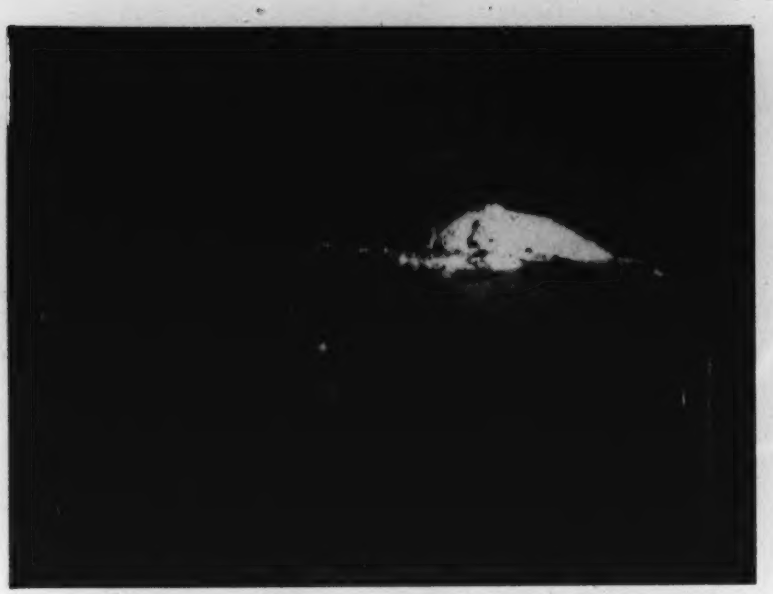

Figure 4.20 The fracture path in the region of a saw cut, sample 148-1, 6x.

The final separation of sample 148-1 is out of the ordinary. It would be expected that the fracture would join up with the saw cut instead of continuing to propagate in the original fracture plane. It is also totally unexpected that an individual would be able to rip an area of ≈18mm² of zirconium metal by hand. Since the area of the fracture surface created by the final fracture was shiny (not oxidized) it is clear that some form of damage or degradation to the metal can extend ahead of the crack front as defined by the oxide bands.

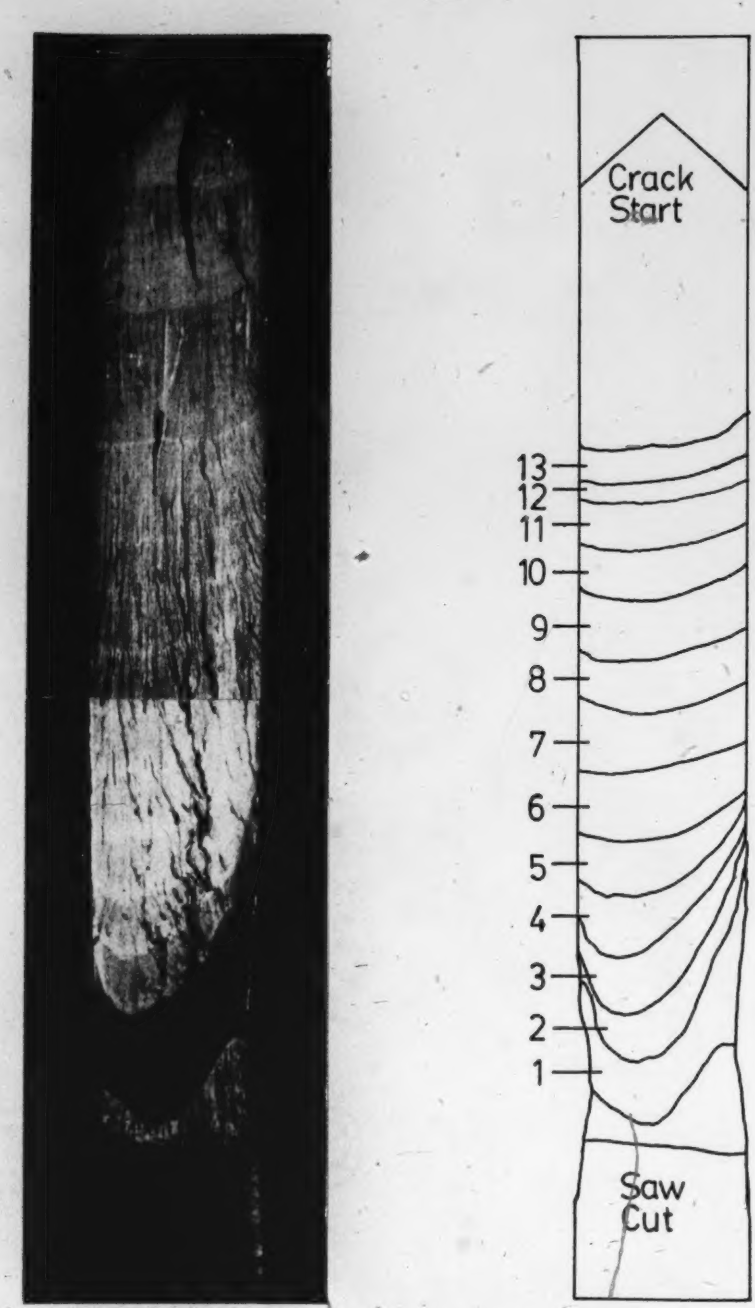
Crack Start
13
12
11
10
9
8
7
6
5
4
3
2
1
Saw Cut

Figure 4.21 The fracture surface of sample 1804-2, 92 ppm hydrogen, 6x.

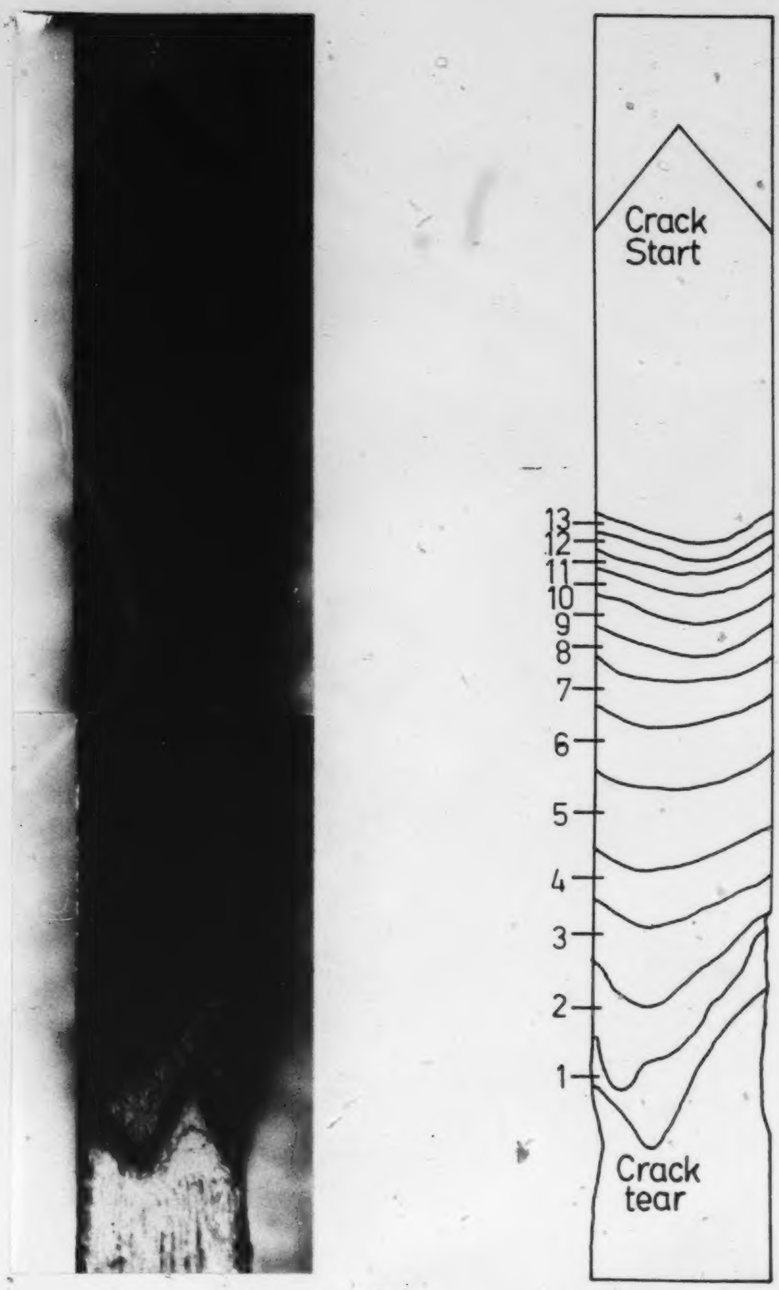
Crack Start
13
12
11
10
9
8
7
6
5
4
3
2
1
Crack tear

Figure 4.22 The fracture surface of sample 148-1, 298 ppm hydrogen, 6x.

Two features of the fracture surface were immediately visible to the naked eye: oxide bands, and texture markings. The oxide bands, which are especially prominent in the lower half of Figure 4.21, consisted of shaded bands about 0.3 mm in width, spaced at intervals in the range of 0.5 to 1.5 mm. These bands were found to be invisible in the scanning electron microscope and are therefore attributed to an oxide layer of varying thickness. Only a few texture markings were visible to the naked eye, but with the aid of the binocular microscope these markings appeared as a series of striations.

Striations, which were prominent on both fracture surfaces, are the vertical lines shown in Figure 4.23. Striation lines run approximately normal to the direction of fracture propagation. In the binocular microscope they appeared as narrow grooves scribed across the sample surface in a thumbnail pattern roughly parallel to one another. They were spaced at intervals varing from approximately 70 microns to less than 20 microns. At a magnification of 40x the striations shown in Figure 4.23 were found to be similar to those illustrated by Dutton (1978).

Figure 4.23 Striations (oriented vertically), sample 1804-2, 40x.

4.4.2 Surface Features in the Scanning Electron Microscope

The fracture surface features were observed in the scanning electron microscope. The surface oxide bands were not visible, but with some difficulty it was possible to locate and observe the striations. Figures 4.24 and 4.25 show fracture surface features and striations on sample 1804-2 (92 ppm hydrogen) which were visible in the scanning electron microscope at different magnifications.

40PM 25KV 02 011 S

Figure 4.24 Striations (oriented horizontally), 500x.

Figure 4.25 A striation line (shown with arrows), 1900x.

Scanning electron fractography has previously been conducted on surfaces resulting from the hydride cracking of Zr-2.5%Nb pressure tubing. The resulting appearance of the fracture surfaces has been described as "feathery platelets" (Ells,80). Electron microscope fractographs from these studies are similar in appearance to those illustrated in Figure 4.24 and 4.25.

Other workers (Dutton,77a) have reported brittle cleavage between the striations. Areas of cleavage were not apparent in samples 1804-2 and 148-1. It is possible that cleavage would have been visible in very small regions of the fracture surface if the higher resolving power of the transmission electron microscope had been used.

4.4.3 Acoustic Emission and Fractography

During the hydride cracking of samples 1804-2 and 148-1 acoustic emissions were monitored as a function of the varying loads and temperatures. It would be expected that some of the events related to changes in emission rate could be correlated with the fracture surface markings. To this end transparencies were placed over enlargments of Figures 4.22 and 4.23 and tracings made of each band or striation group. The areas outlined by the successive bands were then measured using a computerized digitizer board. The result of these area computations are listed in Tables 4.5 and 4.6.

It was also necessary to group the acoustic emissions according to variations in activity resulting from changes in the test parameters. During testing both samples had been subject to repeated temperature profiles such as shown in Figure 4.26.

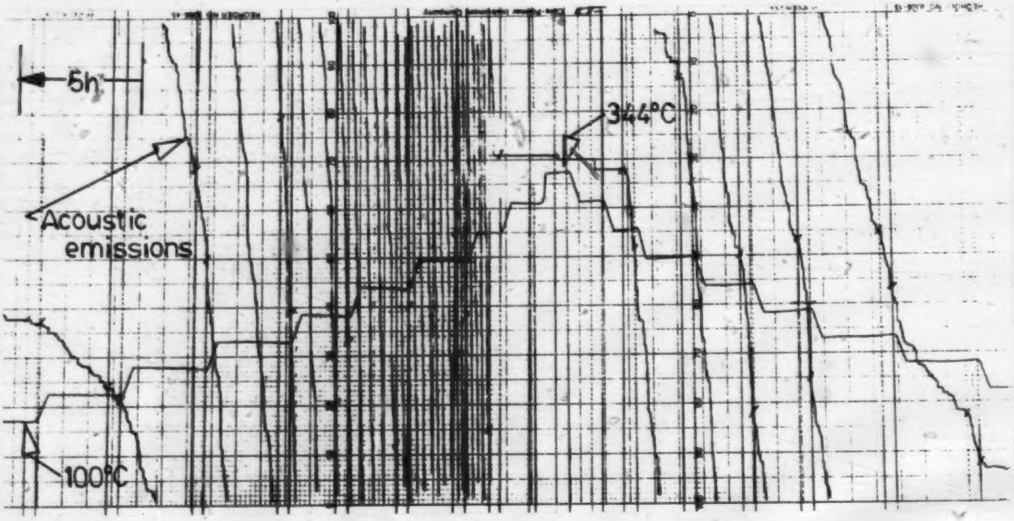

Figure 4.26 A temperature profile and acoustic emissions.

Periods of low acoustic activity were noted during both the low temperature periods and the high temperature periods of each profile. Load changes were imposed during periods of low temperature between the individual temperature profiles. This allowed the acoustic emissions to be grouped in four different ways, corresponding to the following four intervals:

(1) from a period of low activity to the next period of low activity.

(2) from minimum temperature to minimum temperature on one temperature profile.

(3) from peak temperature to the next peak temperature.

(4) from load change to load change.

Of the four methods of grouping the acoustic activity, number three (peak temperature to peak temperature) correlated best with the fracture surface markings. Therefore the emissions from the hydride cracking tests on samples 1804-2 and 148-1 have been divided into groups corresponding to the emissions detected from one to the next peak temperature. The total acoustic emission counts that occurred in these groups is listed in reverse chronological order in Tables 4.5 and 4.6, starting from the last test conducted on each sample in Tables 4.5 and 4.6.

TABLE 4.5 - COUNTS VERSUS FRACTURE AREA ON SAMPLE 1804-2

Region (as per Figure 4.21)	Area (mm^2)	Acoustic Activity (Mcnts)	Mcnts/mm^2	Mcnts/mm^2 (if region 1 disregarded)
1	7.9	3.25	0.41	
2	3.8	2.75	0.72	0.85
3	4.5	2.15	0.48	0.61
4	4.2	2.80	0.67	0.51
5	4.8	3.26	0.68	0.58
6	5.9	3.40	0.58	0.55
7	4.7	3.60	0.77	0.72
8	6.0	3.45	0.58	0.60
9	5.0	3.10	0.62	0.69
10	4.4	2.00	0.45	0.70
11	3.6	1.55	0.43	0.56
12	2.9	1.25	0.43	0.53
13	2.6			0.48

TABLE 4.6 - COUNTS VERSUS FRACTURE AREA ON SAMPLE 148-1

Region (as per Figure 4.22)	Area (mm^2)	Acoustic Activity (Mcnts)	Mcnts/mm^2	Mcnts/mm^2 (if region 1 disregarded)
1	4.2	1.10	0.26	0.26
2	4.2	3.80	0.90	0.70
3	5.4	3.50	0.65	0.50
4	7.0	3.80	0.54	0.97
5	3.9	3.10	0.80	0.56
6	5.5	2.20	0.40	0.47
7	4.7	2.90	0.62	0.63
8	4.6	2.05	0.45	0.68
9	3.0	0.90	0.30	0.41
10	2.2	0.85	0.39	0.47
11	1.8	0.42	0.23	0.28
12	1.5	0.48	0.32	0.48
13	1.0			

From a logical standpoint the fracture surface markings would be expected to correlate very well with acoustic activity generated during the course of the hydride fracture. It is reported in the literature that on a single sample, acoustic emissions produced from a hydride crack are directly proportional to the created fracture surface area, the constant of proportionality being independent of stress intensity and temperature (Ambler,84, Arora,81). Oxide bands have also been used to mark the progress of a hydride crack

(Simpson,77). Accordingly the number of kilocounts per unit area shown in Tables 4.5 and 4.6, should be a constant as it represents the acoustic emissions generated as the hydride crack propagates the distance from one oxide band to another, yet it shows considerable scatter. Furthermore the scatter of this parameter did not change significantly if the last area to fracture (region 1) was disregarded and all the groups of acoustic emissions were correlated to different areas on the fracture surface (last column Tables 4.5 and 4.6). Nor did regrouping the acoustic emissions according to the temperature profiles and correlating these groups with fracture surface features, make a significant change to the parameter.

Thus the conclusion is reached that although acoustic emissions represent cracking that occurs in the sample, perhaps even proportionally to the fracture area, it is not known where in the sample the fracturing originates. For example subsidiary cracking would result in the creation of fracture surface which would produce additional acoustic emissions, but would not contribute to a larger measured fracture surface area.

4.5 Metallography

4.5.1 As-Received Tubing

A section of Zr-2.5%Nb pressure tubing with an outside diameter of ≃110 mm and a wall thickness of ≃4 mm was obtained for metallographic examination. This tubing was manufactured to the same specifications as the Candu reactor pressure tubes and would normally be expected to contain ≃10 to 15 ppm hydrogen. Sections were removed from the tube in order to view three planes as referenced in Figure 4.27. These sections were then mounted, polished and etched for viewing in the optical microscope.

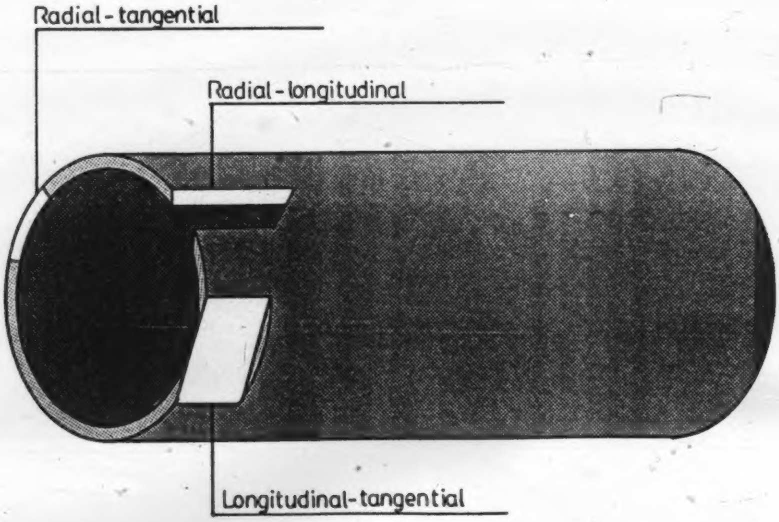
Radial-tangential
Radial-longitudinal
Longitudinal-tangential

Figure 4.27 The orientation of three planes in the pressure tube.

Figure 4.28 shows the microstructure of the radial-longitudinal plane in the pressure tube. This plane displays the most pronounced banding of all three orientations with the major grain elongation occurring in the longitudinal direction. These long narrow grains have the approximate dimensions of 0.3 by 40 microns.

← longitudinal →

Figure 4.28 The radial-longitudinal plane of a Zr-2.5%Nb tube, etched, 1400x.

Figure 4.29 shows the longitudinal-tangential plane. The microstructure has a wood grain appearance and the grain boundaries appear somewhat woolly. The grains are elongated in the longitudinal direction, but appear to have aspect ratios less than those observed in the radial-longitudinal plane.

← longitudinal →

Figure 4.29 The longitudinal-tangential plane, etched, 1400x.

The radial-tangential plane is shown in Figure 4.30. The grains are approximately 0.4 by 7 microns in size with the banding occurring in the tangential direction.

← tangential →

Figure 4.30 The radial-tangential plane, etched, 1400x.

The microstructure of the pressure tube consisted of two phases. The white colored phase in the above figures is representative of the α zirconium which is outlined by a network of retained β_{Zr} phase. Each individual grain of the α zirconium resembled a squashed sausage with the major axis generally parallel to the axis of the pipe while the minor axis showed some random deviation about the tangential direction. These results are similar to those from other metallographic studies (Yuan,82) completed on Zr-2.5%Nb pressure tube, with some differences noted in the estimation of the grain dimensions.

4.5.2 Hydride Orientation

Sample 1804-3 (92 ppm hydrogen) was sectioned to view three planes in the pressure tube as referenced in Figure 4.26. These sections were mounted and polished in order to ascertain the orientation and morphology of the zirconium hydride phase. The appearance of the radial-longitudinal plane is shown in Figure 4.31. The dark markings in the figure are hydrides elongated parallel to the longitudinal direction of the pressure tube.

← longitudinal →

Figure 4.31 The hydride orientation in the radial-longitudinal plane, unetched, 110x.

Figure 4.32 shows the hydrides in the longitudinal-tangential plane. Here it is seen that a small amount of elongation occurs in the longitudinal direction, but hydrides also appear as rounded wispy blotches without any discernible orientation.

← longitudinal →

Figure 4.32 The hydride orientation in the longitudinal-tangential plane, unetched, 110x.

The hydrides in the radial-tangential plane as shown in Figure 4.33 were oriented primarily in the tangential direction. A certain amount of deviation from this direction was noted along with a waviness in the hydride platelets. This feature is possibly related to the waviness in the grain structure which is also apparent in the radial-tangential plane shown at higher magnification in Figure 4.30

← tangential →

Figure 4.33 Hydrides in the radial-tangential direction, unetched, 110x.

4.5.3 Grain Structure and Hydrides

Figure 4.34 shows optical micrographs taken from the same region of a delayed hydride cracking specimen before and after etching. The hydrides in this orientation appear as worm like entities extending vertically from the region of the crack tip at the bottom of the micrographs. It can be seen that the original grain structure has been maintained in the hydrided region, and that each of the hydrides encompasses more than one grain.

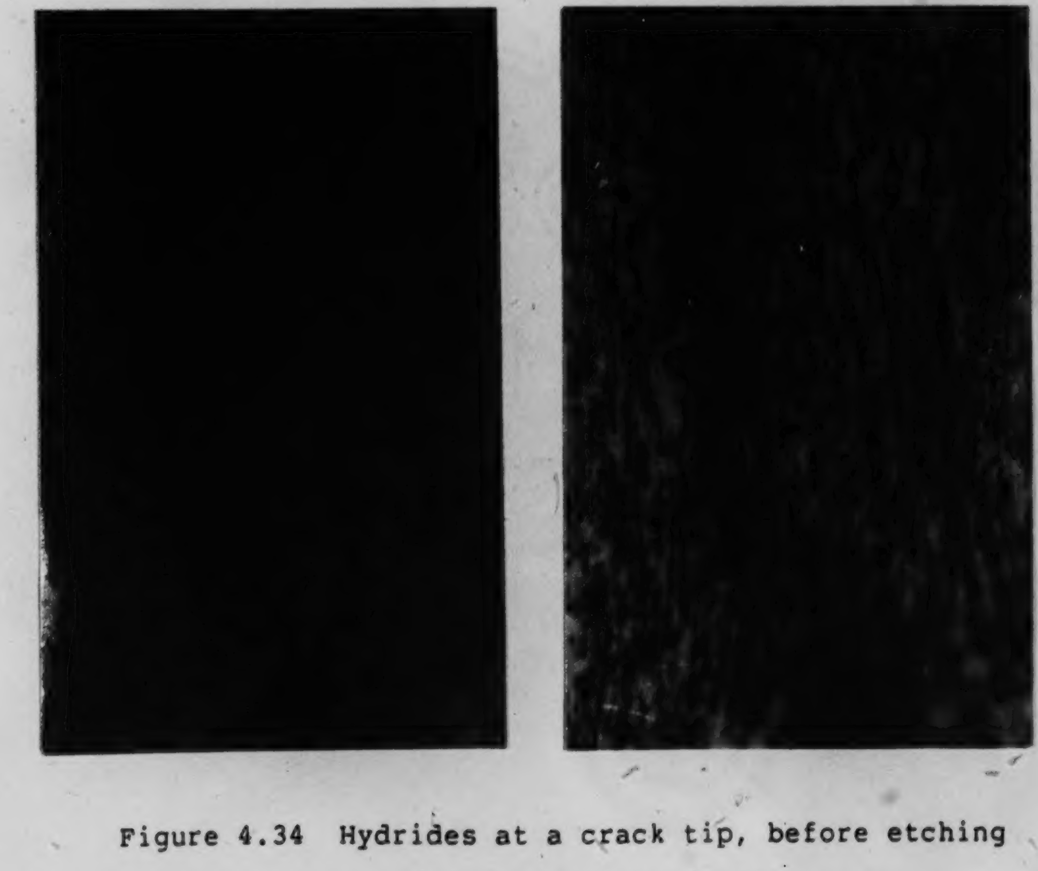

Figure 4.34 Hydrides at a crack tip, before etching (left), and after etching (right), 1400x.

As Figure 4.34 shows, the hydrides are difficult to identify at high magnification in the optical microscope, especially after the specimen surface has been etched. The hydrides appear slightly darker on the etched sample, but the boundaries of the hydrides are masked by the appearance of the retained β phase that also marks the α grain boundaries. Therefore for optical microscopy, in order to differentiate hydrides from the background, the best method of sample preparation was found to be light pressure hand polishing to 1/4 micron diamond paste. This provided some surface relief on the sample surface in which hydrides were slightly pronounced. This appeared as contrast in the light optical microscope.

4.5.4 Microhardness

The difficulty in identifying hydrides with the optical microscope led to the use of other techniques to differentiate the hydrides from the matrix. In this vein a microhardness tester was employed using a 15 gram load on a diamond pyramid indentor for a 5 second duration to ascertain the hardness values of the microstructural components. At these low loads the hydrides gave the appearance of being slightly harder than the base metal as Figure 4.35 shows.

Figure 4.35 Hardness indents of 15 grams on the Zr-2.5%Nb matrix containing a hydride, 1400x.

The computation of 20 hardness values confirmed that the hydrides were slightly harder than the matrix material. The hydrides had an average Vickers hardness of 233 while the average hardness values for the 10 hardness tests conducted on the matrix was 213. These results compare favorably with those reported by Mueller et al. (1968).

4.6 Artifacts in the Metallographic Preparation of Fractures

A metallographic sample prepared for viewing with the optical microscope is subject to damage and modification during preparation. Fine cracks are especially troublesome as they can be approximately the same size as the abrasive polishing compound and are often too small to allow infiltration by the mounting material. This allows at least three types of artifacts to exist when specimens containing fine cracks are prepared for metallographic examination. One type of artifact occurs when the polishing compound is wedged into the open crack. With the advent of the energy dispersive analysis on the scanning electron microscope, this is often the easiest to distinguish. A quick qualitative analysis will identify grinding components such as silicon (from silicon carbide), magnesium (from magnesium oxide), etc. leaving diamond to be determined by other means. The other two types of artifacts that occur during polishing are more difficult to recognize and evaluate; these being the filling-in of the crack and the widening of the crack.

A diamond stylus scratched across a crack will pull a small amount of ductile material into the opening. If just enough polishing is done afterwards to remove the scratch, a small jetty of material will extend beyond the regular crack surface. This is an artifact in that it was not present before scratching the surface and would serve to fill-in or narrow the crack opening. It is therefore a basic requirement that each polishing step must remove all the material disturbed by the prior polishing. However, there is nothing to support the edges of the crack and thus they are especially susceptible to degradation and removal. In the case of hydride cracking, the hydride is very brittle and is often found at the edge of the cracks. It is therefore extremely prone to fracturing and degradation during the polishing procedures which would serve to widen or enlarge the crack opening.

The innate brittleness of the hydride phase allows the possiblity of another type of artifact, that is, the creation of a crack. A small very brittle phase might well be coherent in plane strain but sectioning the sample changes the stress state. This factor combined with the stresses applied in cutting, grinding and polishing, could cause the inclusions to fracture.

It is therefore apparent that a certain amount of deliberation is required, both in preparation and interpretation of a fracture in a metallographic sample.

4.6.1 Fracture Path

For this study the hydride cracks in the samples were propagated in the radial-longitudinal plane, in the longitudinal direction as referenced to the original pressure tube as shown in Figure 4.27. When viewed in the longitudinal-tangential plane the metallographic features associated with the hydride fracture showed a high degree of diversification. Therefore the fracture, which is the progression of one or more cracks, is characterized in terms of four zones.

The first zone occurs near the crack root, that is the region associated with the tip of the crack. Here, as Figure 4.36 shows, the wispy crack-like entity is barely discernible in the optical microscope. This micrograph is not sharp simply because the dimensions of the fracture cause the features to fade in the twilight zone that marks the limit of the resolving power of light optics. An estimation of the crack opening in this region without an applied load is something less than 3000 Å.

Figure 4.36 The root of the hydride crack polished to show hydrides (above) and polished flat (below), 2000x.

The cracks of zone one become increasingly visible as they are followed away from the crack root. The fracture appears to be made up of a series of small cracks and may also show major branching. Hydrides are generally associated with the the fracture.

Etching the fracture surface created more contrast between the crack and the background once the opening of the cracks reached a certain size. The etched surface also demonstrated that the fracture propagated both transgranularly and intergranularly as shown in Figure 4.37.

Figure 4.37 The intergranular and transgranular components of the fracture path, 1400x.

Zone two is characterized by a coarse phase that has the appearance of an oxide and is associated with the wispy crack of zone one. Figure 4.38 shows the interface of the wispy cracks of zone 1 on the right and dark coarse phase of zone 2 on the left.

Figure 4.38 The interface of zone 1 and zone 2, 2000x.

Zone three is marked by a region of material that appears to contain a multitude of cracks, oxides and cavities as shown in Figure 4.39. In the samples studied the width of this region ranged from about 5 microns towards the crack root and increased in size up to about 30 microns near the fracture mouth.

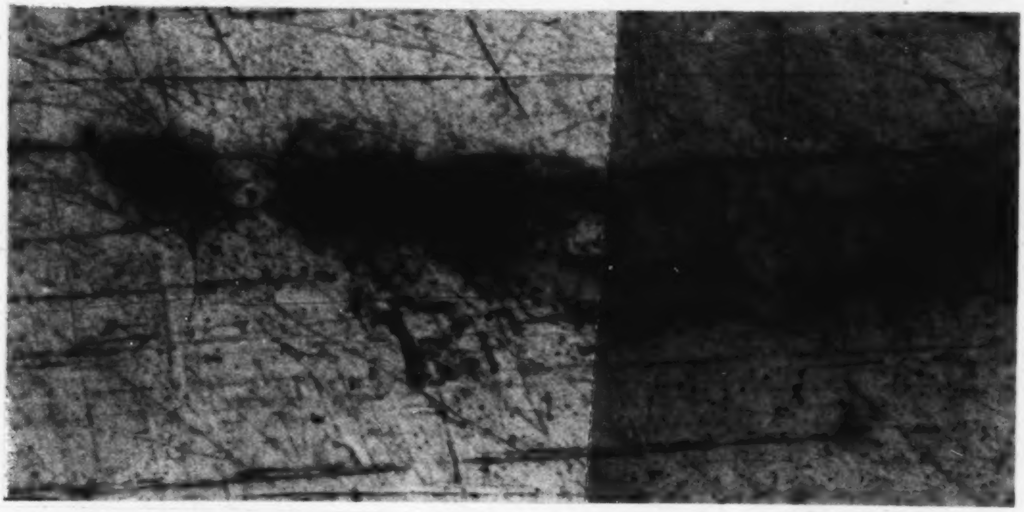

Figure 4.39 The powdery cracking of zone three, 1400x.

Zone four is the final separation of the fracture surfaces. Figure 4.40 shows cracking in zone 4 along with some of the zone three material.

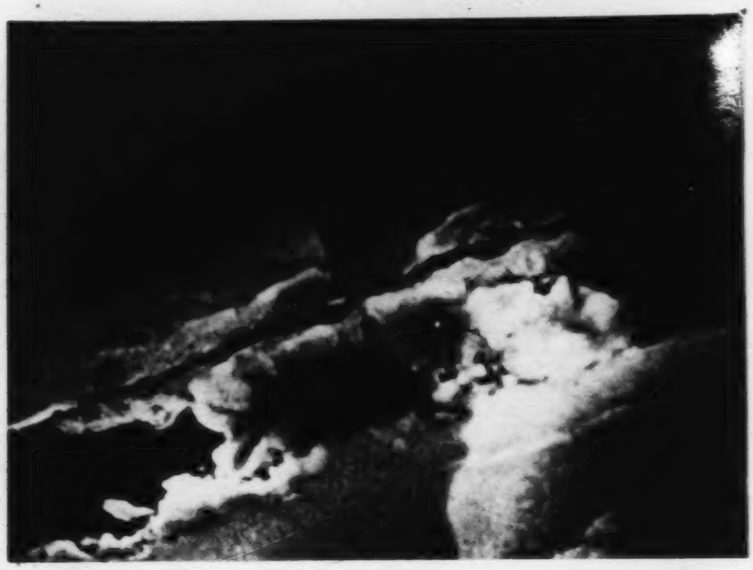

Figure 4.40 The final fracture separation with some of the zone three material, 650x.

From the preceding discussion on artifacts it is apparent that some changes will have been made to the fracture during the sample preparation. Some questions may arise concerning the powdery component in zone three; in particular whether it is entirely an artifact that has been packed in during polishing, or whether it is a region perhaps consisting of fractured zirconium metal, oxides and hydrides that slowly increases in the thickness direction towards the mouth of the crack. With this question in mind several experiments were carried out on the material in this region, and the fracture was examined in detail after various stages of the polishing procedure. Figure 4.41 shows that three heavy scratches from polishing tended to remove the phase.

Figure 4.41 The effect of heavy polishing scratches on the stage three material, 1400x.

Particles in the phase showed sufficient cohesion and adhesion to allow hardness tests to be carried out as shown in Figure 4.42.

Figure 4.42 A hardness indent of 15 grams on the stage three material, 600x.

Etching revealed that many of the large particles associated with the fracture in zone three have elongated grain structures and orientations similar to the bulk material. Figure 4.43 shows a wedge-shaped particle in this region after etching.

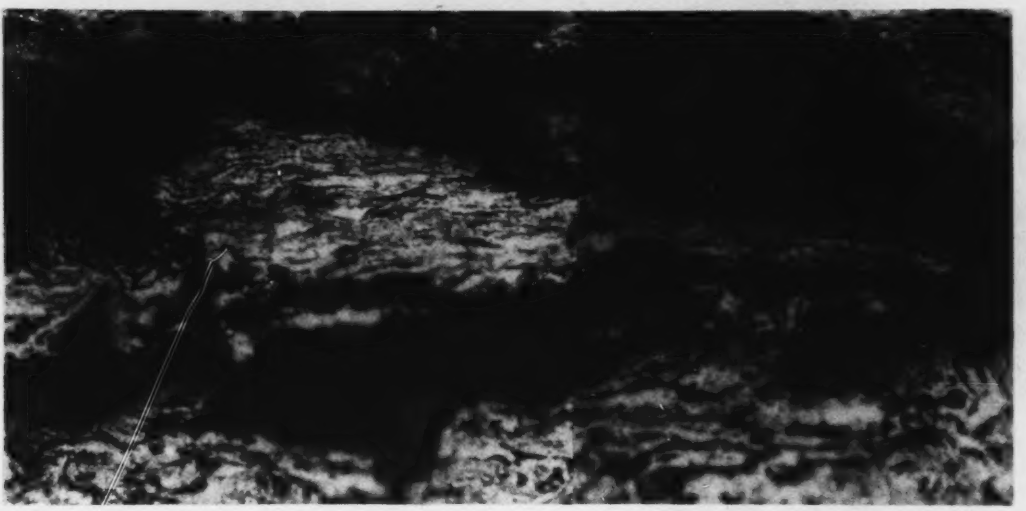

Figure 4.43 An etched section of zone three, 1400x.

An energy dispersive analysis using the scanning electron microscope was conducted on the material appearing in the region of the third fracture zone. This analysis showed no significant amounts of the elements associated with polishing or grinding compounds that would have been present had such material been packed in during the sample preparation.

The oxide phase that made up part of the material in the third zone was identified by comparing the appearance of this phase with that of other phases known to be oxides. For this purpose it was assumed that oxides would be visible in the surface regions of the metallographic samples and perhaps in some regions near the fracture surface. To facilitate the observation of these oxides 45° taper sections were made. The fracture surface as shown in Figure 4.44 showed a dark rounded phase comparable in morphology to the phase associated with the hydride crack of Figure 4.38.

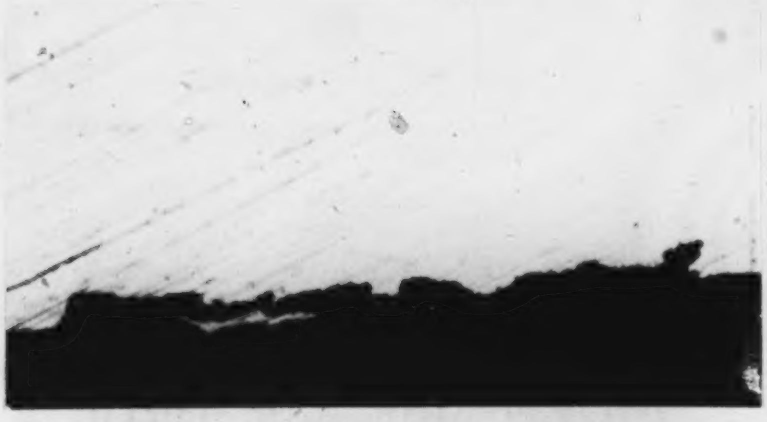

Figure 4.44 The oxide phase adjacent to the fracture surface of a tube sample as shown by a 45 degree taper section of sample 148-1, 1400x.

When the external surface of the sample was viewed, a rounded dark phase also appeared as shown in Figure 4.45.

This phase appeared to be very similar to those associated with the fracture, as in zone 2 through zone 4. Thus on the basis of this optical comparison it was concluded that the rounded dark phase associated with the hydride crack was an oxide.

Figure 4.45 The oxide phase adjacent to the outside surface of a tube sample as shown by a 45 degree taper section of sample 148-1, 1400x.

As a final test as to what type of material could be accumulated in a crack during the preparation of Zr-2.5%Nb, a hole was drilled in sample 148-2 and a plug was machined out of sample 1804-2. The plug was then filed on two sides and pressed into the hole with a vise. This provided two crevices of varying thickness that were prepared concurrently with the hydride crack for microscopic examination. Figure 4.46 shows a portion of the hydride crack and a portion of the artifical crack after polishing.

Figure 4.46 Material found in a hydride crack (above) and material found in a crack-like defect created in the same sample (below), 1120x.

At first glance the section of the artifical crack appeared similar to the hydride crack. However closer examination revealed that the artifical crack did not contain the oxide phase nor did it exhibit the same type of geometry as the hydride crack. If the material found in the region of the third zone of the hydride fracture was totally a result of sample preparation it should have been identical to the material seen in the artifical crack. Since this was not the case the material in zone three must represent some aspect of hydride cracking.

There were regions in the artifical crack where the surfaces were in close contact with one another. When the sample was polished to expose the hydrides this tight interface between the plug and the hole was accented by a narrow dark zone as shown in Figure 4.47.

Figure 4.47 Hydrides associated with a drilled hole and plug in a hydrided zirconium sample, 320x.

The dark zone did not have the appearance of a layer resulting from a work hardening process, and it formed preferentially on the outside of the interface where a tensile stress would be encountered. Since a tensile stress is conducive to hydride formation and the phases in the zone had the same appearance as hydrides in the optical microscope, this zone was assumed to be a series of hydrides that formed after the plug was pressed into place. It may be noted that the hydrides appear to be oriented incorrectly with the tensile stresses that would be expected around the drilled hole. However the orientation of the submicroscopic plates that make up the hydride could still be normal to the tensile stress while the hydrides, as they appear in the optical microscope, would run parallel to the tensile stress.

The appearance of the artifical crack is important in the analysis of the microstructure for it emphasizes that the hydride phase, as it appears in metallographic samples, may not have been present during the fracturing process.

4.6.2 Load and Crack Displacement

The above descriptions of the hydride fracture are limited because the fracture is viewed in a condition of zero load, and because the amount of degradation that occurs during the sample preparation is unknown. In order to obtain a better understanding of the hydride cracking process, metallographic information was required in addition to that obtained by viewing the unstressed crack in one plane. To this end a cracked sample under a tensile load was observed in the optical microscope and in the scanning electron microscope.

The hydride crack created in 1804-3 was loaded to 80 kg while the crack opening displacement was monitored with an extensometer. Prior to loading the sample had been polished on the longitudinal-tangential plane for microscopic examination. The preparatory procedures had reduced the thickness to approximately 3.4 mm. Once the sample was extended to full load a steel wedge was inserted in the machined opening near the crack mouth. This provided a residual strain in the region of the fracture equivalent to a tensile load of about 57 kg after the sample was removed from the tensile machine.

The sample was then viewed in the scanning electron microscope. The mouth of the radial-longitudinal crack is shown in Figure 4.48. The crack does not appear to be a continuous straight line but contains a number of steps or protrusions from each fracture face. Since the sample had been previously mounted in epoxy, it is likely that at least some of the matter seen in the crack is mounting material.

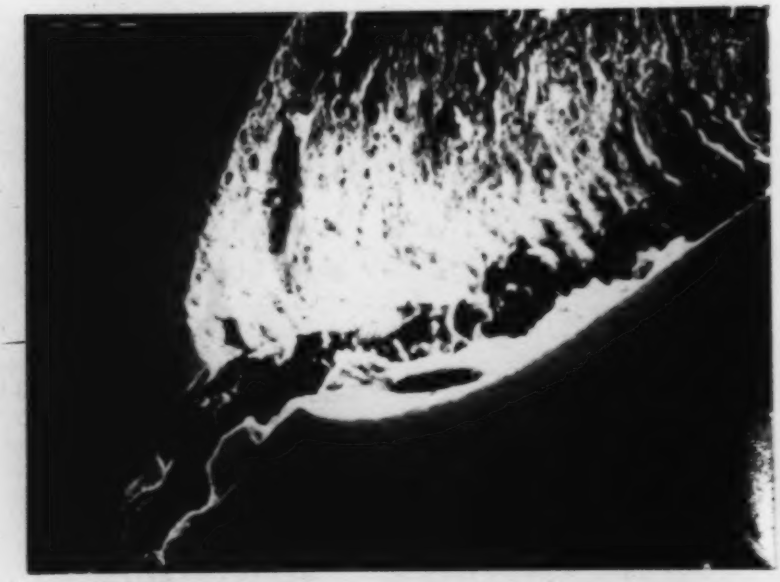

Figure 4.48 An electron micrograph of a stressed hydride crack (the longitudinal direction of the crack extends from the lower left corner at ≈45°), 300x.

The sample was also viewed in the optical microscope and a portion of the hydride crack is shown in Figure 4.49.

Figure 4.49 The hydride crack under load, 56x.

The areas surrounding the two hydride cracks near the hardness indents seen in Figure 4.49 are shown enlarged before and after stressing in Figure 4.50.

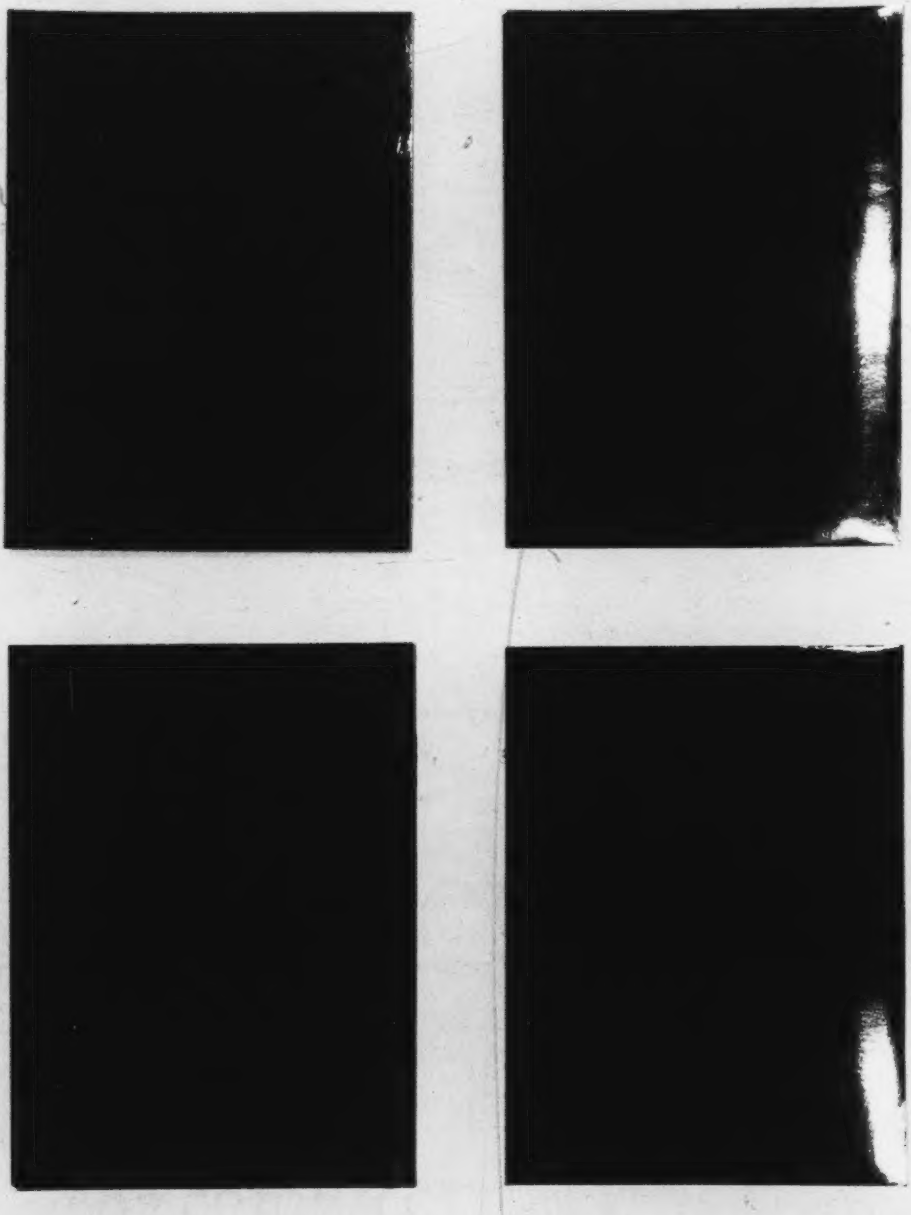

Figure 4.50 A prepared hydride crack without load (left) and with load (right). The upper crack of Figure 4.49 is shown above while the longer, lower crack is shown below, 800x.

The above micrographs serve to substantiate the concept that at least locally a hydride crack can propagate on two or more parallel planes. Furthermore the secondary crack that runs close to the major crack has also been opened by the application of the tensile stress. It would be expected in the presence of a continuous crack that the tensile stresses in adjacent regions, normal to the crack face would be very low. This implies that the hydride cracks are not continuous.

4.6.3 Fracture Appearance in the Radial-Tangential Plane

The expansion of parallel cracks under load (section 4.6.2) and the appearance of protrusions on the fracture surface (Figure 4.48) necessitated further metallographic investigations in the radial-tangential plane. To acomplish this, sample 1804-3 was mounted in epoxy while under a residual stress as described in the previous section. The sample was then sectioned in the radial-tangential plane as referenced to the original pipe in order to view the hydride fracture from a direction parallel to the direction of crack propagation. Figure 4.51 shows the hydride fracture in this plane near the mouth of the crack.

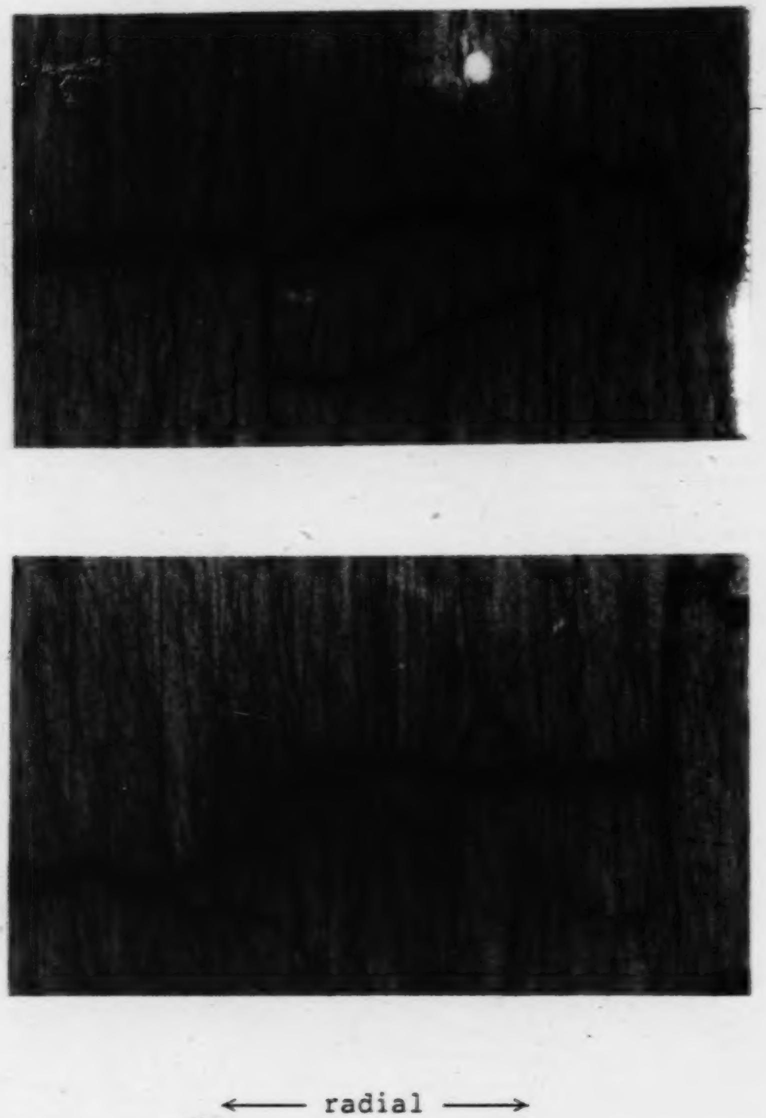

Figure 4.51 The appearance of two regions of the hydride fracture viewed in the radial-tangential plane near the mouth of the crack, 112x.

In some regions of the fracture the hydride crack appeared reasonably continuous. Figure 4.52 shows a continuous section of the crack at two magnifications near the root of the fracture.

Figure 4.52 A region of the hydride fracture at 240x (above) and 1400x (below) near the root of the crack in the radial-tangential plane, sample 1804-3.

Transverse cracking in the radial-longitudinal plane, that is cracking parallel to the applied stress, was apparent near the root of the crack as well as in regions near the crack mouth. Figures 4.53 and 4.54 show examples of transverse cracking.

← radial →

Figure 4.53 Cracking parallel to the applied stress viewed in the radial-tangential plane near the crack tip, 1400x.

There were also some instances of the transverse crack progressing ahead of the major crack. Figure 4.54 shows a number of these transverse cracks propagating near the crack root.

Figure 4.54 Transverse cracking ahead of the major crack in the radial-tangential plane, 225x.

The discontinuous nature of the hydride crack front was also apparent in the radial-tangential plane. Figure 4.55 shows a number of reoriented hydrides that were observed near the root of the hydride fracture. Some of these hydrides were fractured, but the fractures were only visible when viewed at higher magnification. It is apparent that the fracture normal to the applied stress originates as a number of individual cracks growing in different planes.

Figure 4.55 The root of the fracture in the radial-tangential plane, 230x.

The metallographic observations in the radial-tangential plane have served to validate the findings of the previous sections. The material in zone three is now seen as a logical consequence of a fracture that is made up of a multitude of closely spaced branching cracks. Furthermore the discontinuous nature of hydride cracking has been reiterated from a slightly different perspective. It has also been shown that reoriented hydrides that appear uncracked in the light optical microscope occur in the region of the root of the fracture. Unfortunately it is not known precisely when these hydrides formed relative to the formation of the hydride crack.

4.7 The Modelling of Delayed Hydride Fracture

4.7.1 Introduction

The purpose of a scientific model is to consolidate a series of results into an abstraction that will describe the behavior of a phenomenon within a given set of boundary conditions. If the boundary conditions are too narrow or if data appears that cannot be accommodated by the model, it loses value, and eventually it will be modified or replaced by something more useful.

In this section a data base for hydride cracking will be assembled and the current model will then be evaluated in terms of this data. Since a substantial disparity exists between the actual behavior of hydride cracking and the behavior predicted by the current model, a new model will be conceptualized and evaluated.

4.7.2 Components of Hydride Cracking

4.7.2.1 Hydrides

The role that hydrides play in delayed hydrogen fracture is difficult to assess since hydrogen is quite mobile at room temperature and above. This has been demonstrated by the series of hydrides that formed in the tensile region of the artifical crack shown in section 4.6.1. It is therefore apparent that the hydride formation visible in the metallographic samples may not have been present at the time the crack formed.

It has been shown in the literature section that hydrides are a necessary prerequisite for hydride fracture. This is consistent with the observation of reoriented hydrides that appeared to be uncracked near the root of the fracture. These reoriented hydrides indicate that the hydride formation precedes cracking, assuming of course, that the hydrides do not contain cracks below the resolution of the optical microscope.

Fractured transverse hydrides were also seen ahead of the main crack. The fractured transverse hydrides have a similar appearance to other hydrides in the same orientation. This indicates that the hydride cracking process at least partially involves the fracture of hydrides that are normally found in the hydrided Zr-2.5%Nb material.

An equilibrium is reached between the hydrogen in solid solution and the hydrides in the metal matrix.

Both the hydrides and the hydrogen in solid solution are affected by changes in stress. An increase in tensile stress tends to increase the solubility of hydrogen which would tend to dissolve hydrides. However hydrides are seen near the root of the fracture indicating that the anisotropy of the volume expansion that occurs during the formation of a hydride, and the unequal distribution of hydrogen in the metal matrix arising from stress gradients, makes the hydride formation favorable in these areas. Hydrides tend to form in these areas of high tensile stress even though the partial molar volume of hydrogen in the form of a hydride may be lower than that of hydrogen in solid solution. (MacEwen et al. (1985) have reported the partial molar volume of hydrogen in solid solution to be 1.67×10^3 mm^3/mole as compared to 1.4×10^3 mm^3/mole in the δ hydride and 1.7×10^3 mm^3/mole in the γ hydride)

A tensile stress is necessary for hydride cracking. However because of the associated volume increase the formation of a hydride involves the creation of a compressive stress, or at least a partial relief of tensile stresses at root of the fracture. Thus it is apparent that conditions could arise where the hydride fracture is self arresting.

Experiments have also shown that hydrogen migrates down a temperature gradient. Thus it must be concluded that the hydrides are more stable at low temperatures.

Changes in the terminal solid solubility line with stress are assumed to occur, yet have never been shown experimentally. However since the stability of the hydride decreases with increasing temperature the effect of stress on the TSS temperature may indeed be more pronounced at higher temperatures. In other words stresses at high temperatures may cause hydrides to dissolve and also act as a limiting factor to hydride cracking.

4.7.2.2 Hydrogen

The movement of hydrogen is required in order to reorient and form hydrides prior to the crack formation. The migration of hydrogen is dependent on three factors: the amount of hydrogen available to move, the speed at which the individual hydrogen atoms can move, and the driving force for the movement to occur.

The amount of hydrogen available is dependent on the condition of the hydride phase. In conditions of a waning temperature the hydrides are growing in volume. This implies that the atomic hydrogen is supersaturated to some extent in the metal matrix since elastic strains are created by a growing hydride. Conversely a waxing temperature implies an unsaturated condition for the hydrogen which results from the plastic strains that were created previously by the prior growth of the hydride. These plastic strains would tend to leave the shrinking hydride in tension which would shift the equilibrium and tend to preserve the shrinking hydride. In short the hydrides act as large hydrogen traps in the Zr-2.5%Nb system controlling the amount of hydrogen in solid solution. Other traps, along grain boundaries or dislocation lines may also be operational but would be expected to play a lesser role than the hydrides.

The speed at which hydrogen moves is dependent on temperature. As the temperature increases the diffusion rate increases which decreases the time necessary for equilibrium to occur.

The driving force to move hydrogen is dependent on concentration gradients, temperature gradients, and stress gradients. Hydrogen moves down a concentration gradient, but in the case of these tests the samples were annealed after hydrogen was added. Thus a concentration gradient would only be possible on a microscopic level. It has also been shown that hydrogen will migrate down a temperature gradient in zirconium. However with the sample configuration and furnace design utilized here, temperature gradients would not be expected except during temperature changes. Therefore the only major driving force remaining to move hydrogen is the one provided by stress gradients.

4.7.2.3 Crack Morphology

The metallographic samples showed that the hydride crack was discontinuous both in the radial-tangential plane and the tangential-longitudinal plane. Many instances of parallel cracks were apparent, and transverse cracks were also observed when the fracture was viewed in the radial-tangential plane.

The morphology of the hydride fracture gave the impression that cracking continued in a region even after the major crack had propagated through. Thus it is necessary to differentiate between the fracture formation that results in the primary separation of the metal and the fracture processes that continue afterwards. On this basis any region of the fracture that contains an oxide will be considered to have been affected by a process that occurred subsequent to the opening of the major crack in that area. Therefore only zone one cracking, as defined in the microscopy section will be considered to be revelant to the critical hydride cracking mechanism.

4.7.2.4 Acoustic Emission

There is little doubt that acoustic emissions arise from the brittle propagation of cracks. Examples of previous work showing this effect have been mentioned in the literature survey for the case of hydride fracture in zirconium alloys, but acoustic emissions have also been detected in other materials undergoing different types of failures. In the case of a ductile failure in carbon manganese steels the source of acoustic emissions has been attributed to the propagation of cracks which form at the interface between the inclusions and the matrix rather than to void growth and ligament rupture in the steel (Jaffrey,81). Therefore if ligament rupture and void growth are occurring in the hydride fracture process they are most likely not detected under the conditions employed in these tests.

Monitoring the acoustic emissions during the delayed hydride fracture of Zr-2.5%Nb gives an indication as to the amount of brittle fracture that occurs. Therefore in regions where parallel cracks or transverse cracks occur the number of counts per unit crack extension will be high. Conversely in regions where crack extension occurs by void formation and ligament rupture fewer counts per unit crack extension will be detected. This would provide a partial explanation as to the difficulty in correlating acoustic emissions with crack extension as mentioned previously.

4.7.2.5 Temperature

The temperature regime in which delayed hydride cracking takes place is bounded above by the terminal solid solubility temperature or if sufficent hydrogen exists, by the Tcat temperature. At low temperatures the cracking becomes too slow to be of practical significance.

Cracking can occur in two modes depending on whether the test temperature is approached from above (fast cracking mode) or below (slow cracking mode). In both cracking modes, increasing the test temperature causes an increase in cracking rate up to a maximum temperature. An increase in temperature above this maximum causes a decrease in cracking rate. In terms of the dynamic effects, a waxing test temperature can produce a burst of acoustic emissions in both cracking modes.

Above the Tcat temperature a delayed hydride fracture goes into a condition of remission if held for a sufficient time. This condition produces: bulk plastic deformation of the sample, reoriented hydrides if cooled under load, and a long incubation period at lower temperatures before cracking restarts.

Temperature affects the system in other ways. As the temperature is raised the diffusion rates increase allowing spheroidization and growth of microconstituents as well as affecting the availability and mobility of hydrogen. Temperature also affects the strength, ductility and cohesive properties of all the phases present.

4.7.2.6 Load

A lower limit of load exists for hydride cracking. As the load is increased above this value the cracking rate increases to ~~a max~~imum. After the maximum cracking rate has been reached further additions of load either have no effect on cracking rate or cause a reduction in cracking rate. If plane strain conditions persist a load will be reached at which the K_{IC} for the metal matrix is exceeded. This produces a fast propagating unstable fracture not related to hydride cracking, but possibly assisted by hydrides in the matrix.

Cracking rate is also dependent on the prior test load. Increasing load to the test load will cause a faster rate of cracking than decreasing to test load.

A waxing load will cause extra acoustic emissions in addition to those expected at the normal cracking rate, while a waning load will cause a lower rate of cracking or complete arrest of the hydride crack.

4.7.3 Limitations of the Current Hydride Cracking Model

The current model for hydride cracking as described in the literature section, is based on the transport of hydrogen atoms to the region of the crack tip. Each striation of the fracture surface is considered to be a result of hydrides building up in a region ahead of the crack tip until this region becomes embrittled to the point of fracture. The fracture then initiates and quickly runs through this embrittled zone to be arrested in the ductile matrix. Thus the crack propagates simultaneously all along the crack front in a stepwise fashion. This concept of hydride cracking has been expressed in terms of a quantitative mathematical model (section 2.8) which is reported to predict the average crack velocity for a given condition of stress and temperature (Puls,82).

There are many problems with the mathematical model:

(1) There is no provision for the changes in the stress state at the crack tip which result from the formation of hydrides or the movement of atomic hydrogen.

(2) The crack is reported to be arrested in the zirconium matrix (Simpson,77), yet no provision is provided in the model for the fracture of the zirconium metal.

(3) The model is based on the assumption that the hydride crack moves continuously, whereas it is actually reported to propagate in a series of jumps (Dutton,77a)

(4) Transverse cracking is not considered. This would change the loading conditions and produce acoustic emissions that would not represent fracture penetration.

(5) A threshold stress intensity factor exists that is not incorporated into the mathematical model (Puls,82).

(6) The fracture toughness of zirconium hydride is given at 1-3 MPa$\sqrt{m}$ yet delayed hydride fracture occurs over a wide range of stress intensities above this value. This indicates that something other than hydrides is fracturing (Puls,82), which is not accounted for in the model.

(7) Hydrogen is said to come from source hydrides yet there has been no documentation of shrinking of the bulk hydrides in the vicinity of a hydride crack.

(8) There is no provision for the reduction in cracking rate that occurs above 250°C when the test temperature is approached from above, that is when the crack arrest temperature, Tcat, is approached.

(9) There is no provision for the dependency of cracking rate on prior load in the model.

(10) The critical length of a hydride at the crack tip is given as somewhere between 10 and 50 microns (Dutton,77). In the present work there were no indications of regions in this size range having failed in a brittle manner when the fracture surface was viewed in the scanning electron microscope.

(11) There is no provision for striations in the mathematical model.

(12) If variations in the hydride thickness occur as stated in the model, loading conditions of 20 $MPa\sqrt{m}$ would produce a hydride of 12 microns in thickness. A hydride of this size has not been reported as a product of normal hydride cracking.

(13) Acoustic emissions generated from a sample undergoing hydride cracking continue to oscillate around an average value rather than reaching a true steady state. There are no provisions for this type of behavior in the model.

(14) The model does not provide an upper temperature limit for cracking, nor are there provisions for a change in cracking behavior when the load is reduced or when the fracture is in a state of remission.

4.7.4 The Proposed Delayed Hydride Cracking Model

The failure of a metal is normally classified as brittle or ductile. Generally a brittle failure occurs quickly by cleavage or intergranular fracture with little distortion of the metal in the vicinity of the fracture surface while a ductile failure occurs slowly with a substantial amount of plastic deformation. A hydride crack in Zr-2.5%Nb does not fall clearly into either classification. On a microscopic level cracking occurs quickly, as characterized by the acoustic emission behavior yet severe distortion of the fracture surface is observed in the scanning electron microscope. At the same time on a macroscopic level the cracking progresses slowly with almost no detectable amount of plastic deformation. Therefore both the brittle and ductile modes of fracture are incorporated into the delayed hydride cracking model.

In the construction of a model the assumption will be made that the delayed hydride failure occurs by the propagation of two crack "fronts." The discontinuous brittle crack "front" in which hydrides are fracturing is followed by the mainly continuous ductile crack "front" where void growth and ligament rupture are taking place. Other changes in the metal matrix are also expected to occur in order to accommodate these fracture processes. If it were possible to "freeze frame" a propagating hydride crack it would have many of the characteristics depicted schematically in Figure 4.56.

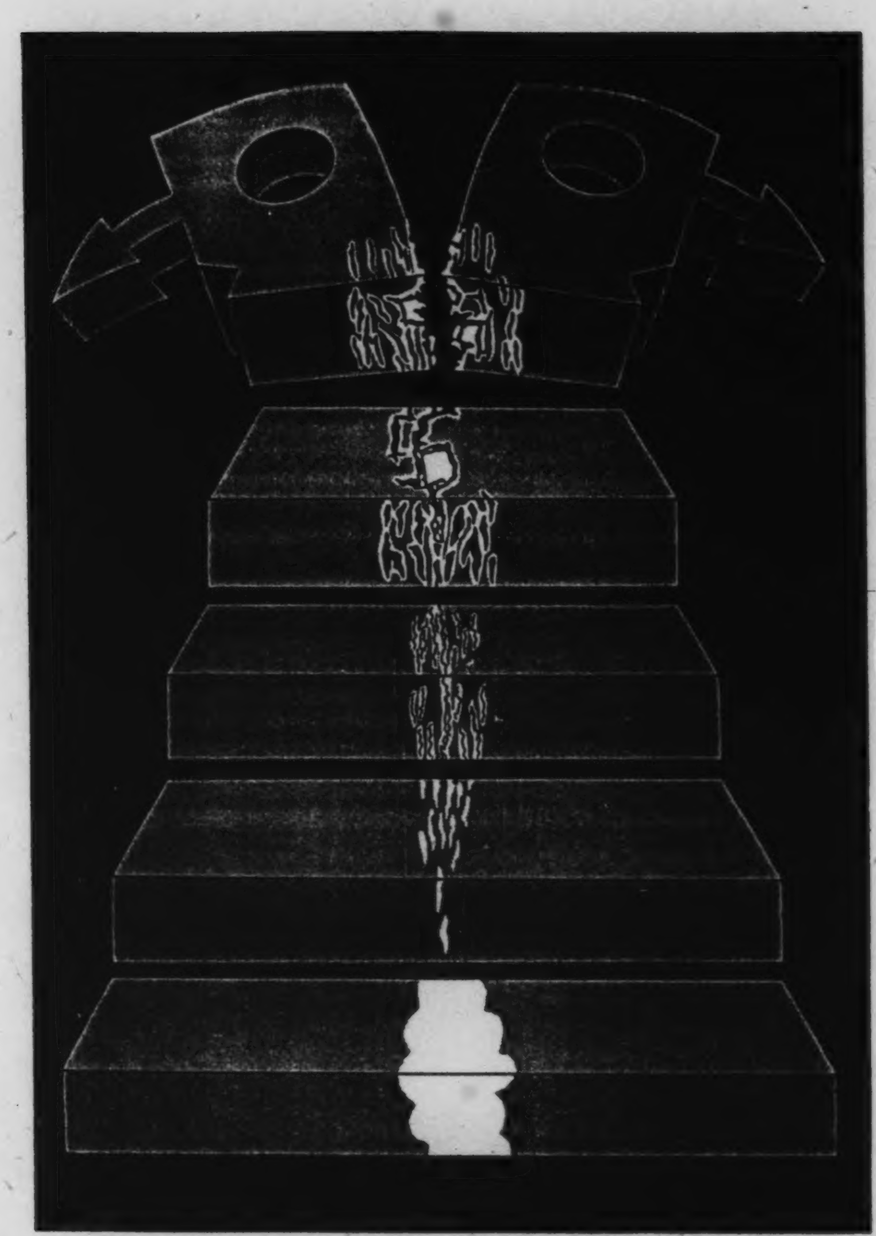

Figure 4.56 A schematic representation of the five stages of hydride cracking (not to scale).

The delayed hydride failure is not conceptualized as an "on-off" occurrence such as the movement of a dislocation, but rather the manifestation of a malady that can be broken down into five stages of development.

The first stage involves the movement of the atomic hydrogen in response to the stress field created by the applied load in the region of the crack tip. This is assumed to be similar to movement of hydrogen in niobium and vanadium which is referred to as the Gorsky effect (Völkl,72). Hydrogen would be expected to preferentially diffuse into this region causing further lattice distortion but reducing the stress concentration and increasing the elastic (anelastic) deformation caused by the applied load.

Once the atomic hydrogen has begun to migrate up the tensile stress gradient other changes take place in the metal matrix prior to fracture. Stage two involves the creation of the prerequisites necessary for the brittle fracture to occur. This process is then followed by stage three: the brittle fracture event that produces acoustic emissions.

The specific prerequisites and the actual fracture processes of stage two and stage three are left open for future experimental work. In this study hydrides ≈2 microns in thickness containing fractures have been observed, but just how this condition arose in the metal matrix is not known. Nucleation, growth and fracture of γ hydrides in Zr-2.5%Nb have been observed in the transmission electron microscope (Cann,80), but these processes were observed in the condition of plane stress and cannot be simply adopted to describe the stage two and stage three fracture that occurs in plane strain.

The outcome of the second and third stages of hydride cracking is a ribbon of material that is not plastically deformed, but contains a multitude of discontinuous cracks. Thus the mechanical properties of this region are dependent only on the cracked area and the properties of the ligaments of unfractured material. The density of the brittle cracks would increase as stage four is approached.

Stage four is the propagation of a ductile crack through the metal matrix which is riddled with pre-existing cracks. Since the ductile crack is relatively continuous and tends to be a singular event all of the cracks that occurred in stage three will not open up to form the stage four crack. The onset of this stage begins with plastic deformation of the ligaments and it terminates with the creation of two separated fracture surfaces. Since the propagation of this ductile crack occurs by the processes of void formation and ligament rupture, it would not be expected to create a significant quantity of acoustic emissions.

After the stage four fracture has progressed through a region the stage five cracking processes continue in the material. These processes arise from stresses created by: differential expansions and contractions of the hydride and metal matrix during thermal fluctuations, the growth of oxide layers in the unopened cracks, and the propagation of the main crack. These stresses manifest themselves near the main crack by the nucleation, growth and fracture of hydrides, and the consequent generation of secondary cracks. Acoustic emissions generated from this stage of cracking could be incorrectly attributed to the progression of the main crack.

Stage five, in the hydride cracking process, is not expected to contribute significantly to the main fracture event. Rather, it acts in conjunction with the growth of hydrides that occurs during the cooldown of the sample to obfuscate features that were associated with the main fracture event when the samples are observed metallographically.

4.7.5 Discussion of the Five Stage Model

The delayed hydride cracking phenomenon has been described in terms of a five stage cracking model which involved the propagation of a brittle and a ductile crack front. This model will now be discussed in the light of the experimental evidence reported in the literature and the experimental results obtained in this study.

4.7.5.1 Load

A sample containing a sharp crack normal to a tensile force will resist the force by the creation of an uneven elastic stress field around the crack tip. The elastic stress will be greatest next to the crack tip and will decrease with distance away from this region. A number of processes, including hydride cracking, respond to this situation and serve to mitigate the intense tensile stress gradient that has been created.

Partial alleviation of high stresses occurs by the generation and/or movement of dislocations to form a plastic zone at the crack tip. Permanent deformation of the sample occurs and the region of the surrounding elastic strain field becomes enlarged.

In the case of zirconium containing hydrogen, the atomic hydrogen in the metal matrix begins to migrate up the tensile gradient as soon as it occurs. Hydrogen causes a further dilation of the strained metallic bonds creating an anelastic deformation that increases the size of the elastic strain field, thereby reducing the stress gradient.

A large volume expansion, especially in the thickness direction takes place when the hydride plates form. In the bulk matrix the volume expansion normally creates a compressive strain field around the hydride, but when hydrides form at the crack tip the expansion overcomes part or all of the tensile strain in this region which causes a redistribution of the surrounding elastic strain field.

The hydrides that form are not limited to one plane in this region, but form in a dispersed fashion on a number of roughly parallel planes, possibly dependent on the location of most favorable nucleation sites created by propitious crystallographic orientations, and stress states. The overall effect is the creation of a layer or ribbon (with a finite thickness) of material containing hydrides that is roughly parallel to the crack plane. Should the load be increased, the size of the highly stressed region at the crack tip will increase. This will allow more hydrides to form over a wider region, increasing the thickness and the length of the hydrided ribbon.

The nucleation of hydrides has an autocatalytic effect in that the formation of one hydride will help to nucleate another. This creates a tendency for hydride growth to continue in the plane of a formed hydride rather than nucleate in a new area. Therefore the thickness of the ribbon in the second stage has a reluctant dependency on stress.

Since the hydrides grow in an elongated fashion and have the above-mentioned autocatalytic tendency, it is favorable for the hydride to grow further into the region of tensile stress rather than expand laterally. Thus as the hydrided ribbon grows ahead of the crack tip causing more dilation of material, the region at the crack tip again undergoes an increase in tensile strain. This can cause further nucleation of hydrides in this area and/or, the fracture of existing hydrides which is the third stage of the cracking process.

The cracking that occurs in stage three causes additional elastic strain at the crack tip in the zirconium ligaments and increased stress at the tip of the growing hydrides in stage two. It is then apparent that a sudden load increase will cause a burst of cracking (stage 3) from the (stage two) hydrides.

If an experiment was conducted in which the test load was reached by increasing the load, the stage two ribbon would be expected to grow at a faster rate, rather than additional hydrides being nucleated. Conversely lowering to test load would tend to propagate the same stage two ribbon thickness; this would cause a slower than normal cracking rate since the stress gradient would have been reduced. If the load was reduced further, a condition could result in which the region at the crack tip would be in compression. In this situation cracking would not occur until the hydrides were redistributed, or stage two continued to grow to the point that the crack tip was again in tension.

It is also apparent that a competition takes place between the nucleating and growing hydrides. If hydrides can nucleate and grow to cause dilation in the thickness direction, and are able to mitigate the tensile stresses in the plane of the crack faster than the stage two ribbon can propagate in the direction of the crack and increase tensile stresses at the root of the crack, the cracking will stop. This is thought to cause the load dependency of crack velocity at high temperatures in which crack velocity will only increase with temperature at high loads.

It has been shown that an increase in load can also cause a decrease in cracking rate. It is thought that this effect is at least partially caused by the appearance of transverse cracking. In a loaded sample a tensile stress is felt parallel to the crack front as well as perpendicular to the crack plane. As the load increases the stress parallel to the crack front builds up to a point where cracking is able to occur normal to this transverse stress. These secondary transverse cracks serve to change the stress state felt by the major crack toward conditions of plane stress, which would reduce the cracking rates.

Load also has an effect on stage four cracking. As the load is increased more ductile ligaments can be torn and the ductile crack front will become physically closer to the stage one region.

It has been reported that acoustic emission per unit fracture surface area is relatively independent of load even though the surface roughness increases with load. This can be explained if only stage three cracking produces acoustic emissions, and an increase in load extends the thickness of the stage three layer without a change in the number of stage 3 cracking events. Thus the same amount of stage three cracking could take place even though an increased amount of ductile tearing is necessary to propagate the fracture.

4.7.5.2 Striations

The utilization of the five stage hydride fracture process allows qualitative explanations of striations visible on the fracture surface. Striations would mark the stepwise progress of the stage four crack. The process which results in striations could be described in terms of a hydride cracking cycle. The start of the cycle could be defined as the instant after the stage four crack propagation has taken place. An opening remains separating the fracture surfaces at the crack tip. Still remaining ahead of the crack tip there are regions of stages 1 through 4. The thickness of the stage 2 and stage 3 ribbons are assumed to be relatively constant as they are expected to be primarily dependent on external load and temperature which are fixed for this particular example.

As time progresses hydrogen diffuses into the stage two region adding to the length of the ribbon as the hydrides form. This decreases the tensile stresses in the region that was previously the stage 1-2 interface. This causes a redistribution of the elastic strain field, an increase in the tensile strains in the stage 2-3 interface from which some acoustic emissions result, and an increase in the opening of the stage four crack tip. This process continues until the crack is ready to propagate. At this point the tensile strain at the stage 1-2 interface is at a minimum, and the individual lengths of stages 2 through 4 are at a maximum.

The stage four crack then begins to propagate. This causes an increase in the tensile strain ahead of the crack which results in additional stage 3 cracking, additional hydrogen migrating to the growing hydrides at the stage 1-2 interface, and an extension of the elastic strain field. Since the progression of the stage four crack is faster than the growth of the stages 2 through 4, the crack opening continues to decrease until the crack stops progressing. This marks the end of a striation cyle.

The striation spacing is dependent on the relative crack tip openings that are required to initiate and propagate the ductile crack, and the relative velocities of the ductile fracture and stage three advancement. It is apparent that striations would disappear if the ductile fracture was either very fast or very slow in comparison to the advancement of stage three cracking.

In the explanation of striations it has been mentioned that the stresses in the regions of the cracking stages would oscillate. Variations of stress on the stage three events would be expected to have a direct relationship to the acoustic emissions generated by the sample. Therefore it would be expected that the acoustic emission rate would also oscillate around an average value rather than reach steady state. This deviation from the steady state production of acoustic emissions during hydride cracking has been observed experimentally in this study.

4.7.5.3 Temperature

Temperature affects hydride cracking by its influence on the mobility and availability of hydrogen, on the nucleation and growth rates of the hydride, and on the mechanical properties of the matrix.

The mobility of the hydrogen in terms of temperature is straightforward as it is a result of the diffusion process, but the availability of hydrogen depends on the hydrogen traps in the matrix. Either of these processes (diffusion and trapping) can be rate determining in that they affect the speed at which hydrogen atoms can be delivered to the crack tip. In the fast cracking mode the rate determining process would likely be diffusion because an increase in load has been shown to cause a substantial increase in the cracking rate in this cracking mode. This idea is based on the concept that the driving force for diffusion is the stress gradient. In the slow cracking mode the rate determining factor is expected to be the amount of hydrogen in solid solution that is available to be moved. The slow cracking mode could result from a lower concentration of hydrogen in solid solution or from an increased difficulty in transferring hydrogen atoms from the bulk hydrides into solid solution.

A temperature exists below which both cracking modes produce approximately the same cracking rate. The conclusion can be reached that one of the rate determining components has become dominant in both cracking modes. An increase in load can cause a lowering of the temperature at which the cracking rates are similar. This results from a larger cracking rate increase in the fast cracking mode compared to the slow cracking mode, when the load is increased. It is therefore possible that the rate determining process that has become dominant at low temperatures is hydrogen diffusion.

Supersaturation of hydrogen is also expected to affect the nucleation rates of the hydrides. If the nucleation rate is high, as may be possible in the case of high hydrogen supersaturation and high temperature, cracking may be stopped due to the relief of the tensile stress by the formation of hydrides.

A temperature increase will cause a decrease in the yield strength of zirconium and may possibly activate some relaxation process in the material that would lower the stress gradient at the root of the crack. If the stress gradient became too low hydride nucleation and growth would no longer take place which would also cause cracking to cease.

Fracture toughness tests (Simpson,79a) performed on the zirconium hydride have shown it to be a very brittle material with little, if any, perceptible increase in ductility with temperature. Thus it has been reported, since the toughness of the hydride is so low, that changes in cracking rate due to temperature are not attributable to changes in hydride properties. However as the temperature increases, small changes in ductility, which would be difficult to measure, could make large changes in cracking rates. These changes in cracking rate could arise because the response to stress may be either fracture of hydrides, or nucleation of hydrides. Therefore if the nucleation stress is very close to the fracture stress of the hydrides, a small increase in the fracture toughness could make nucleation more favorable than hydride fracture, causing fracture to cease.

4.7.5.4 Hydride Cracking Arrest

Conditions of crack arrest should also be included in a comprehensive hydride cracking model. Crack arrest can be achieved by: decreasing load, temperature increases to the crack arrest temperature, Tcat, and by reaching the condition of crack remission.

Reduction of load causes crack arrest by the removal of tensile stresses in the crack tip region. The previous load caused plastic and anelastic strains in this region that are not immediately recovered as the load is removed. It is then possible for these regions to go into compression removing the driving force for hydride cracking.

Tcat was differentiated from crack remission since the remission was associated with plastic deformation of the sample and produced a long term stoppage of hydride cracking. In this condition cracking did not resume immediately when the temperature was lowered, as was observed in the case of the crack arrest temperature.

In terms of temperature there are a number of changes that could occur in the hydride fracture process that would cause cracking to stop. These changes will now be discussed in order to determine the mechanisms most likely responsible for Tcat and crack remission.

Changes in material parameters could directly stop cracking, for example if a large increase in the toughness of zirconium or zirconium hydride occurred at some temperature the cracking would be terminated. Based on the studies of changes of the material parameters (Ambler,84, Simpson,79a) with temperature this appears unlikely.

The subtle changes in material properties would be more likely to produce crack arrest. This would include cases in which the stress gradients are lowered due to relaxation of the metal and cases where there is a change in the ratio of hydride nucleation stress and hydride fracture stress. The relaxation of the matrix could be so pronounced that hydride formation at the crack tip would no longer be favorable, whereas small increases in the fracture stress could make additional hydride nucleation more feasible as a stress relief mechanism rather than the fracture of the hydrides.

Changes in the hydride nucleation and growth behavior may directly stop cracking. This would be the case if a temperature existed where nucleation and growth of hydrides were no longer feasible, or if the stress began to have a major effect on TSS, causing the dissolution of all hydrides in the region of the crack root. Cracking would also be stopped if hydride thickening began to predominate over hydride growth in the length direction. By the same token if the activation energy for hydride nucleation became very low, hydrides would nucleate throughout the crack tip region eliminating the tensile stress gradient.

The proposed explanation of Tcat is based on the experimental evidence that showed: a decrease in cracking rate as Tcat was approached, the load dependence of cracking rate as Tcat was approached, the quick return of cracking velocity when temperature was reduced below Tcat, and the insensitivity of Tcat to applied load. Based on these observations it appears there are two mechanisms which occur, one during the approach to Tcat, and the other at the time of crack arrest. The approach to Tcat likely involves a competition between processes, either hydride nucleation versus hydride fracture or, hydride growth versus hydride nucleation, or hydride growth in the thickness direction versus hydride growth in the length direction. With any of these combinations an increase in load would still increase the possibility of stage three cracking before stress relaxation could occur from the development of the hydrides in directions normal to the crack.

The actual temperature at which Tcat occurs must represent a dramatic change in the mechanism of hydride cracking. One possibility here would be the existence of a critical temperature above which precipitation of a hydride in a stressed region is no longer energetically favorable. Alternatively a temperature could be reached whereupon the uneven distribution of atomic hydrogen was sufficient to reduce the stresses below the cracking threshold of the hydrides at the crack tip. Thus any increase in the toughness of the hydride that occurred with temperature would work concurrently in this process of crack arrest. Whatever the mechanism is that so curtly stops the cracking, it does not make large changes in the stress state at the crack tip, since cracking resumes almost immediately after the temperature is lowered.

The process of crack remission in which hydride fracture terminates must involve large scale changes in the stress distribution at the crack tip. Test samples showed bulk plastic deformation after crack remission was achieved, while the metallographic specimen showed a region of reoriented hydrides approximately 8 mm by 5 mm in size. Thus it seems readily apparent that a major relaxation took place at the crack tip. Since the thermodynamic state of the hydrogen at the crack tip is not known, the effect could be caused by the deformation of zirconium possibly assisted by atomic hydrogen, or assisted by massive amount of hydride nucleation and growth. This plastic deformation would serve to drastically lower the stress concentration at the crack tip and eliminate the possibility of cracking.

4.7.5.5 Literature Support for the Cracking Model

As previously mentioned the stage one movement of hydrogen has been validated in the literature. The effect has been well documented in similar materials such as niobium and vanadium (Völkl,72) and hydrogen diffusion rates in Zr-2.5%Nb have been calculated by use of this method (Mazzolai,76).

Metallographic studies (Tangri,82) have shown the formation of hydride platelets on adjacent planes along the fracture surface. These hydrides are assumed to be either stage 2 or stage 3 hydrides.

Simpson (1980) has reported discrepancies between the potential drop and acoustic emission outputs of a delayed hydride cracking sample. The suggestion is made that the hydride platelets fracture soon after they form, but the crack faces do not separate. This suggestion is easily accommodated in the stage three of the proposed hydride cracking model.

Support for the concept of a propagating ductile crack, that is stage four cracking, seems to appear only through the micrographs of the fracture surface. The features of the fracture surface have been described as "feathery platelets" (Ells,80), or as ductile tear ridges connecting brittle regions (Yuan,81).

In summary, the hydride cracking behavior both observed in this study and reported in the literature gives support to the proposed model. As further experimental data is collected the model may have to be modified or even deleted entirely, but at this time of writing the qualitative aspects of delayed hydride cracking can be accommodated within the five stage cracking model.

5. Conclusions

This study has been primarily based on the observed acoustic emission behaviour supplemented by the fractographic and metallographic characteristics of delayed hydride fractures in Zr-2.5%Nb pressure tube material. The conclusions arising from this study are presented below in point form.

(1) Acoustic emissions appear to represent only the brittle component of the fracture process, likely involving fracture of hydrides.

(2) Oxide bands, visible on the fracture surface, are associated with acoustic activity but not directly.

(3) The metallographic studies have shown parallel cracking and transverse cracking which would generate acoustic emissions but would not be reflected in amount of fracture surface area observed fractographically.

(4) The secondary transverse cracking would tend to impede the progress of the main fracture by changing the stress state to plane stress in regions along the crack front.

(5) The delayed hydride fracture process consists of the propagation of two crack fronts: a brittle crack front, and a ductile crack front.

(6) From the experimental results a five stage model for delayed hydride cracking has been conceptualized which includes the brittle and the ductile mode of fracture.

(a) Stage one is the migration of atomic hydrogen up the stress gradient at the crack tip which in turn serves to reduce this stress gradient.

(b) Stage two involves the creation of a hydride entity that relieves tensile stresses in the region of its formation.

(c) Stage three is the brittle fracture associated with the hydrides which produces the measurable acoustic emissions.

(d) Stage four represents the full separation of two fracture surfaces. The heavily deformed fracture surface features indicate the ductile nature of this final fracture.

(e) Stage five is the product of the sample response to minor stresses associated with the newly created fracture surface. These stresses would consist of: residual stresses from the main fracture event, stresses created from uneven expansion of the hydrides during thermal fluctuations, and stresses arising from the formation of oxides on the fracture surfaces.

(7) The propagation of the hydride crack is sensitive to subtle changes of temperature, and stress.

(8) The two modes of cracking have been attributed to changes in the microstructural proportion of the hydrides in the matrix which in turn affects the availability of atomic hydrogen to the forming hydrides.

(9) Bursts of brittle cracking that are apparent during a waxing temperature are most likely the result of stress changes due to the large coefficent of expansion of the hydride compared to that of the matrix.

(10) An upper temperature boundary exists for hydride cracking both in terms of a crack arrest temperature, Tcat, and the full termination of crack propagation referred to as cracking remission. These temperature boundaries appear to be independent of the terminal solid solubility temperature which until now has been considered to be the upper temperature limit for hydride cracking.

(11) Changes in test load were found to have a major influence on cracking rate.

(12) Load was thought to influence the thickness of the region in which the second stage of cracking occurred. This combined with the autocatalytic nature of the hydride formation allowed more than one cracking rate to be attained at the same test load by changes in the load applied prior to the test.

(13) Use of the five stage hydride cracking model is expecially useful in the explanation of the striation spacing on the fracture surface and also explains the tendency for the acoustic emissions to oscillate around an average value rather than reaching steady state conditions.

(14) Hydride cracking will continue to be a potentially fertile research topic since its true mechanisms are physically hidden underneath the metal surface where plane strain conditions exist, and the adroit nature of hydrogen serves to obfuscate whatever cracking evidence may be attainable through metallographic techniques.

6. Further Study

Ultimately further work on the topic of delayed hydride cracking Zr-2.5%Nb will lead to a complete understanding of the fracture process. This would include a quantitative mathematical model that could be used to accurately predict the cracking velocity under all conditions. Some of the research topics that would assist in reaching this objective are listed below:

(1) A quantitative analysis of the effect of prior temperature on cracking rate would be valuable. It has been shown that a temperature spike or trough of 40 to 60°C changes the cracking mode. However changes that occur in cracking rate with variations of size, shape, and duration of this prior temperature profile over a range of temperatures are not known.

(2) Experiments could be undertaken to demonstrate the quantitative aspects of load changes over a range of temperature. The immediate burst of emissions that occurs when a load increase is applied to a cracking sample could be investigated or the long term changes that occur in acoustic emmision rate after an increase or decrease in load.

(3) The positive identification of the hydride and oxide phases would clarify some doubts on the microstructural constituents in various positions along the hydride crack. This could be done with an electron microprobe for the oxide phase and with a lithium nuclear

microprobe for the hydride phase.

(4) A degradation of properties has been noted in the Zr-2.5%Nb metal ahead of the oxide bands as seen on the fracture surface. A research project could be undertaken to determine the volume of material involved, the properties of this material and the metallurgical nature of this damage.

(5) It is also apparent that the acoustic emissions contain more information than just number of counts. In terms of this study it was noted that the same acoustic emission rate could be attained by a large number of small bursts or a small number of large bursts. This would be expected to represent a difference in cracking characteristics, that could perhaps be identified. Other information may be apparent if signal processing packages were available similar to the energy dispersive analysis used on the scanning electron microscope. Perhaps a distinction could then be made between the acoustic output of a pencil lead breaking and the output of a running delayed hydride crack.

(6) The effects of hydrogen content are not well known, and would also be expected to play a role in hydride cracking. For instance increasing the hydrogen content may slow the cracking rate by providing locations for extra transverse cracking, thus creating additional areas of plane stress, or it may increase the cracking rate by increasing the rate of hydrogen migration to the crack tip.

(7) Most work has been done in which the delayed hydride crack propagation occurs in the radial-longitudinal plane of the pressure tube material. For a complete understanding of the system other planes would also be worthy of investigation, especially the longitudinal-circumferential plane which would be parallel to the existing hydrides.

7. Bibliography

Ambler J.F.R., Zirconium in the Nuclear Industry: Sixth International Symposium, ASTM STP 824 (1984) p. 653

Ambler J.F.R. and Coleman C.E., Second International Congress on Hydrogen in Metals, paper $3C_{10}$ (1977)

Arora A. and Tangri K., International Advances in Nondestructive Testing, 8(1981)217

Arunachalam V.S., Lehtinen B. and Östberg G., Journal of Nuclear Materials, 21(1967)241

Barraclough K.G. and Beevers C.J., Journal of Less-Common Metals, 35(1974)177

Beck R.L., Transactions of the ASM, 55(1962)542

Bradbrook J.S., Lorimer G.W. and Ridley N., Journal of Nuclear Materials, 42(1972)142

Cann C.D. and Sexton E., Acta Metallurgica, 28(1980)1221

Cann, C.D., Puls M.P., Sexton E.E. and Hutchings W.G., Journal of Nuclear Materials, 126(1984)197

Carpenter G.J.C., Journal of Nuclear Materials, 48(1973)264.

Carpenter G.J.C., Acta Metallurgica, 26(1978)1225

Cheadle B.A. and Coleman C.E., Hydrogen in Metals, Japan Institute of Metals,(1979) p. 517

Cheadle B.A., Coleman C.E. and Ipohorski M., Zirconium in the Nuclear Industry: Sixth International Symposium, ASTM STP 824, American Society for Testing and Materials,(1984) p. 210

Coleman C.E., Zirconium in the Nuclear Industry: Fifth Conference, American Society for Testing and Materials, ASTM STP 754 (1982) p. 393

Coleman C.E., AECL memorandum to G.J. Field, March 16,1984 (a)

Coleman C.E. and Ambler J.F.R., Zirconium in the Nuclear Industry, ASTM STP 663, American Society for Testing and Materials (1977) p. 589 (a)

Coleman C.E. and Ambler J.F.R., AECL memorandum to C.E.Ells, August 19,1977 (b)

Coleman C.E. and Ambler J.F.R., Hydrogen in Metals, The Metallurgical Society of CIM, Annual volume (1978) p. 81

Coleman C.E. and Ambler J.F.R., Reviews on Coatings and Corrosion, 3(1979)105

Coleman C.E. and Ambler J.F.R., Scripta Metallurgica, 17(1983)77

Coleman C.E. and Cox B., Zirconium in the Nuclear Industry:Sixth International Symposium, ASTM STP 824 (1984) p. 675 (b)

Coleman C.E., Cheadle B.A., Ambler J.F.R., Lichtenberger P.C. and Eadie R.L., Canadian Metallurgical Quarterly, 24(1985)245

Coleman C.E. and Hardie D., Journal of the Less-Common Metals, 11(1966)168

Dutton R., Hydrogen in Metals, The Metallurgical Society of CIM, Annual Volume (1978) p. 16

Dutton R., Nuttall K., Puls M.P. and Simpson L.A., Metallurgical Transactions A, 8A(1977)1553 (a)

Dutton R., Woo C.H., Nuttall K., Simpson L.A. and Puls M.P., Second International Congress on Hydrogen in Metals, paper $3C_6$ (1977) (b)

Ells C.E., Journal of Nuclear Materials, 28(1968)129

Ells C.E., The Metallurgical Society of CIM, Annual Volume (1978) p. 1

Ells C.E. and van der Kuur J.H., AECL-6853, March, 1980

Erickson W.H. and Hardie D., Journal of Nuclear Materials, 13(1964)254

Hardie D. and Shanahan M.W., Journal of Nuclear Materials, 55(1975)1

Hehemann R.F., Canadian Metallurgical Quarterly, 11(1972)201

Jaffrey D., Ninth World Conference on Non-destructive Testing, 4J-1 (1981)

Johnson H.H. and Hirth J.P., Metallurgical Transactions A, 7A(1976)1543

Kearns J.J., Journal of Nuclear Materials, 22(1967)292

Kearns J.J., Journal of Nuclear Materials, 43(1972)330

Libowitz G.G., Journal of Nuclear Materials, 5(1962)228

MacEwen S.R., Coleman C.E., Ells C.E. and Faber J. Jr., Acta Metallurgica, 33(1985)753

Marshall R., Trans TMS-AIME, 233(1965)1249

Mazzolai F.M. and Ryll-Nardzewski J., Journal of the Less-Common Metals, 49(1976)323

Mishima Y. and Okubo T., Canadian Metallurgical Quarterly, 11(1972)157

Mostovoy S., Crosley P.B. and Ripling E.J., Journal of Materials, 2(1967)661.

Mueller W.M., Ed. Metal Hydrides, Academic Press, (1968)

Nath B., Lorimer G.W. and Ridley N., Journal of Nuclear Materials, 58(1975)153

Northwood D.O. and Lim D., The Metallurgical Society of CIM, Annual Volume (1978) p. 68 (a)

Northwood D.O. and Gilbert R.W, Journal of Nuclear Materials, 78(1978)112 (b)

Nuttall K., Second International Congress on Hydrogen in Metals, paper $3C_7$ (1977)

Nuttall K. and Rogowski A.J., Journal of Nuclear Materials, 80(1979)279

Östberg G., Journal of the Institute of Metals, 93(1964-65)223

Perovic V., Weatherly G.C. and Simpson C.J., Acta Metallurgica, 31(1983)1381

Perovic V. and Weatherly G.C., Journal of Nuclear Materials, 126(1984)160

Perryman E.C.W., Nuclear Energy, 17(1978)95

Petch N.J. and Stables P., Nature, 169(1952)842

Pressouyre G.M., Acta Metallurgica, 28(1980)895

Puls M.P., Acta Metallurgica, 29(1981)1961

Puls M.P., Simpson L.A. and Dutton R., Fracture Problems and Solutions in the Energy Industry, Pergamon (1982) p. 13

Rogers B.A. and Atkins D.F., Journal of Metals (1955)1034

Sawatzky A., Ledoux G.A., Tough R.L. and Cann C.D., Proc. Miami Intern. Symp. on Metal-Hydrogen Systems (1981) p. 109

Simpson L.A., Proceedings of the 3rd International Conference on the Mechanical Behavior of Materials, 2(1980)445

Simpson L.A., Metallurgical Transactions A, 12A(1981)2113

Simpson L.A. and Cann C.D., Journal of Nuclear Materials, 87(1979)303 (a)

Simpson L.A. and Cann C.D., Journal of Nuclear Materials, 126(1984)70

Simpson L.A. and Puls M., Metallurgical Transactions A, 10A(1979)1093 (b)

Simpson L.A. and Nuttall K., Zirconium in the Nuclear Industry, ASTM STP 633, American Society for Testing and Materials (1977) p. 608

Takano S. and Suzuki T., Acta Metallurgica, 22(1974)265

Tangri K., Proceedings of the Institute of Acoustics, paper 417 (1977) p. 1

Tangri K. and Yuan X.Q. Fracture Problems and Solutions in the Energy Industry, Pergamon Press (1982) p. 27

Thompson A.W. and Wilcox B.A., Scripta Metallurgica, 6(1972)689

Troiano A.R., Transactions of the ASM, 52(1960)54

Vitikainen E. and Nenonen P., Journal of Nuclear Materials, 78(1978)362

Völkl J., Berichte der Bunsen-Gesellschaft für physikalische Chemie, 76(1972)797

Waisman J.L., Toosky R. and Sines G., Metallurgical Transactions A, 8A(1977)1249

Weatherly G.C., Acta Metallurgica, 29(1981)501

Weinstein D. and Holtz F.C., Transactions of the American Society for Metals, 57(1964)284

Westlake D.G., Transactions of the ASM, 62(1969)1000

Wilkins B.J.S. and Wasylyshyn A., Journal of Nuclear Materials, 29(1969)235

Yuan X.Q. and Tangri K., Journal of Nuclear Materials, 105(1982)310